Characterization of Two Novel Voltage-gated Calcium Channel Beta Subunits from *Lymnaea stagnalis*

by

Taylor F. Dawson

A thesis
presented to the University of Waterloo
in fulfillment of the
thesis requirement for the degree of
Master of Science
in
Biology

Waterloo, Ontario, Canada, 2010

AUTHOR'S DECLARATION

I hereby declare that I am the sole author of this thesis. This is a true copy of the thesis, including any required final revisions, as accepted by my examiners.

I understand that my thesis may be made electronically available to the public.

Abstract

In excitable tissues, voltage-gated calcium channel activity is critical in the linkage of electrical stimuli to physiological responses, and so modulation of calcium channels therefore has significant implications. The exact mechanisms of calcium channel modulation and membrane expression, however, remain elusive. Previous work suggests that the calcium channel β subunit (*Cavβ*) modulates the expression and biophysical properties of the pore-forming α_1 subunit. Previous research has shown that the core domains of $Ca_v\beta$ subunits are highly conserved, although alternative splicing in the highly variable N-terminus and HOOK regions is commonly observed in invertebrates, teleost fish and mammals. Splicing in these regions can produce unique isoforms that differentially modulate the membrane trafficking and gating properties of high voltage-activated calcium channels. With this in mind, two novel isoforms of an invertebrate *Cavβ* subunit have been identified and cloned from the pond snail *Lymnaea stagnalis,* which contain a novel N-terminus not previously identified. In addition, one of these novel isoforms excludes an optional, short exon in the HOOK region of $LCa_v\beta$. Intron sequencing and amino acid alignments of the variable N-terminal and HOOK regions with mammalian and fish homologs have revealed that the genomic structure of $Ca_v\beta$ subuinits is conserved, despite the divergence in sequence and function between genes and splice isoforms. It was determined that the previously characterized $LCa_v\beta$ isoform, as well as the two new isoforms, can act to fine-tune calcium channel activity by modulating the membrane expression, voltage-dependencies of activation and inactivation and gating kinetics of invertebrate homologs of L-type (LCa_v1) and neuronal (LCa_v2) calcium channels. It is hoped that broadening our knowledge of simplified invertebrate calcium channels, like those found in *Lymnaea*, may advance our understanding the workings of our own highly elaborate and dynamic calcium channel complexes, and the nervous system as a whole.

Acknowledgements

I owe many individuals a great deal of gratitude for all they have given me since starting in the Spafford laboratory more than three years ago as an undergraduate student. Most notably, I would like to thank my supervisor, Dr. David Spafford for taking me on as a relatively inexperienced undergraduate student and giving me the opportunity to work in his laboratory. His motivation and enthusiasm for neuroscience have been a constant source of inspiration for me, especially at times when results were scarce. Next, I would like to thank the members of my graduate committee, Drs. Brian Dixon and Mungo Marsden, for their continuing advice and constructive criticism of my research- your insight has been much appreciated. Finally, I would like to acknowledge those faculty members who introduced me to the world of research by providing me with my first two laboratory positions- Drs. Kirsten Müller and Trevor Charles.

There are also many other to whom I am greatly indebted, especially my colleagues, past and present, in the Spafford Lab. I owe a great deal thanks to Adriano Senatore, who taught me almost everything I know with regard to techniques in molecular biology. I extend my most sincere thanks to Adriano for his patience and selfless commitment to sharing his expertise with others. Along the way I have also been helped by several other at various times in my career including Xuan (Sherry) Huang, Patrick McCamphill, Adrienne Boone, Stanley Lam and Dale Weber. I would like to extend a sincere thankyou to Linda Zepf who has alwys gone above and beyond in her willingness to help myself and others in the department.

Lastly, I am grateful to have been surrounded by such great friends and family over the past six years in Waterloo. Most importantly I would like to acknowledge my mom (Karen Dawson), stepdad (Sandy Horbatiuk), grandparents (Ray and Jenny Rudyk), great aunt (Sonja Halyk) and all of my friends who have made Waterloo home for the past six and a half years- thank you!

Dedication

To Baba and Gigi

(Jenny and Raymond Rudyk),

Your constant encouragement and support have always been greatly appreciated.

Thank You.

Table of Contents

List of Figures

List of Tables

Chapter 1
Introduction

1.1 Voltage-gated Calcium Channels

Voltage-gated calcium channels (VGCCs) perform critical functions in excitable membranes. VGCCs mediate the transduction of electrical signals (in the form of membrane potentials) into physiological responses, such as neurotransmitter release or muscle contraction (Jones, 1998), which are initiated by a rise in intracellular calcium levels (Hille, 1992). Although diversity exists among the total population of VGCCs, they can be divided into two broad classes based on their functional characteristics.

One class of VGCCs, referred to as the low voltage-activated (or LVA) channels, are open at resting membrane potentials (around -60 mV) and require only a weakly depolarizing stimulus to become activated (Carbone and Lux, 1984). The LVA VGCCs also display rapid inactivation (Carbone and Lux, 1984). Channel activation and inactivation will be discussed further in section 1.1.3. These LVA VGCCs (also referred to as T-type or Ca_v3 channels) are responsible for slow, repetitive pacemaker activity in the thalamus and in cardiac tissue (Hugenard, 1996). The functions more commonly associated with VGCCs are performed by a different class of VGCCs known as high voltage-activated (or HVA) channels.

As the name suggests, HVA VGCCs need a strong depolarization to activate and their inactivation properties are highly variable. Several subclasses of VGCCs fall into this group based on their electrophysiological characteristics. One class of VGCCs are known as the L-type calcium channels (also referred to as $Ca_v1.1$, $Ca_v1.2$, $Ca_v1.3$ and $Ca_v1.4$), so-called

because of their large conductance as compared to other VGCCs (Nowycky *et al*., 1985). The non-L-type channels include three groups: P/Q-, N- and R-type channels also referred to as $Ca_v2.1$, $Ca_v2.2$ and $Ca_v2.3$ respectively (Jones, 1998). The non-L-type channels are responsible for synaptic transmitter release, while L-type channels can also be found outside of the nervous system, where they can be detected in skeletal, cardiac and smooth muscle as well as retinal tissue. It is also possible to differentiate HVA channels according to their differing responses to various drugs that affect channel conductance and kinetics (their pharmacological properties) (Plummer *et al.*, 1989; Mintz *et al.*, 1992). Although the HVA class of VGCCs is functionally, molecularly and pharmacologically diverse, intriguingly they have striking structural homology.

1.1.1 Voltage-gated Calcium Channel Structure

VGCCs are multimeric complexes comprised of up to four distinct protein subunits, although as few as one may be sufficient for channel operation (Jones, 1998). All VGCCs must at least contain the primary α_1 subunit, which is endowed with all the major attributes of VGCCs including the ion-selective pore, selectivity filter, voltage sensors and drug binding sites (Catterall, 1996). Aside from the α_1 subunit, several auxiliary subunits may or may not be present in HVA VGCCs, including a β subunit, an $\alpha_2\delta$ subunit and a γ subunit which act to modulate the gating and membrane expression of VGCCs. This section will concentrate on the structure of the primary α_1 subunit. For a discussion of β subunit structure, please refer to section 1.2.1.

The α_1 subunit is comprised of four repeated, homologous domains (I-IV) connected by loops, each of which contains six transmembrane α-helical segments (referred to as S1-S6) as seen in figure 1.1 (Tanabe *et al.*, 1987). Together, these four homologous domains form a tubular pore through the membrane through which calcium ions may pass. Mutagenesis experiments of homologous voltage-gated sodium and potassium channel domains have hypothesized that the voltage-sensing mechanism is found in the S4 helix of the transmembrane domains, which contains positively charged amino acid residues in every third position exposed to the surface of the channel or the pore (Stuhmer *et al.*, 1989; Yang and Horn, 1995; Mannuzzu *et al.*, 1996). When this region is altered by site-directed mutagenesis, channel activity is abolished. Aside from sensing changes in membrane potential, the α_1 subunit must also contain a mechanism which is selective for the passage of calcium ions over other ionic species.

It is believed that the selectivity filter, as it is known, is contained in the extracellular, re-entrant loop between transmembrane segments S5 and S6 (also known as the P-loop). Each loop, contributed from all four domains, contain a critical glutamate residue which is necessary to attract and bind calcium ions (two at a time) with high affinity in the interior of the pore. It has been hypothesized that the rapid flow of ions through the pore is a balance of the opposing effects of calcium ions binding with high affinity to the glutamate residues and the repulsion between the two calcium ions bound in the pore (Yang *et al*., 1993). Studies have shown that if these residues are altered using site-directed mutagenesis, then the preference of the channel to pass calcium ions is severely attenuated, if not abolished depending on which residues are mutated (Kim *et al.*, 1993; Yang *et al.*, 1993). It is these

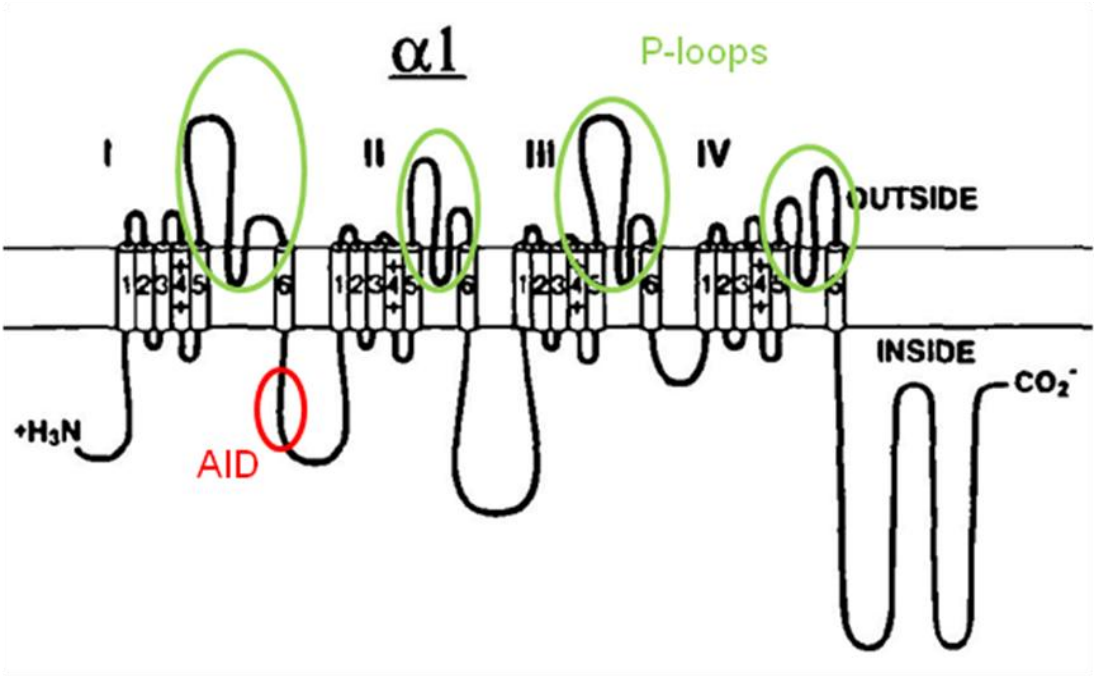

Figure 1.1: Domain structure of voltage-gated calcium channel α1 subunit. Cylinders represent transmembrane α-helicies and lines represent linker peptides. The α interaction domain (AID) found in the I-II linker is highlighted by a red circle and the p-loops (hypothesized to form the selectivity filter) are surrounded by green circles, while the putative voltage sensor found in S4 is identified by (+) , which is indicative of the charged residues contained within. Modified from Catterall , W.A. (2006). *J.Bioenerg.Biomembr. 28*(3), 219-230.

structural elements contained within the α_1 subunit that allows them to function independent of any of the auxiliary subunits.

1.1.2 Kinetics of Voltage-gated Calcium Channels

As described in section 1.1.1, VGCCs function by allowing calcium into a cell upon the detection of a depolarizing stimulus. The amount of calcium allowed into cells is determined by two factors, the extent to which calcium channels are expressed in the membrane and the gating kinetics of these channels. Logically, as the level of membrane expression is increased, so will the total amount of calcium entering the cell (this is referred to as the peak calcium current). The role of kinetics in modulating calcium entry is more complex.

VGCCs exist in three functional states: activated, closed and inactivated (reviewed in Jones, 1998). Upon detection of a depolarizing stimulus, VGCCs will activate by undergoing a change in conformation which allows calcium ions to pass through the pore and into the cytosol. This occurs very rapidly, on the scale of a few milliseconds after receiving a depolarizing stimulus. However, after a prolonged depolarization, VGCCs become inactivated. In their inactivated states, VGCCs transition to a "reluctant" state where they are refractory to opening regardless of the membrane potential. In whole-cell recordings of peak Ba^{2+} or Ca^{2+} currents, the inactivation is seen as an exponential decay in the total current, even though the level of depolarization remains high. Calcium channels recover from inactivation by hyperpolarization, which promotes the transition of channels from the refractory, inactivated state to the closed state, where they are in a "willing" state for re-

opening. Several factors can influence channel kinetics, including membrane potential, calcium concentration, or interactions with other proteins including the VGCC β subunit ($Ca_v\beta$).

1.2 Voltage-gated Calcium Channel β Subunits

The $Ca_v\beta$ subunit of VGCCs was first discovered in 1987 as a 54 kDa component of purified skeletal muscle dihydropyridine receptors (Takahashi *et al.*, 1987). The $Ca_v\beta_1$ subunit was then cloned (Ruth *et al.*, 1989), followed by the identification and cloning of three other mammalian $Ca_v\beta$ subunit genes ($Ca_v\beta_2$, $Ca_v\beta_3$ and $Ca_v\beta_4$) over the next five years (Hullin *et al.*, 1992; Perez-Reyes *et al.*, 1992; Castellano *et al.*, 1993a,b). In addition to the multiple genes encoding $Ca_v\beta$ subunits, a further level of complexity is added by the frequent occurrence of alternative splicing in $Ca_v\beta$ subunits (Foell *et al.*, 2004). All $Ca_v\beta$ subunits are expressed in the brain, but $Ca_v\beta$ subunits can be differentially expressed in other excitable tissues such as the heart, lungs and skeletal muscle (as reviewed in Arikkath and Campbell, 2003). Despite the variation among $Ca_v\beta$ subunits at the sequence level, their domain structure is highly conserved.

1.2.1 Structure of the Voltage-gated Calcium Channel β Subunit

For years after their discovery and cloning, the structure of $Ca_v\beta$ subunits were unknown. It was not until the late 1990s that homology modelling was employed to predict the five

domain structure. Hanlon and colleagues predicted a core structure of $Ca_v\beta_{1b}$ resembling that of the membrane-associated guanylate kinase (MAGUK) protein family (Hanlon *et al.*, 1999). MAGUKs contain Src Homology 3 (SH3) and guanylate kinase (GK) domains, as well as PDZ domains (Montgomery *et al.*, 2004). The predicted structure of the $Ca_v\beta_{1b}$ subunit contains putative SH3 and GK domains, located at residues 100-165 and 220-430 respectively, and a PDZ-like domain in the N-terminus (Hanlon *et al*., 1999). The N- and C-termini are structures with little identity to known motifs and so their structure was not clearly predicted, nor was the region bounded by the SH3 and GK domains (referred to as the HOOK region). These predictions based on homology have recently been confirmed by studies of the crystal structure of the $Ca_v\beta$ subunit core (which corresponds to the SH3, HOOK and GK domains) (Chen *et al*., 2004). A ribbon diagram illustrating the crystal structure of the $Ca_v\beta$ subunit can be seen in figure 1.2A.

MAGUKs and $Ca_v\beta$ subunits share both structural and functional similarities. MAGUKs are scaffolding proteins found in synaptic active zones and act to organize and assemble a plethora of multimeric signalling complexes (as reviewed in Montgomery *et al.*, 2004) as well as cluster *Shaker*-type potassium channels (Kim *et al.*, 1995). SH3 domains are often found in proteins that are localized to the inner surface of the plasma membrane (like $Ca_v\beta$ subunits), and are also known to assist in the assembly of signaling complexes (Hanlon *et al*., 1999). The $Ca_v\beta$ subunit SH3 domain consists of five β-sheets, which run antiparallel to each other in two groups which are arranged perpendicular to each other. However, unlike in MAGUKs, the SH3 domain of the $Ca_v\beta$ subunit is interrupted between β-sheets four and five by an intervening HOOK region, a difference that does not lead to disruption in the

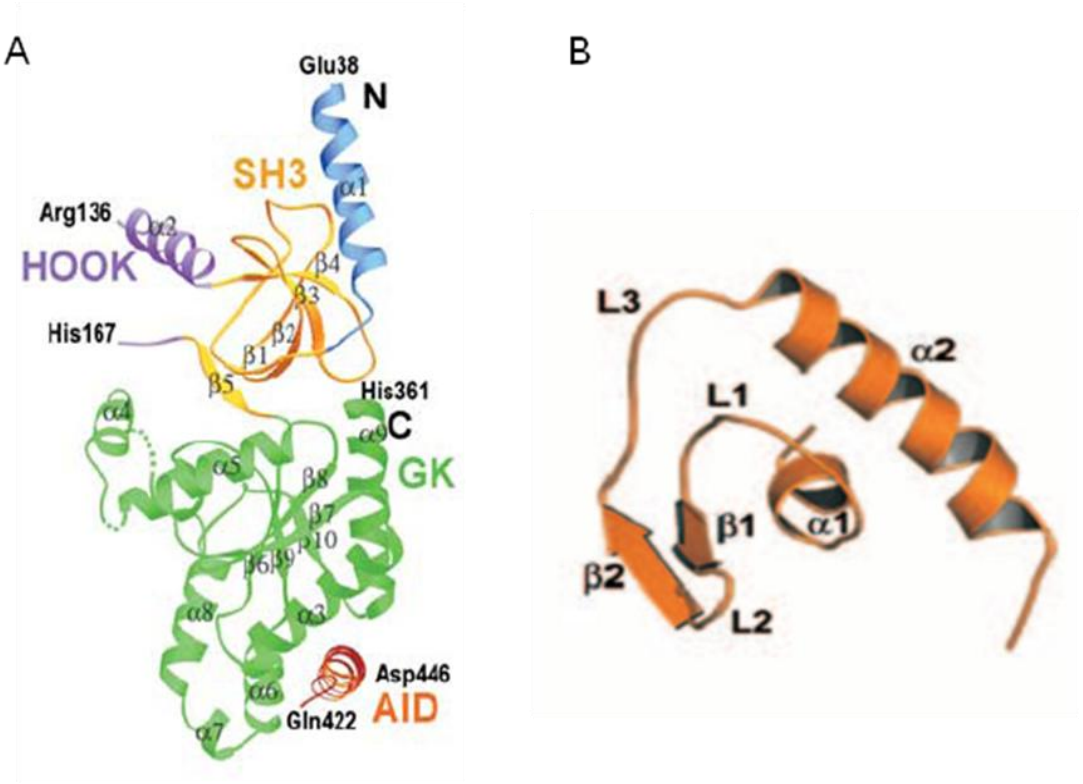

Figure 1.2: Crystal structure of the voltage-gated calcium channel β subunit. (A) Cyrstal structure of conserved Src Homology 3 (SH3, yellow) and Guanylate Kinase (GK; Green) domains. The structures of N-terminal and HOOK domains are incomplete due to the high degree of variability found in these domains. The position of AID peptide binding is also shown (orange, right hand side). From Chen, Y. (2004). *Nature* . 429, 675-680. (B) Crystal structure of the N-terminal A-domain of the $Ca_V\beta_{4a}$ subunit . From Vendel, A.C. *et al.* (2006). *Protein Sci.* 15, 2, 378-383.

domain folding. Typically, MAGUK-SH3 domains are involved in the binding of proline-rich peptides (McPherson, 1999), but the crystal structure of the $Ca_v\beta$ subunit reveals that these putative binding sites are occluded in the $Ca_v\beta$-SH3 domain (Chen *et al.*, 2004). Recent work has shown that the SH3 domain can bind to the I-II linker and C-terminus of the primary α_1 subunit (Dubuis *et al.*, 2006), and that dynamic rearrangements of this domain are possible in order to expose the putative proline binding sites (Gonzalez-Gutierrez *et al.*, 2007) allowing for the possible interaction of many proteins with the SH3 portion of the $Ca_v\beta$ subunit. Further work is needed to validate the role of the SH3 domain in VGCC modulation and trafficking.

The putative $Ca_v\beta$-GK domain was identified by its homology to GK domains found in yeast proteins, as it contains a repeating β-α-β motif but lacks the ATP-binding site necessary for kinase activity (Hanlon *et al.*, 1999). Interactions with other proteins, most notably the VGCC α_1 subunit, occur via the GK domain. Studies of the crystal structure of the GK domain (Chen *et al.*, 2004), as well as biochemical assays and analysis of truncated proteins (De Waard *et al.*, 1994; Pragnell *et al.*, 1994) have shown that the GK domain contains a β Interaction Domain (BID) which is required for binding to the primary α_1 subunit. The BID is 30 amino acids long and by mutating key residues within it, De Waard *et al.* were able to abolish the high-affinity binding of β subunit to the α_1 subunit, and show that the functional effects of the β subunits had disappeared (De Waard *et al.*, 1994). Similar studies were completed in α_1 subunit to determine that a region of 18 amino acid residues in the linker between domains I and II, known as the α Interaction Doman or AID (see figure 1.1), is responsible for interacting with the $Ca_v\beta$ subunit (Pragnell *et al.*,1994).

More recent studies have questioned the nature of the interaction between the AID of α_1 subunits and BID of the $Ca_v\beta$ subunit. The crystal structure of the $Ca_v\beta$ subunit shows that the BID does not interact directly with the AID, but instead that the AID interacts with a small hydrophobic groove in the GK domain, opposite the SH3 domain (Chen *et al*., 2004). This leaves the majority of the surface of the $Ca_v\beta$ subunit free to interact with other regions of the α_1 subunit or other proteins. It has been postulated that the role of the BID is structural, in that it acts as a stabilizing bridge between the SH3 and GK domains (Chen *et al.*, 2004). This hypothesis is supported by other studies that have shown that truncated $Ca_v\beta$ subunits which lack the BID and most of the GK domain still have modualtory effects on VGCC biophysics (Harry *et al.*, 2004; Cohen *et al.*, 2005).

To further investigate the nature of the AID-$Ca_v\beta$ interaction, other groups have transferred the AID region from HVA VGCCs to the I-II loop of LVA T-type channels, which are not known to be associated with auxiliary subunits. Interestingly, when the AID domain was added to the I-II loop of the T-type channel, some (but not all) of the typical modulatory effects of $Ca_v\beta$ subunits- increased peak current and hyperpolarization of the activation curve- were observed (Arias *et al.*, 2005). This work builds upon the direct coupling hypothesis, which states that channel gating is modulated by the $Ca_v\beta$ subunit regulation of the conformational changes seen in the IS6 transmembrane segment of α_1 during activation and inactivation (Hering, 2002). In order for this to occur there must also be a rigid link between the end of IS6 and the AID. To test this hypothesis, deletions and mutations were made to the 22 amino acid region which connects IS6 to the AID in $Ca_v2.2$ and assessing the biophysical effects. If amino acids in the IS6-AID linker thought to

represent β-sheets are replaced by glycine residues (to increase flexibility and disrupt β-sheet formation) all $Ca_v\beta$ subunit effects were removed (Vitko *et al.*,2008). It was also found that deletion of even a single amino acid in this region was sufficient to abolish all of the effects of $Ca_v\beta$ subunit expression, with the exception of its ability to assist in the assembly and membrane trafficking of the α_1 subunit (Vitko *et al.*, 2008). It was determined, using bimolecular fluorescence complementation (BiFC) analysis, that deletions in the IS6-AID linker had disrupted β-sheet formation and had shifted the orientation of the $Ca_v\beta$ subunit by 180˚, leading to the conclusion that the role of the AID is to anchor the $Ca_v\beta$ subunit so that it is positioned towards other regions of α_1 where lower affinity binding promotes modulation of channel gating (Vitko *et al.*, 2008). Furthermore, studies investigating the specific roles of the individual domains have raised speculation that the SH3 domain is more active in promoting interaction with α_1 than the crystal structure data suggests. For instance, Maltez *et al.* (2005) showed that some β subunit functions can be achieved without interaction with the AID, and that the SH3 domain can bind directly to the I-II linker *outside* of the AID region. Although it is clear that the SH3 and GK domains interact with α_1 to modulate its biophysical properties, much work remains in order to fully understand the true nature of VGCC modulation by the $Ca_v\beta$ subunit core.

As discussed, the SH3 and GK domains are highly conserved among all $Ca_v\beta$ subunits. So how are $Ca_v\beta$ subunits able to interact with the various classes of VGCCs in an isoform specific manner? The answer may lay in the hypervariable A domain, located at the N-terminus. The recently published solution structure of the N-terminal A domain of $Ca_v\beta_{4a}$ (seen in figure 1.2B) shows that this domain folds independently and points away from the

SH3-HOOK-GK core (Vendel *et al.*, 2006). The domain is comprised of two α-helicies positioned antiparallel to one another with two β-sheets and three connecting loops which surround a small hydrophobic core (Vendel *et al*., 2006). The second α-helix is stabilized through an interaction with the SH3 domain which is important in ensuring that the N-terminus is oriented away from the rest of the protein. Since it has been shown that the A domain does not directly interact with the α_1 subunit (Maltez *et al*., 2005), perhaps this domain exerts its influence on channel function indirectly by interacting with other proteins that bind to and modulate α_1. This notion is especially attractive as it is known that the A domain has a high rate of alternative splicing, and previous work has shown α_1 isoform-specific modulation by $Ca_v\beta_{4a}$ splice variants of the A domain (Helton and Horne, 2002). Alternative splicing in the N-terminus and HOOK regions likely plays a large role in the specific modulation of various α_1 subfamilies, especially in invertebrates like the freshwater pond snail *Lymnaea*, where only a single $Ca_v\beta$ subunit homolog is present (Spafford and Zamponi, 2003).

1.2.2 Functional Effects of β Subunit Expression

$Ca_v\beta$ subunits serve as critical modulators of VGCC expression and gating, and these tasks are achieved independently of one another (Gerster *et al.*, 1999). It has long been known that the overexpression of all four mammalian $Ca_v\beta$ subunits in excitable cells results in increased density of calcium currents through both L-type and non-L type HVA VGCCs (Neuhuber *et al*., 1998; Raghib *et al.*, 2001; Colecraft *et al.*, 2002). This increase in current density (seen

as increased whole-cell peak calcium current) is due to the role of $Ca_v\beta$ subunits in the membrane trafficking of the primary α_1 subunit.

It has been shown that the I-II loop of α_1 contains an endoplasmic reticulum (ER) retention signal which can be antagonized by the $Ca_v\beta$ subunit (Bichet *et al.*, 2000). If the $Ca_v\beta$ subunit is not co-expressed with α_1, immunolabeling and deletion analysis reveals that the ER retention signal drastically restricts the level of α_1 expressed in the membrane and α_1 remains confined to the ER (Bichet *et al.*, 2000). Masking of the ER retention signal, presumably through AID-BID interaction, allows α_1 to escape the ER and become inserted in the membrane. Despite their similar roles in the membrane trafficking of α_1, the four mammalian $Ca_v\beta$ subunits (and their splice isoforms) differ in their modulation of channel gating and kinetics.

The ability of the various $Ca_v\beta$ subunits to uniquely alter the gating properties of α_1 is one of the primary ways in which VGCCs are regulated temporally and spatially. The modulation of VGCC kinetics is specific to the unique combination of α_1 and $Ca_v\beta$ subunits which are expressed in a given cell (Sokolov *et al.*, 2000), and therefore the functionality of VGCCs in a given cell can be fine-tuned by modifying the expression of the four $Ca_v\beta$ subunit genes. The gating properties of α_1 may be altered by modulating the voltage-dependency and/or kinetics of activation, inactivation or both. All of the mammalian $Ca_v\beta$ subunits induce a hyperpolarizing shift in the voltage-dependence on activation (He *et al.*, 2007), which translates functionally to the channels activating at a more negative potential (i.e. less depolarization above resting potential is required). When inactivation induced by $Ca_v\beta$ subunit overexpression was studied, it was noted that $Ca_v\beta_{1b}$, $Ca_v\beta_3$ and $Ca_v\beta_4$ all

increased the speed of inactivation, and shifted the voltage-dependence in a hyperpolarizing direction (He *et al.*, 2007). This means that a greater fraction of VGCCs will begin to close at more negative potentials after being open for less time, resulting in a calcium current which will disappear more rapidly than if $Ca_v\beta$ subunits are not expressed. Conversely, inactivation was significantly slowed by the expression of $Ca_v\beta_{2a}$ and the voltage dependence on inactivation was shifted to more depolarizing potentials (He *et al.*, 2007), meaning VGCCs can remain open longer and do not significantly inactivate at lower potentials. Knowing that the core structure of the β subunit is remarkably conserved, how can these functional differences be accounted for? Many studies have implicated the hypervariable N-terminus and HOOK regions in the endowment of isoform-specific properties.

As shown by Bichet and colleagues, $Ca_v\beta$ subunits mask an ER retention signal found in the I-II linker of α_1 in order to facilitate membrane expression. It was later shown that the same effect could be achieved by the co-expression of α_1 with a truncated $Ca_v\beta$ subunit comprised of only the BID-containing GK domain (He *et al.*, 2007). Although the trafficking of α_1 was enhanced by $Ca_v\beta$-GK expression, there was only a slight modulation of the gating properties. Co-expression of α_1 with $Ca_v\beta$-GK resulted in whole-cell currents which inactivated rapidly, showing only a slight, insignificant deviation amongst all four mammalian $Ca_v\beta$ subunits (He *et al.*, 2007; Richards *et al.*, 2007). Therefore, it was concluded that although the AID-GK interaction firmly anchors $Ca_v\beta$ to α_1 to assist with trafficking, gene- and isoform-specific modulation must occur via lower affinity interactions in the more variable regions which flank the GK domain (He *et al.*, 2007).

In order to elucidate the role of the N- and C-termini, as well as the HOOK region, several studies of truncated $Ca_v\beta$ subunits were carried out. It was clear that the C-terminus, although relatively divergent between subfamilies was not responsible for modulating the changes in gating, as channels expressed with $Ca_v\beta$ subunits truncated at the C-terminus were biophysically identical to wild-type (He *et al.*, 2007). Evidence suggests that the distal N-terminus and the HOOK region are involved in modulating the inactivation of VGCCs. When α_1 was co-expressed with either full-length $Ca_v\beta$ subunits or $Ca_v\beta$ subunits containing only the core domains (SH3-HOOK-GK) it was noted that the inactivation kinetics of each pair (e.g. β_2: full length versus truncated) were markedly different (He *et al.*, 2007). This suggests that the N-terminus is participating in the subfamily-specific regulation of α_1 since both constructs contained the same HOOK region and C-terminus. He and colleagues (2007) hypothesized that the HOOK region must also be involved in channel inactivation since there was remarkable variation in the inactivation properties among the four $Ca_v\beta$ subunit cores.

To test this theory, the HOOK regions of $Ca_v\beta_{1b}$ and $Ca_v\beta_{2a}$ were swapped, and it was noted that $Ca_v\beta_{1b}$ (which usually facilitates inactivation) was inhibiting inactivation (as is usually the case for $Ca_v\beta_{2a}$) and vice versa (He *et al.*, 2007). This model is further supported by experiments which demonstrate that if the HOOK region of $Ca_v\beta_{2a}$ is deleted, rapid inactivation is observed (Richards *et al.*, 2007). Other work shows that expression of the GK domain alone is sufficient to inhibit inactivation of α_1 even among $Ca_v\beta_1$, $Ca_v\beta_3$ and $Ca_v\beta_4$, which suggests that the facilitation seen in those $Ca_v\beta$ subunits is controlled by regions outside of the GK domain (Gonzalez-Gutierrez *et al.*, 2008). Overall, it is safe to say that

much remains to be learned about how the biophysical properties of the α_1 subunit are modulated by mammalian $Ca_v\beta$ subunits.

Finally, an additional level of complexity is added by the fact that modulation of channel function is possible through the interaction of $Ca_v\beta$ subunits with other proteins outside of the VGCC complex. These include enzymes like mitogen-activated protein kinase (MAPK) (Fitzgerald, 2002), and protein kinase A (PKA) (as reviewed in Arikkath and Campbell, 2003) and regulatory proteins, including members of the G-protein family such as Gem (Beguin *et al.*, 2001). The interaction of other proteins with $Ca_v\beta$ subunits can produce a variety of effects on membrane trafficking and gating of the primary α_1 subunit.

1.3 Lymnaea stagnalis as a Model Organism in Neuroscience

The fact that mammals express four genes for $Ca_v\beta$ subunits can quickly confound our ability to understand the fundamental concepts involved in their modulation of VGCCs. For this reason, molluscs such as the freshwater pond snail *Lymnaea stagnalis*, are ideal as they contain only a single $Ca_v\beta$ subunit homolog ($LCa_v\beta$) and two HVA α_1 homologs (known as LCa_v1 and LCa_v2) for the seven mammalian α_1 genes (Spafford *et al*., 2006; Spafford *et al.*, 2003). $LCa_v1$and LCa_v2 are homologs to the L-type and non-L-type HVA channels, respectively. As reported by Spafford *et al.* (2004), the *L* $Ca_v\beta$ subunit has little effect on the membrane expression and overall kinetics of LCa_v2 channels. The only significant finding was that the co-expression of $LCa_v\beta$ with LCa_v2 caused a slowing of inactivation decay

(Spafford *et al.,* 2004). Since it is a common feature of $Ca_v\beta$ subunits to facilitate membrane trafficking of α_1, but invertebrates do not contain multiple $Ca_v\beta$ subunit genes, it is very likely that unidentified alternative splice isoforms exist in *Lymnaea* in order to facilitate channel type-specific membrane trafficking.

It is the goal of this project to identify novel splice isoforms of $LCa_v\beta$ in the N-terminal region, which is thought to be highly variable. These isoforms will then be cloned and characterized electrophysiologically (with both LCa_v1 and LCa_v2), and the patterns of localization with α_1 will be investigated.

Chapter 2
Materials & Methods

2.1 Screening of cDNA Library for Novel $LCa_v\beta$ Subunit Variants

In order to determine if alternative splice isoforms of the $LCa_v\beta$ N-terminus were present, cDNA libraries were screened by nested polymerase chain reaction (PCR) using degenerate primers. Amplified products were then purified and sequenced before being cloned into a full-length $LCa_v\beta$ subunit in the mammalian expression vector pMT-2SX(R). These steps are described in further detail below.

2.1.1 Degenerate Primer Design for Library Screening

In order to determine if alternative splicing is present in the N-terminus of $LCa_v\beta$, a cDNA library constructed from *Lymnaea* cerebral ganglia was screened using a degenerate primer set and vector specific primers. These nested primers are referred to as $LCa_v\beta$ 1exon1b-outer and *Lymnaea*-beta-degen and their sequences are displayed in table 2.1. The relative locations of all primer sites used in cloning and sequencing are illustrated in figure 2.1. The vector used in the construction of the cDNA library, λZAP, contained universal primer sites for the following primers (whose sequences are also displayed in table 2.1): T77, T33, EV2 and EV3. Since the orientation of the cDNA insert in the library was unknown, each fraction was screened in either direction using either the EV3/T33 or EV2/T77 primer sets. Therefore,

Table 2.1: Primer Sequences used in library screening and cloning (restriction sites are highlighted)

Primer Name	Primer sequence (5' to 3')
*LCa$_v\beta$*1exon1b-outer	AGCAAACGCAACAGGTTTGGCCTTAGC
Lymnaea-beta-degen	TCGTAGTGCCTCCTTCTCTTCATCTAG
T77	GTAATACGACTCACTATAGGGCGA
T33	AATTAACCCTCACTAAAGGGAAC
EV2	CGCCCAGGGTTTTCCCAGTCACGAG
EV3	AGCGGATAACAATTTCACACAGGA
*LCa$_v\beta$*Mf	GGCGTGTTTCCTATCTGTACAAAC
*LCa$_v\beta$*1bNotATG	CGACGCGGCCGCCACCATGCGAATCAAGGCTGGGGAGACC
*LCa$_v\beta$*BlpIbb	TTCTGCCTGAACTTCAGCTAAGCC
*LCa$_v\beta$*BlpIb	TTCAGCTAAGCCTGAAGCTCTTGG
LCa$_v\beta$-aKpnf	CCAAGGGTACCTCATTTTTATGAATATCTTATTC
LCa$_v\beta$-aSacb	CCAAGAGCTCCTGTCGTATAAAACTGTTGGAGCT
LCa$_v\beta$-bKpnf	CCAAGGGTACCTTTAAGTGCATCTTTACAAACAC
LCa$_v\beta$-bSacb	CCAAGAGCTCCAGAGAATCGATGTCGCTGAGCCC
end-LBetaBexon	GCATGAGACTTTGCCCCAAGGCAGGATGG
CB5'Nco1b	CTGTAAGAACCAATGTGTCCTATG
CBSB2	GCCAAACCTGTTGCGTTTGCTGTA
LBetaNdeI	GTAAATGCGGGCCGTTCAATATC

for the primary PCR the primers used were "*LCa$_v\beta$*1exon1b-outer" with either EV2 or EV3, while "*Lymnaea- LCa$_v\beta$* -degen" and either T77 or T33 were used for the secondary PCR.

2.1.2 Polymerase Chain Reaction

Polymerase chain reactions (PCRs) were preformed in a volume of 25µL. In preparation for the primary PCR, each reaction component was diluted to the following concentrations in sterile Milli-Q water: 1X Taq Buffer with $(NH_4)_2SO_4$ (Fermentas, #B33), 2.5mM $MgCl_2$, 0.2mM of each deoxyribonucleotide (dATP, dGTP, dCTP, and dTTP; Fermentas #R0192) and 1µM each of the forward and reverse primers (described in section 1.1.1). Next, 0.2µL of cDNA template was added, as was 0.2 units of Taq DNA polymerase (Fermentas, #EP0404). Each fraction of the library was screened and a control with no DNA template

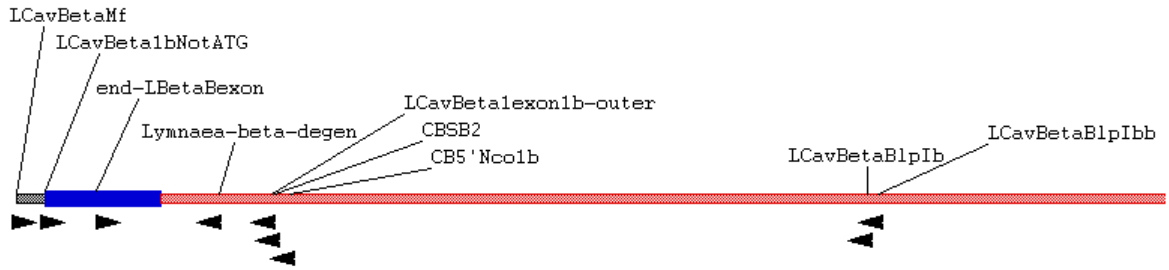

Figure 2.1: Location of primer sites utilized in the cloning and sequencing of LCa_vB_B. Primer sites and directions are indicated by black arrows. Black regions represent 5' UTR sequence, while blue represents the N-terminus and the rest of LCa_vB_B is shown in red.

was prepared for each round of PCR, for a total of 25 reactions. Each reaction was then placed in an Eppendorf AG Mastercycler ep thermocycler (Eppendorf, # 950000015) and heated to 95°C for two minutes to denature the DNA. Next, the reactions underwent 30 cycles of heating to 94°C for one minute, 56°C for 45 seconds then 72°C for four minutes. A final elongation of ten minutes at 72°C was added after the cycling was complete.

For the secondary PCR, the same reaction conditions and cycling parameters were used as described above except that 0.2µL of the primary PCR was added in place of 0.2µL of cDNA library for template. Upon completion of the secondary PCR, results were visualized on an agarose gel.

2.1.3 Agarose Gel Electrophoresis

To visualize PCR products, a 1% agarose gel was made by dissolving 0.7g of agarose in 70mL of boiling Tris-Acetic acid-Ethelenediaminetetraacetic acid (EDTA) buffer (TAE buffer). Before casting, the gel was allowed to cool, and three to five drops of 0.1% ethidium bromide were added. The gel was then cast and a comb was inserted into the molten agarose.

After solidification of the gel, 5µL of 6X loading dye was mixed with the secondary PCR product and loaded into the agarose gel, as was 6µL of GeneRuler 1kb DNA Ladder Plus (Fermentas, #SM1333) to mark the size of any amplified products. Gels were then run at 120V for approximately 30 minutes to allow for separation of the ladder. The gel was

visualized under ultraviolet (UV) light on an AlphaImager HP gel documentation system (Alpha Innotech, # 92-13823-00) and a digital photograph was taken.

2.1.4 PCR Product Purification

Any PCR products visualized on the gel were excised and purified using the QIAquick PCR Purification Kit (QIAGEN, #28104). The protocol was carried out according to the manufacturer's instructions with the following deviations: the DNA-buffer mixture was run through the column twice at 4500 x g, the water used for elution was pre-heated to 65°C, and the eluted fraction was run through the column a second time. To ensure samples were not lost during purification, 5µL of each sample were run on an agarose gel as described in section 2.1.3.

2.1.5 Sequencing of PCR Products

The concentration of purified PCR products was adjusted to approximately 20ng/µL using a NanoDrop ND-1000 Spectrophotometer (NanoDrop Technologies). The samples were then sent for DNA sequencing using the dye-termination method at the University of Waterloo's Molecular Core Facility.

2.2 Cloning of the Novel $LCa_v\beta$ Subunit N-terminus

In order to express the novel $LCa_v\beta$ splice isoforms in mammalian cells, the genes were cloned into a suitable mammalian expression vector. To achieve this task, new, specific primers containing restriction sites were designed and used to amplify the N-terminus of $LCa_v\beta$ from freshly prepared cDNA. These products were then cut with restriction enzymes and ligated into a mammalian expression vector containing the downstream portion of *LCavβ*, known as *LCavβ*-pMT2SX(R).

2.2.1 Primer Design for Cloning the Novel $LCa_v\beta$ N-terminus

In order to clone the novel $LCa_v\beta$ N-terminus, known as $LCa_v\beta_B$, into the full-length $LCa_v\beta$ subunit, new nested primer sets containing restriction sites were ordered from Sigma-Aldrich. To target the N-terminal start site the primers $LCa_v\beta$Mf (outer) and $LCa_v\beta$1bNotATG (inner) were created. The inner primer, $LCa_v\beta$1bNotATG contains a NotI restriction site (5'- GCGGCCGC -3') four base pairs upstream of the start of the open reading frame (ORF) to facilitate cloning. The reverse primers, $LCa_v\beta$BlpIbb (outer) and $LCa_v\beta$BlpIb (inner), were designed to target a region one kilobase (kb) downstream of the start of the ORF and were chosen because they contain a BlpI restriction site (5'-GCTNAGC-3') to be used in later cloning steps. All primer sequences are given in table 2.1.

2.2.2 Reverse Transcription and Polymerase Chain Reaction for Full-length Clone

Total RNA was extracted from *Lymnaea stagnalis* tissue (frozen in liquid nitrogen and ground to a fine powder) using a modified TRIZOL-reagent (Applied Biosystems, #AM9738) protocol carried out by Adriano Senatore. To carry out the reverse transcription and create cDNA, 2µL of BlpIbb primer (1µM) were combined with 1µL of dNTPs (10mM) and 5.5µL of milli-Q water, which was then heated to 65°C for five minutes before adding 4.5µL of total RNA extract. This mixture was incubated at 65°C for an additional five minutes, followed by a five minute incubation on wet ice to denature any secondary structure present in the RNA. Next, the sample tube was briefly centrifuged to collect the sample at the bottom of the tube before adding 4µL of 5X First Strand Buffer (Invitrogen, # 18080-093), 1µL of 100mM Dithiothreitol (DTT), 1µL of RNase Inhibitor, and 200 units of SuperScript III Reverse Transcriptase (Invitrogen, # 18080-093). The total reaction volume of 20µL was then incubated at 54°C for 80 minutes, followed by 15 minute incubation at 70°C. The cDNA was then held at 4°C or frozen at -20°C until used in PCR.

PCRs were performed as described in section 2.1.2, except that 1µL of cDNA was added to the reaction instead of 0.2µL. The primers sets (forward/reverse) employed for the primary and secondary PCRs were $LCa_v\beta$Mf/ $LCa_v\beta$BlpIbb and $LCa_v\beta$1bNotATG/ $LCa_v\beta$BlpIb, respectively. The PCRs (both primary and secondary) were then visualized by loading 5µL on a 1% agarose gel as described in section 2.1.3.

2.2.3 Phenol-Chloroform Extraction and Ethanol Precipitation

Next PCR products were purified by phenol-chloroform extraction. Remaining PCR products were diluted to a final volume of 100µL with milli-Q water and transferred to a 1.5mL tube before one volume (100µL) of phenol-chloroform (1:1 volume ratio) were added. The mixture was vortexed at maximum speed before being centrifuged at 21,130 x g for five minutes. After centrifugation, the aqueous phase was removed and placed in a new 1.5mL tube. This process was repeated until no white precipitate was visible between the aqueous and organic phases. To remove traces of phenol from the aqueous phase, one volume (100µL) of pure chloroform as added. This mixture was vortexed and centrifuged as before and the aqueous phase was then placed in a new tube.

To precipitate the DNA from the aqueous phase, an ethanol precipitation was carried out by adding one tenth volume (10µL) of 3M sodium acetate (pH5.2) and vortexing. Next, two volumes (220µL) of 100% ethanol were added. The tube was mixed by inversion and placed on ice for one hour before being centrifuged at 16,100 x g at 4°C for ten minutes to pellet precipitated DNA. The pellet was washed with 70% ethanol and allowed to air-dry. The air-dried pellet was then resuspended in 47.5µL of milli-Q water that was warmed to 65°C.

2.2.4 Restriction Digestion and Gel Purification

To prepare the N-terminal $LCa_v\beta_B$ PCR fragment and full-length $LCa_v\beta$-pMT2SX(R) for ligation, both were double-digested with the restriction enzymes NotI (New England Biolabs, # R0189S) and BlpI (New England Biolabs, # R0585S) in separate 200µL tubes. Each digest contained the appropriate volume of 10X NEBuffer2 (New England Biolabs, # B7002S) supplemented with Bovine Serum Albumin (BSA; New England Biolabs, # B9001S) to a final concentration of 0.1mg/mL, 4µL of NotI and 2µL of BlpI. The entire purified PCR product was added to one tube for a final volume of 60µL. To the other tube 10µg of $LCa_v\beta$-pMT2SX(R) was added and Milli-Q water was used to reach a final volume of 60µL. Both tubes were incubated at 37°C overnight to ensure complete digestion.

The restriction digest reactions were then visualized on a 1% agarose gel as described in section 2.1.3. In the gel lane containing the N-terminal PCR product digested with NotI and BlpI, the single 1014bp band was excised. In the lane containing $LCa_v\beta$-pMT2SX(R), the 5.4kb band was excised, while the 1kb band was discarded. The excised bands were purified using the Illustra GFX PCR DNA and Gel Band Purification kit (General l Electric Healthcare, # 28-9034-70) according to the manufacturer's instructions with the same exceptions described in section 2.1.4.

2.2.5 Ligation

Following digestion and purification, the PCR fragment (hereafter referred to as the "insert") and the 5.4kb fragment purified from the digest of $LCa_v\beta$-pMT2SX(R) (hereafter referred to

as the "vector") were ligated to form the novel construct $LCa_v\beta_B$-pMT2SX(R) (the previously cloned $LCa_v\beta$ subunit will hereafter be referred to as $LCa_v\beta_A$). Five ligation reactions were preformed in total, each of which contained a different ratio of insert to vector. Each ligation reaction contained 1µL of T4 ligase enzyme (New England Biolabs, #M0202), 1.5µL of 10X T4 ligase buffer (new England Biolabs, #B0202), and 0.5µL of vector. To each of the five tubes 0, 1, 3, 5 or 10µL of insert were added and the final volume was adjusted to 15µL with milli-Q water. The ligation reaction containing no insert served as a negative control for the presence of background colonies. These reactions were incubated overnight at 16°C.

2.2.6 Heat Shock Transformation into DH5α Cells

The ligations were then transformed into bacteria, where the plasmids could be grown-up, purified and screened for the presence of $LCa_v\beta_B$-pMT2SX(R). For transformation, the *Escherchia coli* strain DH5α was chosen because it is capable of transformation by heat shock and grows rapidly. Aliquots of frozen DH5α were thawed on wet ice. In separate pre-chilled 200µL tubes, 100µL of thawed cells were mixed thoroughly with 5µL of each of the ligation reactions, including the negative control, and chilled on wet ice for 20 minutes. The tubes were then heated to 42°C for 90 seconds before rapid chilling on wet ice for an additional two minutes.

The contents of each tube were then transferred to 1mL of Luria Bertani (LB) broth in a 1.5mL tube and incubated at 37°C for 45 minutes while shaking at 450 rpm. Upon completion of the incubation, each tube was centrifuged at 4500 x g to pellet the bacterial

cells. The supernatant was discarded and the cells were resuspended in 50µL of fresh LB broth before being plated on LB agar plates containing 0.1mg/mL ampicillin (EMD Chemicals, #171254). The plates were then inverted and incubated at 37°C overnight. The following morning, plates were inspected for the presence of colonies and two colonies from each plate (including the negative control plate) were used to inoculate 5mL of LB broth containing 0.1mg/mL ampicillin. These cultures were incubated at 37°C for two days while shaking at 450rpm to allow the bacteria to multiply and produce large quantities of plasmid.

2.2.7 **Plasmid Isolation by Alkaline Lysis** (Adapted from Birnboim and Doly, 1979)

In order to isolate the plasmids contained in each bacterial culture sample, a modified alkaline lysis method was employed. The following method describes the isolation procedure for one sample. The entire procedure is carried out in 1.5mL plastic tubes. To the tube, 1.5mL of bacterial culture was decanted and centrifuged at 4500 x g for two minutes to pellet the bacteria. The supernatant was then discarded and if there was not a large pellet (roughly filling the bottom 5mm of the tube), then this process was repeated. The pellet was then resuspended in 150µL of Glucose Tris-EDTA (TE) buffer (50mM glucose, 25mM Tris-HCl, 10mM EDTA, pH8.0). To lyse the cells, 300mL of freshly prepared lysis buffer [1%(w/v) sodium dodecyl sulfate (SDS), 0.2N NaOH) was added and the tube was gently mixed by inversion and placed on ice for up to five minutes before the addition of 225µL of ice-cold potassium acetate solution [3M potassium acetate, 11.45% (w/v) glacial acetic acid] to precipitate the cellular debris and genomic DNA. The mixture was then vortexed for

approximately five seconds or until a cottage cheese-like precipitate was visible. The tube was then centrifuged at maximum speed at 4°C for five to ten minutes (until the cellular debris and genomic DNA had formed a tight pellet against the wall of the tube).

The supernatant was transferred to a fresh tube and 405µL of 2-propanol was added. The tube was mixed by inversion before incubation at -20°C for at least 30 minutes to allow plasmid DNA to precipitate. The tube was then spun in a centrifuge for ten minutes at maximum speed at 4°C to pellet the precipitate. The supernatant was discarded and the pellet was allowed to air dry prior to resuspension in 100µL of TE buffer (10mM Tris-HCl, 1mM EDTA, pH 8.0). RNase A (Sigma, #R4875) was then added to a final concentration of 20µg/mL, and the sample was incubated at 37°C for 15 minutes. To complete the plasmid isolation, phenol-chloroform extraction and ethanol precipitation were preformed as described in section 2.2.3. The plasmid pellet was resuspended in 50µL of warm Milli-Q water. This procedure was repeated for all ten samples.

2.2.8 Screening Clones by Restriction Digestion

In order to determine if isolated plasmids contained the $LCa_v\beta_B$ insert, sequential digestions with the restriction enzymes SalI (New England Biolabs, #R0138) and BlpI were preformed. These enzymes were chosen because BlpI is found inside of $LCa_v\beta_B$, whereas SalI is found in the vector, pMT2SX(R), just upstream of the NotI site used in cloning. Approximately 2µg of each plasmid was combined with 1µL NEBuffer1 supplemented with BSA to a final concentration of 0.1mg/mL, 1µL of SalI and diluted to a final volume of 10µL with Milli-Q

water. These digests were incubated at 37°C for four hours then purified by phenol-chloroform extraction and ethanol precipitation as in section 2.2.3. The DNA pellets were resuspended in 17μL of warm Milli-Q water.

To perform a second digest with BlpI, 2μL of NEBuffer4 and 1μL of BlpI were added to the resuspended DNA. The digest was then incubated another four hours before the results were visualized on a 1% agarose gel as in section 2.1.3.

2.2.9 Sequencing of *LCavβ*$_B$-pMT2SX(R)

Isolated plasmids which gave positive results in the restriction fragment length polymorphism (RFLP) screening were sent for sequencing at Robarts Research Institute at the University of Western Ontario. Plasmids were sequenced in the reverse direction with the primer *LCa*$_v$*β*BlpIb.

2.3 Creation of In Situ Probes for Southern Blotting

It was necessary to clone out small, unique sequences of the untranslated region (UTR) upstream from each *LCa*$_v$*β* subunit isoform into pBluescriptII SK(+), a shuttle vector, so that probes could be created to identify each isoform uniquely. Similar to the methods described in section 2.2, the desired regions were amplified by PCR, then digested with restriction enzymes, ligated into the vector, transformed and screened for the presence of the insert.

2.3.1 Primer Design

Unique sequences of each *LCa$_v$β* subunit isoform were chosen based on their small size and GC content (approximately 50%). Primers were designed to amplify these regions and incorporate 5' KpnI and 3' SacI restriction sites into the fragment to facilitate cloning into pBluescriptII. These restriction sites were chosen since they are the most distal in the multiple cloning site which enables one to amplify the cloned regions using primer sites found in the vector with minimal amplification of vector sequence. The primers (forward/reverse) for *LCa$_v$β*$_A$ and *LCa$_v$β*$_B$ are known as *LCa$_v$β*-aKpnf/ *LCa$_v$β*-aSacb and *LCa$_v$β*-bKpnf/ *LCa$_v$β*-bSacb, respectively. The sequences of the primers can be found in table 2.1.

2.3.2 Polymerase Chain Reaction

Unique N-terminal regions were then amplified by PCR from specific DNA library fractions. For *LCa$_v$β*$_A$, parasitized *Lymnaea* library fraction #11 was used as the template, whereas for *LCa$_v$β*$_B$, *Lymnaea* cerebral ganglion cDNA library fraction C was used. The reactions were carried out as described in section 2.1.2, with the following deviations: the total reaction volume was increased to 50µL, the concentration of $MgCl_2$ was decreased to 1.5mM, the Taq was replaced by 0.25µL of a Taq/Vent polymerase (20:1) mixture (Vent DNA polymerase, New England Biolabs, #M0254), and the extension time during the 72°C cycle was decreased to one minute. Also, each reaction was performed in duplicate. The results were then visualized by loading 5µL of each reaction on a 1% agarose gel as in section 2.1.3.

2.3.3 Restriction Digestion with KpnI and SacI

Prior to restriction digestion, the duplicate PCR reactions were combined and purified by phenol-chloroform extraction and ethanol precipitation as in section 2.2.3. The DNA was resuspended in 47.4µL of Milli-Q water. To the DNA, 6µL of 10X NEBuffer1 was added, as was 3µL each of SacI (New England Biolabs, #R0156) and KpnI (New England Biolabs, #R0146). This mixture was supplemented with 0.6µL of 10mg/mL BSA. To facilitate cloning, 10µg of pBluescriptII SK(+) was also cut with SacI and KpnI in a similar fashion, except that water was added to bring the final volume to 60µL. All digestions were incubated overnight at 37°C. The next day, the pBluescript vector was dephosphorylated by supplementing the digest with 4µL of 10X Antarctic Phosphatase buffer (New England Biolabs, #B0289), 5µL of milli-Q water and 1µL of Antarctic Phosphatase (New England Biolabs, #M0289). This reaction was incubated for 30 minutes at 37°C. Dephosphorylation helps to reduce the occurrence of vector re-circularization.

Results were visualized on a 1% agarose gel as in section 2.1.3. The bands representing the unique N-terminal fragments and the large band of the pBluescript vector were excised from the gel and purified as in section 2.2.4. Concentrations of the purified DNA were measured on the NanoDrop.

2.3.4 Ligation

Ligations were performed by diluting 10X T4 ligase buffer to a final concentration of 1X in the presence of 53.1ng of pBluescript vector and 1μL of T4 ligase. The $LCa_v\beta$ subunit sequences were added in various amounts to give an insert to vector ratio (I:V) of 0 (negative control), 1, 3, 5 and 10, which was calculated using the following formula:

$$ng_{(insert)} = [I:V][ng_{(vector)} x\ kb_{(insert)}]/[kb_{(vector)}]$$

where ng represents mass and kb represents size in kilobases. These ligation reactions were incubated at room temperature for four hours. Ligation reactions were then transformed into DH5α cells and the plasmids were isolated as in sections 2.2.6 and 2.2.7, respectively.

2.3.5 Screening Plasmids by Restriction Fragment Length Polymorphism

Plasmids were screened for the presence of the unique N-terminal inserts by restriction fragment length polymorphism (RFLP). One microgram of each plasmid was cut with 1μL each of KpnI and SacI in the 2μL of NEBuffer2 supplemented with 0.1mg/mL BSA. Water was added to a final volume of 20μL, and digests were incubated at 37°C overnight. Results were analyzed on an agarose gel as in section 2.1.3.

2.3.6 Sequencing

Isolated plasmids which gave positive results in the RFLP screening were sent for sequencing at the Molecular Core Facility at the University of Waterloo. Plasmids were sequenced bi-directionally using the primers T7 and T3 found in pBluescriptII SK(+).

2.3.7 Synthesis of Digoxigenin-labeled DNA Probes by Polymerase Chain Reaction

In order to identify the localization of $LCa_v\beta$ subunits in digested genomic DNA, DNA probes will be labeled with digoxigenin (DIG). The DIG-labeled nucleotides will be incorporated using PCR, and will be compared to a control PCR without DIG-labeled nucleotides. The DIG-labeling should cause a slight shift in band position on an agarose gel, as the DIG-labeled nucleotides are of a higher molecular weight. Both reactions contained the following: 1.125mM $MgCl_2$, 0.5µM each of the forward and reverse primers (as in section 2.3.1) and 0.25µL of Taq DNA polymerase, and 0.25ng of plasmid (either $LCa_v\beta_A$ or $LCa_v\beta_B$ fragments in pBluescript) as template. Also, for both $LCa_v\beta_A$ and $LCa_v\beta_B$, these reactions were carried out in duplicate, except that one contained 0.1mM dNTPs, while the other contained 0.1mM each of dATP, dGTP and dCTP, 85µM dTTP and 15µM DIG-11-dUTP (alkali-liable; Roche, # 11573152910).

Each reaction was then placed in an Eppendorf AG Mastercycler ep thermocycler and cycled as in section 2.3.2. The entire PCR reaction was then loaded on an agarose gel as and

visualized as in section 2.1.3. The bands representing DIG-labeled fragments were excised and purified as in section 2.2.4. The purified, double-stranded, DIG-labeled DNA probes were eluted in 50µL of water and stored at -20°C.

2.4 *Genomic DNA Extraction from Lymnaea stagnalis*

In order to examine the genomic structure of the $LCa_v\beta$ gene, genomic DNA must be freshly extracted from *Lymnaea* tissue in a procedure modified from *van Moorsel et al.* (2000). To prepare for extraction, about five large snails were anesthetized in tank water containing 10% Lysterine mouthwash which was placed on ice for approximately ten minutes or until snails were unresponsive to touch. Each snail was then de-shelled and ground to a fine powder in liquid nitrogen using a mortar and pestle. Ground snail tissue was then placed in 1.5ml plastic tubes and flash frozen in liquid nitrogen before storing at -80°C.

To extract genomic DNA, approximately 3g of ground, frozen tissue was divided roughly equally between two 50mL Falcon tubes containing 40mL TE buffer, 1mL of 10mg/mL Proteinase K (Sigma, #P4850), 2.4mL of 20% SDS and 3.4mL of water. The tubes were mixed gently by inversion and then incubated at 55°C for 15 minutes, then 45°C until the tissue has dissolved (this step may take overnight). After the tissue has dissolved, the tubes were placed on ice for five minutes then 31.2µL of 20mg/mL RNase A was added. The RNase A is then incubated at 37°C overnight. The following morning, an additional 31.2µL of RNase A was added and incubated another one hour.

After the incubation has finished, the contents of each tube were divided between four 45mL falcon tubes and 14.6mL of ice-cold 5M potassium acetate was added to each. The tubes were incubated on ice for 20 minutes prior to spinning at 5250 x g for ten minutes. After centrifugation, the supernatant was then filtered through cheesecloth and divided equally between two 50mL falcon tubes. To precipitate DNA, 15mL of 2-propanol was then added to each tube and they were rocked gently on a shaker overnight at room temperature.

The following morning, precipitated DNA was spooled on a hooked Pasteur pipette and transferred to a new 15mL tube. This tube was centrifuged quickly for 30 seconds and the supernatant was removed with a pipette. The pellet was then washed in 70% ethanol and air dried before resuspension in 5mL of Milli-Q water. To this, 5mL of ice-cold 5M lithium chloride was added and incubated on ice for one hour before centrifugation at 5250 x g for 15 minutes. The supernatant was decanted into a fresh tube and 9µL of 20mg/mL RNase was added and allowed to incubate at 4°C overnight. The next morning, phenol-chloroform extraction and ethanol precipitation were preformed as in section 2.2.3. The genomic DNA pellet was resuspended in 2mL of milli-Q water and 1mL of TE buffer. The concentration of the extracted genomic DNA was measured using the NanoDrop spectrophotometer, and genomic DNA was diluted to an approximate concentration of 1µg/µL.

2.5 Southern Blot Analysis

In an attempt to examine the genomic structure of the *LCa$_v\beta$* gene, Southern blotting was carried out. *Lymnaea* genomic DNA was digested with four restriction enzymes (EcoRV,

HindIII, EcoRI and XhoI), separated on a gel, transferred to a nylon membrane and probed using the double-stranded DIG-labeled DNA probes created previously.

2.5.1 Restriction Digests of Genomic DNA

Approximately 20µg of genomic DNA was digested with each of the four restriction enzymes- EcoRV, HindIII, EcoRI and XhoI. Digests were set up by adding 10µL of the appropriate 10X buffer (NEBuffer3 for EcoRI and EcoRV, NEBuffer2 for HindIII and XhoI; EcoRV and XhoI reactions were supplemented with 0.1mg/mL BSA) to the DNA. Reactions were diluted to 93µL with milli-Q water and 7µL of enzyme was added. These reactions were then incubated overnight at 37°C, followed by heat inactivation of enzymes at 80°C for 20 minutes. After heat inactivation, 16µL of loading dye was added to each digest and samples were decreased in volume by approximately 75% using a DNA dehydrator with no heat. These samples were then run on a 1% agarose gel and visualized as in section 2.1.3.

2.5.2 Transfer to Nylon Membrane

To facilitate transfer of large genomic DNA fragments by capillary action to the nylon membrane, the agarose gel was first soaked in DNA degradation solution (0.5M NaOH, 1.5M NaCl) twice for 15 minutes. The gel was then rinsed well in milli-Q water before soaking twice for 15 minutes in neutralization solution (3M NaCl, 0.5M Tris, pH7.5). The gel was then ready for transfer of the genomic DNA by capillary action.

To achieve this, a square glass pyrex dish was filled halfway with 20X SSC buffer (3M NaCl, 30mM sodium citrate, pH 7.0) and a large platform (an upside down pipette tip box was used here) was placed in the middle of the dish, above the level of the buffer. Next, four pieces of blotting paper (VWR, #28298-020) were cut, each as tall as the height of the gel. Two of these pieces were then cut to match the width of the gel, while the other two were cut so they were 3-4 times as wide as the gel. The wide strips of blotting paper were centered over the platform and bent into the buffer to serve as a wick. On top of these sheets, the denatured and neutralized gel was placed face down. Next, a sheet of positively charged nylon membrane (Roche, #11 417 240 001) which was cut to the same size of the gel was placed directly on top of the gel, followed by the other two sheets of blotting paper. A large stack of paper towels was placed on top of the blotting paper and a weight (two textbooks) was placed on top of the paper towels. This setup was left at room temperature overnight. The following morning, the apparatus was disassembled and the DNA was cross-linked to the nylon membrane by exposure to UV light.

2.5.3 Hybridization of DIG-labeled DNA Probes

A hybridization oven was preheated to 40°C for the Southern blot of $LCa_v\beta_{A+}$, and 37°C for $LCa_v\beta_{B+}$ (these will be referred to as the hybridization temperature). In hybridization tubes, 12mL of EasyHyb solution (Roche, #11 603 558 001) was pre-heated to the hybridization temperature. After pre-heating the EasyHyb solution, it was used to wash the nylon membrane for 30 minutes. During the wash, the DIG-labeled probes were heated to 95°C for

ten minutes, and then rapidly chilled on wet ice for another ten minutes. The entire volume of probe was then diluted in 20mL of EasyHyb solution and filter sterilized through a 0.4μm filter. After the 30 minute incubation, the EasyHyb was decanted and replaced with the diluted DIG-labeled probe solution. The probe was allowed to incubate overnight at the hybridization temperature.

The next morning, the probe solution was decanted and saved for later use. The nylon membrane was then washed twice with 20mL of low stringency buffer [2X SSC, 0.1%(w/v) SDS], first for 15 minutes, then 20 minutes at room temperature. Next, the low stringency buffer was decanted and the membrane was washed twice in 20mL of High Stringency buffer [0.5X SSC, 0.1%(w/v) SDS], for 20 minutes. The first and second high stringency washed were at different temperatures. For $LCav\beta_{A+}$, the membranes were washed at 55°C then 65°C, whereas for $LCav\beta_{B+}$ the membrane was washed at 50°C and 55°C. The high stringency buffer was then decanted and the membrane was washed in 20mL of wash buffer [100mM maleic acid, 150mM NaCl, 0.3%(v/v) Tween-20, pH 7.5] for one minute at room temperature, then blocked for one hour at room temperature with blocking buffer [100mM maleic acid, 150mM NaCl, 1%(w/v) blocking reagent (Roche, #11 096 176 001)].

During blocking, 1.5μL of sheep anti-DIG antibody conjugated to alkaline phosphatase (Invitrogen, # G-21079) was diluted in 7.5mL of detection buffer (0.1M Tris, 0.1M NaCl, pH 9.5) to give a 1:5000 dilution. Upon completion of blocking, the blocking buffer was decanted and the diluted antibody solution was added. The antibody was allowed to incubate for 30 minutes at room temperature before it was removed.

Following incubation with the enzyme-conjugated antibody, the nylon membrane was placed on a shaker and washed twice in 80mL of wash buffer for 15 minutes at room temperature. The membrane was then washed in detection buffer for two minutes. During the washes a colour substrate solution was prepared by combining 10mL of detection buffer, 45µL of 4-Nitro blue tetrazolium chloride (NBT; Roche, #11 383 213 001) and 35µL of 5-bromo-4-chloro-3-indolyl-phosphate (BCIP; Roche, #11 383 221 001). After washing with the detection buffer, it was decanted and replaced with colour substrate solution. The membrane was allowed to incubate in colour substrate solution overnight in the dark (no shaking). The next morning, the colour substrate solution was decanted and the blot was briefly washed in Milli-Q water. A digital image was then taken of the blot using a desktop scanner.

2.6 Determination of Genomic Structure of LCa$_v$β Subunit N-terminus

In order to better characterize the structure of the genomic region which surrounds the N-terminus of *LCa$_v$β*, PCR was performed on a genomic DNA template. This product was then isolated, cloned and sequenced.

2.6.1 Primer Design and Polymerase Chain Reaction

In order to amplify possible introns which could exist downstream of the *LCa$_v$β$_B$* N-terminus by PCR, primers were designed to complement the distal portion of the N-terminus of

LCa$_v\beta_B$ (end-*LBeta*Bexon) and the proximal portion of the SH3 domain (CBSB2 and CB5'Nco1b). The sequence of these primers is listed in table 2.1.

In order to facilitate the amplification of a genomic region of unknown size, nested PCR was preformed with the Expand Long Template PCR System (Roche, #11 681 834 001). Each 50uL reaction contained the following components 350uM of each dNTP, 300nM forward primer (end-LBetaBexon), 600nM reverse primer (CB5'Nco1b for primary PCR; CBSB2 for secondary PCR), 1X Expand Buffer 2, and 0.2uL Expand Long Template enzyme mix. Template for the primary PCR was 200ng of genmic DNA, while for the secondary PCR 1uL of the primary reaction was added. A negative control reaction containing no template was also included. Each reaction was then placed in an Eppendorf AG Mastercycler ep thermocycler and heated to 94°C for two minutes to denature the DNA. Next, the reactions underwent 30 cycles of heating to 94°C for 15 seconds, 56°C for 30 seconds then 68°C for five minutes. From cycles 11 to 30, an additional 20 seconds was added to the elongation with each successive cycle. A final elongation of seven minutes at 68°C was added after the cycling was complete.

2.6.2 Cloning of the *LCa$_v\beta$* Genomic Fragment

Cloning of the *LCa$_v\beta$* genomic fragment was carried out using the TOPO XL PCR Cloning Kit (Invitrogen, K4750-10). All steps up to (but not including) transformation were carried out according to the manufacturer's instructions with no deviation in procedure.

2.6.3 Transformation

Following TOPO cloning, plasmids were transformed into CopyCutter EPI400 Electrocompetent *E.coli* cells (Epicentre Biotechnologies, #C400CH10). The CopyCutter cells were chosen for use because they are more efficient for cloning unstable DNA fragments since they maintain a low copy number until just prior to plasmid isolation. This is accomplished by the addition of CopyCutter Induction Solution just prior to plasmid isolation, which subsequently raises the copy number of the transfected plasmid (see below for more detail).

CopyCutter cells (50uL) were thawed on ice, before adding 1uL of the TOPO ligation reaction and mixing vigorously. The cell-plasmid mixture was then transferred to a sterile, pre-chilled 1mm Electroporation cuvette (VWR, #89047-206) and electroporated at 1200mV for 5ms using an Eppendorf 2510 electroporator. Cells were then immediately transferred to 1mL LB medium and incubated in a 15mL tube at 37°C with shaking at 220rpm for one hour, before plating on LB agar plates containing 50µg/mL Kanamycin (OmniPur, #5880). Plates were then inverted and incubated overnight at 37°C. The following morning 12 colonies were used to inoculate 12 tubes each containing 5mL of LB media supplemented with 50µg/mL of Kanamycin in a 60mL test tube and incubated overnight at 37°C while shaking at 350rpm. The following morning, overnight cultures were diluted to a final OD of 0.2 in LB with Kanamycin and CopyCutter Induction Solution (diluted to 1X concentration) and then incubated for four hours at 37°C while shaking at 500rpm. Plasmids were then isolated by alkaline lysis as in section 2.2.7.

2.6.4 Screening of Plasmids by Restriction Digestion

Isolated plasmids were screened for the presence of the *LCa$_v\beta$* genomic fragment by digestion with the enzyme EcoRI, whose restriction sites bound the multiple cloning site of the TOPO cloning vector. One µg of plasmid was digested in EcoRI Buffer (diluted to 1X) and 0.5µL of EcoRI in a final volume of 10µL for four hours at 37°C. Results of the digest were then visualized on a 1% agarose gel as in section 2.1.3. Plasmids which appeared to contain the correct digestion pattern were sent for sequencing at Robarts Research Institute at the University of Western Ontario. Plasmids were sequenced in the reverse direction with the primer CBSB2 and an intron specific primer LBetaNdeI.

2.6.5 Creation of Amino Acid Alignments and Phylogenetic Tree

All amino acid alignments were created using ClustalW2 and data was exported and formatted using Excel 2007 (Microsoft Corporation). Alignments were then imported into PAUP 4.0 to generate a consensus gene tree using the Branch-and-Bound algorithm. The gene tree was tested for robustness in 100 bootstraps and displayed in TREEVIEW 1.6.6. GenBank Accession numbers of all sequences used can be found in table 2.2.

Table 2.2: GenBank accession numbers of sequences used in amino acid alignments.

Type	Subtype	Organism	GenBank Accession #	Reference
B	β_A	*Amphioxus*	EEN54426	Putnam et al., 2008
		Aplysia californica	EB291128	Moroz et al., 2006
		Lymnaea stagnalis	AF484087	Spafford et al., 2003
		Loligo bleekeri	AB069676	Kimura and Kubo, 2003
	β_B	*Aplysia californica*	EB255159	Moroz et al., 2006
		Musca domestica	X78561	Grabner et al., 1994
		Loligo bleekeri	AB069677	Kimura and Kubo, 2003
β_1	β_{1a}	*Homo sapiens*	AAA35631	Powers et al., 1992
	β_{1b}	*Homo sapiens*	AAA35633	Powers et al., 1992
	β_{1c}	*Danio rerio*	ABB05051	Zhou et al., 2006
β_2	$\beta_{2.1}$	*Danio rerio*	ABY19301	Ebert et al., 2008
	β_{2a}	*Homo sapiens*	AF423189	Colecraft et al., 2002
	β_{2b}	*Homo sapiens*	AF285239	Colecraft et al., 2002
		Danio rerio	DQ372945	Zhou et al., 2008
	β_{2c}	*Homo sapiens*	AF423190	Colecraft et al., 2002
	β_{2cN1}	*Homo sapiens*	AY393860	Foell et al., 2004
	β_{2d}	*Homo sapiens*	AF423191	Colecraft et al., 2002
	β_{2e}	*Homo sapiens*	AF423192	Colecraft et al., 2002
β_3		*Homo sapiens*	AY054985	Helton and Horne, 2002
	β_{3a}	*Danio rerio*	ABD34796	Zhou et al., 2008
	β_{3b}	*Danio rerio*	ABD34797	Zhou et al., 2008
β_4	β_{4a}	*Homo sapiens*	AY054985	Helton and Horne, 2002
		Danio rerio	ABD34798	Zhou et al., 2008
	β_{4b}	*Homo sapiens*	AAB53333	Taviaux et al., 1997
		Danio rerio	ABD34799	Zhou et al., 2008

2.7 Mammalian Cell Culture

In order to assess the functional effects of $LCa_v\beta_{A+}$, $LCa_v\beta_{B+}$ and $LCa_v\beta_{B-}$, it was necessary to express these proteins, in conjunction with LCa_v1 or LCa_v2 and $\alpha_2\delta$ subunits, in a heterologous expression system. Two cell lines were chosen for this purpose: Human Embryonic Kidney (HEK) 293T cells, and GripTite 293 MSR cells (Invitrogen, #R795-07). General electrophysiological and biophysical characteristics were studied using the HEK 293T cells, while the GripTite 293 MSR cells were used in the fluorescent antibody-labeling experiments. The MSR cell line is a HEK derivative but can better withstand multiple wash

steps due to its superior adhesion to substrates. It should be noted that all manipulations involving living mammalian cells were preformed in a sterile biosafety cabinet.

2.7.1 Complete Growth Media

Both HEK and MSR cells were cultured in Dulbecco's Modified Eagle's Medium (DMEM; Sigma, #D5796) supplemented with 10% Fetal Bovine Serum (FBS; Sigma, #F1051) that had been heat-inactivated at 56°C for 30 minutes and 2.5mL of Penicillin-Streptomycin solution (5000 units of penicillin and 5mg streptomycin/mL; Sigma, #P4458). The complete HEK media (500mL) was further supplemented with 5mL of 100mM sodium pyruvate (Sigma, #S8636), while the complete MSR media was supplemented with 5mL of MEM Non-essential amino acids (Gibco, #11140). In all instances complete culture media was heated to 37°C in a water bath before use.

2.7.2 Thawing Cells

Aliquots of low-passage cells had been frozen in liquid nitrogen for long-term storage. To thaw the cells (procedure for both cell lines is the same, except where noted), one tube was removed from liquid nitrogen and rapidly thawed in a 37°C waterbath. During thawing, empty 50mL ($25cm^2$) cell culture flasks were filled with 6mL of complete media. For HEK cells, two flasks were used; while three flasks were used for the MSR cells. When the frozen cells have thawed completely, the aliquot was divided evenly among the flasks and incubated

overnight at 37°C in a humidified 5% CO_2 environment (these will be referred to as standard conditions). The next morning, cells were washed with fresh media and, for the MSR cells, 72µL of 50mg/mL Gentecin (Gibco, #1070) was added to each flask. Cells were incubated under standard conditions until a confluency of 80-90% was reached, then the cells were subcultured.

2.7.3 Subculturing Cells

To subculture cells, the media was removed from the flask and cells were washed twice with phosphate buffered saline (PBS; 6.70mM KCl, 3.67mM KH_2PO_4, 10.82mM Na_2HPO_4-$7H_2O$, 342mM NaCl) that had been pre-warmed to 37°C. To detach cells, 1mL of 0.25% Trypsin-EDTA (Sigma, #T4049) that had been heated to 37°C was added to the flask. The flask was then incubated at 37°C until the majority of cells had detached (to a maximum of five minutes). In the meantime, two new flasks were filled with 5.5mL of fresh complete media (these will be used for the next passage). Also, flasks of cells for transfection were filled with 5mL of fresh complete media. If MSR cells were being subcultured, 72µL of Gentecin was added to each flask. Once the cells were detached, 5mL of fresh complete culture media was added and the cells were resuspended by pipetting up and down several times. The resuspended cells were then divided among the flasks so that each flask had a final volume of 6mL, therefore the flasks to be used in the next passage were split 1:12, while the flasks to be transfected were split 1:6. These cells were then incubated under standard conditions. Cells were allowed to grow to 40-50% confluency prior to transfection. For all transfections (in

both cell lines), *LCa$_v$1* or *LCa$_v$2* were transfected with $\alpha_2\delta$, and either *LCa$_v\beta_{A+}$*, *LCa$_v\beta_{B+}$*, *LCa$_v\beta_{B-}$* or no *LCa$_v\beta$* subunit.

2.7.4 Transient Transfection of Human Embryonic Kidney Cells using Calcium Phosphate

Transfection of HEK 293T cells was done using a calcium phosphate transfection protocol that was carried out by diluting 4µg of each plasmid to be transfected in 30µL of 2.5M $CaCl_2$ and sterile milli-Q water to 300µL. This was then added dropwise to 300µL of 2X HES buffer (280mM NaCl, 50mM Hepes, 1.5mM Na_2HPO_4-$7H_2O$, pH 7.0). The mixture was then mixed well and allowed to incubate at room temperature for 20 minutes to allow for the formation of calcium phosphate crystals.

During the incubation, media was removed from the flask to be transfected and replaced with 5.4mL of fresh complete medium. After incubation, the calcium phosphate solution was added dropwise into the flask of cells. The flask was then incubated under standard conditions for eight to 16 hours. After eight to16 hours, the cells were washed twice with PBS pre-heated to 37°C and 6mL of fresh complete medium was added. These cells were then incubated at 28°C in a humidified 5% CO_2 atmosphere for two days before plating onto glass coverslips (see section 2.6.7).

2.7.5 Transient Transfection of Human Embryonic Kidney Cells using Lipofectamine

Due to lower transfection efficiencies, MSR cells were transfected using Lipofectamine 2000 Reagent (Invitrogen, #11668-019). Transfection with Lipofectamine was achieved by diluting 6.67µg of each plasmid to be transfected in 625µL of DMEM. In a separate tube, 25µL of Lipofectamine was diluted with 625µL of DMEM. These tubes were then incubated at room temperature for five minutes before combining them, mixing well and incubating an additional 20 minutes.

During the incubation, the media was removed from flasks to be transfected, and replaced with 6mL of DMEM supplemented with FBS and non-essential amino acids (same concentrations as complete medium). After the completion of the incubation, the transfection solution was added to the flask which was incubated under standard conditions for six hours. After six hours, the transfection media was removed and replaced with 6mL of complete media. These cells were then incubated at 28°C in a humidified 5% CO_2 atmosphere for two days prior to plating (see section 2.6.7).

2.7.6 Poly-L-Lysine Coating of Coverslips

Prior to plating cells, sterile, round glass coverslips (Fisher Scientific, #12-545-80) were coated in poly-L-lysine. The coverslips were spread out in a single layer at the bottom of a large (100mm diameter) culture dish. A dilute poly-L-lysine solution was made by diluting 1.5mL of 0.1%(w/v) poly-L-lysine (Sigma, #P8920) in 13.5mL of milli-Q water. This

solution was poured over the coverslips and they were allowed to incubate at room temperature for one hour. After one hour, the poly-L-lysine solution was removed and coverslips were washed twice in 15mL of sterile water and then dried in a 56°C oven for two hours. After coating, coverslips were stored at 4°C for up to two weeks.

2.7.7 Plating Cells Onto Coverslips

Two days after transfection, both HEK and MSR cells were plated onto glass coverslips using the same method. Media was removed from the flask and the transfected cells were washed twice with PBS before the addition of 1mL of trypsin, as in section 2.6.3. The cells were resuspended in 6mL of complete media and added to 60mm culture dishes containing the appropriate amount of complete media and four to six coverslips so as to give a split ratio of 1:3 and 1:4 for cells to be used in patch clamp experiments (HEK cells) and 1:6 for cells to be used for antibody staining (MSR cells). These dishes were then incubated at standard conditions for three to four hours before they were moved to 28°C in a humidified 5% CO_2 atmosphere.

2.8 Western Blotting

In order to verify that the $LCa_v\beta$ subunit proteins are being expressed by the HEK cell line, qualitative Western blotting was carried out five days after transfection. The rabbit anti-$LCa_v\beta$ antibody to be used was made by David Spafford and recognizes the epitope

SLDEEKEALRRET, which is downstream of the N-terminus and is common to both $LCa_v\beta$ isoforms.

2.8.1 Human Embryonic Kidney Cell Lysis

Five days post-transfection, media was removed from the flask of transfected cells as well as a flask that had been mock transfected (no DNA present) and then the cells were washed twice with 2mL of PBS that had been warmed to 37°C. After washing, cells were resuspended in 250µL of warm PBS. HEK cells were then lysed by adding 250µL of 2X sample lysis buffer [80mM Tris (pH 6.8), 100mM DTT, 2%(w/v) SDS, 0.006%(w/v) bromophenyl blue, 15%(v/v) glycerol] that had been preheated to 95°C. Lysate was then incubated at 95°C for five minutes before loading on a gel.

2.8.2 SDS-Polyacrylamide Gel Electrophoresis

To separate proteins for Western blotting, proteins contained in the HEK cell lysate were separated by SDS- Polyacrylamide Gel Electrophoresis (SDS-PAGE). Proteins were run on two 5% acrylamide (resolving) gels- one of which will be used for blotting, while the other will be Coomassie stained. The resolving gels were made by adding 2.50mL of 30% acrylamide stock, 3.80mL resolving buffer [1.5M Tris (pH 8.8), 0.40% SDS(w/v)], 115µL of 10%(w/v) ammonium persulfate, 7.50µL of TEMED and milli-Q water to 15.00mL. The resolving gel was poured between glass plates separated by a 1mm gap, topped off with

milli-Q water and allowed to polymerize. During polymerization the stacking gel was prepared by adding 1.28mL of 30% acrylamide stock, 1.88mL stacking buffer [0.5M Tris (pH 6.8), 0.40% SDS(w/v)], 80µL of 10%(w/v) ammonium persulfate, 7.50µL of TEMED and milli-Q water to 7.50mL. After the resolving gel had polymerized, the water was removed and the stacking gel was poured on top of the resolving gel, a comb (to make wells) was inserted and the gel was allowed to polymerize.

Once the gels were polymerized, they were submerged in running buffer [25mM Tris, 19.2mM glycine, 1%(w/v) SDS] and the comb was removed. Next, 30µL of HEK cell lysate was loaded onto the gel as was 10µL of PageRuler Prestained Protein Ladder Plus (Fermentas, #SM1811) and the gel was run at 85V until proteins were appropriately separated. One gel was stained with Coomassie stain [0.1%(w/v) Coomassie Blue R-250, 50%(v/v) methanol, 10%(v/v) acetic acid] and then de-stained with de-staining solution [8%(v/v) acetic acid, 12%(v/v) ethanol]. Digital images of the stained gel were taken using a desktop scanner.

2.8.3 Transfer of Proteins to Nitrocellulose

Once the total protein was appropriately separated by SDS-PAGE, the contents of the gels were transferred to a nitrocellulose membrane. A glass pyrex dish was half-filled with transfer buffer [36.64mM glycine, 47.88mM Tris, 0.037%(w/v) SDS, 20%(v/v) methanol, pH 8.3] and the gel was sandwiched between pads, and membranes in the following order (starting from the side that will face the negative electrode): pad, blotting paper (cut to fit gel

size), gel, 0.45μM nitrocellulose membrane (cut to fit gel size; Mandel, # W-10401196), blotting paper and another pad. The "sandwiches" were submerged in transfer buffer and the air bubbles were removed. The transfer apparatus (with an ice pack and stir bar), was then loaded with the "sandwiches" such that the nitrocellulose is between the gel and the positive electrode. The rig was then filled with transfer buffer and allowed to run overnight at 90mA (at 30V) while stirring. The following morning, the nitrocellulose membrane was temporarily stained with Ponceau stain to confirm that protein transfer has occurred and then de-stained with water.

2.8.4 Membrane Blocking and Antibody Hybridization

Before applying antibody, the nitrocellulose membrane must be blocked to reduce non-specific interactions. Blocking buffer [10mM Tris, 100mM NaCl, 0.1% Tween-20(v/v), 5%(w/v) skim milk powder] was added to the membrane in a shallow dish (enough to completely cover the nitrocellulose), placed on a shaker and allowed to incubate at room temperature for two hours.

After blocking, the membrane was washed five times with Tween-Tris-Buffered Saline [TTBS; 10mM Tris, 100mM NaCl, 0.1% Tween-20(v/v)] for five minutes at room temperature. Next, the primary antibody (rabbit anti-$LCa_v\beta$) was diluted 1:2000 in blocking buffer and poured over the membrane after the last wash with TTBS. The primary antibody was incubated with the membrane overnight at 4°C. The following morning, the antibody was removed and the membrane was washed five times in TTBS for five minutes at room

temperature, and then once in blocking buffer for 15 minutes at room temperature. After the second block, the secondary antibody (Goat anti-rabbit IgG coupled to horseradish peroxidase; Invitrogen, #65-6120) was diluted 1:5000 in blocking buffer and added to the dish containing the membrane. The secondary antibody was incubated with the membrane for 30 minutes at room temperature before it was decanted. The membrane was then washed five times in TTBS for five minutes at room temperature. The membrane was then ready for chemiluminescent staining to detect the presence of $LCa_v\beta$ subunits.

2.8.5 Antigen Detection

$LCa_v\beta$ subunits were detected using the chemiluminescent stain ECL which was made by combining 20mL of freshly prepared solution one (2.5mM luminol, 396µM p-coumaric acid, 100mM Tris, pH8.5) and 20mL of freshly prepared solution two (100mM Tris, 12µL of 30% H_2O_2, pH 8.5). Solutions one and two were combined, poured over the membrane and incubated for one minute at room temperature. The blots were then exposed to x-ray film (Kodak, #819 4540) for one minute in a darkroom before development using an automated developer. Films were then compared to nitrocellulose membranes and the ladder was marked onto the film by hand.

2.9 Creation of EGFP-labeled Channels

In order to visualize the subcellular localization of *LCa_v1* and *LCa_v2*, both channels were fused with an EGFP molecule at the N-terminus. This was accomplished by cloning the channel into the vector pEGFP-C1 which encodes EGFP in reading frame with the insert (*LCa_v1* and *LCa_v2* in this instance) with no intervening stop codons. Described below is the procedure for the construction of *LCa_v1-pEGFP-C1*. *LCa_v2-pEGFP-C1* was constructed in the same manner by Adriano Senatore.

2.9.1 Restriction Digestions

In order to obtain the necessary coding sequence of *LCa_v1* for cloning, the plasmid *LCa_v1-pIRES* was digested with the restriction emzymes XhoI and XmaI (New England Biolabs, #RO180S) as was the p-EGFP-C1 vector. These enzymes are chosen because they bound the *LCa_v1* sequence in pIRES, and are present in the multiple cloning site of pEGFP-C1 (XhoI at the N-terminus; XmaI at the C-terminus). Approximately 10µg of each plasmid were diluted in 1X NEBuffer 4 supplemented with 0.1mg/mL BSA and 2.5µL each of XhoI and XmaI. The volume of both digests was 50µL and they were incubated at 37˚C overnight. The following morning, the digested pEGFP-C1 vector was dephosphorylated by supplementing the digest with 6µL of 10X Antarctic Phosphatase buffer, 2µL of milli-Q water and 2µL of Antarctic Phosphatase (New England Biolabs, #M0289). This reaction was incubated for 30 minutes at 37°C. Following dephosphorylation of the vector, both the vector and the digested

LCa$_v$1-pIRES were run on a 1% agarose gel as in section 2.1.3. The bands representing the vector (5.3kb) and *LCa$_v$1* (6.6kb) were excised and purified as in section 2.2.4.

2.9.2 Ligation and Transformation into ElectroMAX Stbl4 Cells

Ligations were carried out as described in section 2.3.4 with 50ng of pEGFP-C1 vector and insert to vector ratios (I:V) of 1:3, 1 and 3 and 0 (a negative control). The following day, ligation reactions were purified by phenol-chloroform extraction and ethanol precipitation as in section 2.2.3 and resuspended in 10µL of Milli-Q water. Due to the large size of the *LCa$_v$1-pEGFP* construct (11.9kb), plasmids were transformed by electroporation into ElectroMAX Stbl4 Competent Cells (Invitrogen, #11635-018). This was carried out by combining 2.5µL of purified ligation and 20µL of thawed cells in a 1mm electroporation cuvette and applying a 1200mV pulse for 5ms using an Eppendorf 2510 electroporator. Immediately following the application of the voltage pulse cells were added to 1mL of LB media and incubated at 37˚C while shaking at 450 rpm for 90 minutes before plating on LB agar supplemented with 50µg/mL Kanamycin. Plates were incubated at 37˚C for two days. Colonies from each ligation plate were used to inoculate 5mL of LB media supplemented with 50µg/mL Kanamycin and incubated at 37˚C for two days while shaking at 350rpm before plasmids were isolated as in section 2.2.7. In order to confirm the construct is indeed *LCa$_v$1*-pEGFP-C1, approximately 2ug of plasmid was digested with BamHI. Digests were 10µL in volume, and contained 1X NEBuffer 3 supplemented with 0.1mg/mL BSA and 1µL

BamHI. After overnight incubation at 37˚C overnight, digests were run on a 1% agarose gel as in section 2.1.3.

2.10 Antibody Staining of $LCa_v\beta$

Three days after plating, each coverslip of transfected MSR cells was transferred into its own well in a 24-well cell culture plate and washed twice with PBS that had been warmed to 37°C. Cells were then fixed in freshly prepared 1% paraformaldehyde (diluted in PBS) for eight hours at 4°C. After fixation, coverslips were washed twice with PBS, and then permeabilized with 1% Triton X-100 (in PBS) for ten minutes at room temperature. Cells were then washed in TBS twice, once for 15 minutes at room temperature and once overnight at 4˚C before being blocked for three hours at 4°C in TBS (10mM Tris, 100mM NaCl, pH 7.4) supplemented with 1%(w/v) BSA and 0.1%(v/v) Triton X-100. During blocking, rabbit anti-$LCa_v\beta$ antibody was diluted 1:4000 in TBS supplemented with 0.1%(w/v) BSA and 0.1% Triton X-100. After blocking the antibody was applied to the coverslips and allowed to incubate overnight at 4°C on a shaker.

The next morning, the primary antibody was removed and coverslips were washed ten times in TBS supplemented with 0.1%(w/v) BSA and 0.1% Triton X-100. Following the washes, the secondary antibody (Goat anti-rabbit IgG antibody coupled to AlexaFluor 594; Invitrogen, #11072) was diluted 1:800 in TBS supplemented with 0.1%(w/v) BSA and 0.1% Triton X-100 and applied to the coverslips for 45 minutes at room temperature. After incubation with the secondary antibody, cells were washed ten times in TBS and then

mounted on glass microscope slides using 15µL of FluorSave Reagent (Clabiochem, #345789) to help reduce fading of fluorescence. Slides were then imaged on a Zeiss Observer.Z1 fluorescent microscope with a 63X oil objective lens and digital images were taken of ten to 12 cells. Brightness and contrast were adjusted using Photoshop C2 version 9.0.2 (Adobe).

2.11 Electrophysiological Analysis of $LCa_v\beta_{A+}$, $LCa_v\beta_{B+}$ and $LCa_v\beta_{B-}$

The biophysical properties of *LCa_v1* and *LCa_v2* were assessed when co-expressed with $\alpha_2\delta$ and either *$LCa_v\beta_{A+}$*, *$LCa_v\beta_{B+}$*, *$LCa_v\beta_{B-}$* or no *$LCa_v\beta$* subunit using whole-cell patch clamp recording. Cells were recorded three to seven days after plating onto coverslips using an Axopatch 200B amplifier and Clampex 10.2 software (Axon Instruments). Calcium channel currents were measured in a 20mM Ba^{2+} external bath solution (Jarvis and Zamponi, 2001; 20mM $BaCl_2$, 40mM tetramethylammonium chloride, 10mM glucose, 64mM CsCl, pH7.2) and patch pipettes were filled with internal solution (Jarvis and Zamponi, 2001; 108mM cesium methane sulfonate, 4mM $MgCl_2$, 9mM Hepes, 9mM ethylene glycol tetraacetic acid, pH 7.2). During all recording sessions, cells were maintained at a holding potential of -100mV. Prior to recording, a test step to peak current (10mV for *LCa_v1* or 30mV for *LCa_v2*) was preformed to indicate if the cell was producing a current and if the state of the patch was suitable for gathering data.

2.11.1 Current-Voltage Relationship and Steady-State Inactivation Analysis

The current-voltage (IV) relationship was assessed by stepping cells from -100mV to -50mV for 450ms and then increasing the voltage step by 10mV in successive sweeps until reaching a potential of 50mV. To analyze the effect of $LCa_v\beta$ subunits on the steady-state inactivation of the channels cells were stepped from -100mV to peak voltage for 150ms, then allowed to recover for 1s before being held at -100mV until all channels had reached inactivation (this conditioning step may take up to 15 seconds) then immediately stepping to peak again for 150ms. In successive sweeps, the conditioning potential used to inactivate channels was increased by 10mV each time until reaching 30mV.

2.12 Analysis of Electrophysiology Data

For all recordings, leak subtraction was preformed offline and data was filtered using a 500Hz Gaussian filter using Clampfit 10.2 software (Axon Instruments) before further analysis.

2.12.1 Activation and IV Curves

To create activation and IV plots, data was imported into Excel (Microsoft Corp.) where the current (I; in pA) at each voltage step was normalized to peak current (I_{max}; in pA) for that cell. Each normalized IV relationship was plotted and the individual reversal potentials (E_{rev}; in mV) were determined by calculating the y-intercept of the linear portion of the IV curve

(+20 to +40 for *LCa$_v$1*; +30 to +50 for *LCa$_v$2*). The reversal potential represents the membrane potential at which the driving force for Ca^{2+} (or Ba^{2+}) influx is equal to the driving force for Ca^{2+} (or Ba^{2+}) efflux and there is no net movement of Ca^{2+} (or Ba^{2+}) through the VGCCs. The conductance (rate of ions flowing through the channel) was then determined for each voltage step using the equation below (equation 1):

$$G= (I/I_{max})/(V-E_{rev})$$

where G represents conductance (pS) of the channel and V represents the test voltage (mV). For each trace maximum conductance (G_{max}) was then determined. The mean and standard error of the mean (SEM) were calculated for (I/I_{max}), E_{rev} and G_{max}.

Activation plots were created using Origin 8 software (as were all plots; OriginLab) by importing IV data and then performing a Boltzmann transformation using the equation below (equation2):

$$\text{Activation} = I/(V-E_{rev})$$

The Boltzmann-transformed data was then normalized and the a scatter of normalized activation versus voltage was created and curve fit with the following Boltzmann equation (equation 3):

$$\text{Activation}= (G/G_{max})= (A_1-A_2)/(1+e^{((V-V_{0.5})/K_a)})$$

where $V_{0.5}$ and K_a represent the half-activation voltage and slope factor of the activation curves, respectively. The half-activation potential is the voltage at which 50% of the maximal number of channels are open. The slope factor of the activation curve is a value that represents the delay of channels transitioning from the closed to active (open) position. These values were determined by the Origin software. A_1 and A_2 equal one and zero,

respectively, and correspond to maximum and minimum values allowed in the curve fit. The normalized activation data [(I/I_{max}), $V_{0.5}$, K_a] was then averaged and the SEM was determined. The mean data was then plotted and a curve was simualted using these parameters and equation 3.

IV plots were created by plotting voltage against mean (I/I_{max})±SEM and then fitting with an Ohmic-Boltzmann curve using the following equation (equation 4):

$$(I/I_{max})=G_{max}(V-E_{rev})(A_2 + (A_1-A_2)/(1 + e^{((V-V_{0.5})/K_a)}))$$

2.12.2 Steady-State Inactivation Curves

Steady-state inactivation values were determined by dividing the current after the inactivating (conditioning) pulse by the current prior to the inactivating pulse. Each data set was then imported into Origin and curve fit with the Boltzmann equation (equation 5):

$$(I/I_{max})= (A_1-A_2)/(1+e^{((V-V_{0.5})/K_i)})$$

where $V_{0.5}$ and K_i represent the half-inactivation voltage and the slope factor of inactivation, respectively. The half-inactivation potential is the voltage at which 50% of the channels are available and the other 50% of channels have transitioned from the open to the inactivated state. A_1 and A_2 are parameters that represent the maximum and minimum and are equal to one and zero, respectively. The values of $V_{0.5}$ and K_i (determined by Origin) and (I/I_{max}) were then averaged and the standard error of each mean was calculated. The mean steady-state activation data was then plotted ± SEM and this data was used to simulate a Boltzmann curve derived from the parameters determined above.

2.12.3 Gating Kinetics

All kinetic analysis was performed using Clampfit 10.0 software and plotted using Origin 8. Due to the much slower kinetics of *LCa$_v$1* channels, time-dependent methods were used in the kinetic analysis, where as statistical methods were used in the kinetic analysis of *LCa$_v$2*.

For *LCa$_v$1*, time to peak after the start of the depolarization was determined as a measure of activation kinetics which describes the latency in opening of channels in whole-cell currents. The total population of channels is likely to show some delay between depolarization and activation as the α_1 subunit undergoes conformational changes. In order to compare the relative inactivation of each *LCa$_v$1* dataset the fraction of current remaining 350ms after peak (R_{350}) was determined. Larger R_{350} values correspond to a channel which has slowed inactivation kinetics, since there is relatively larger fraction of the current remaining at a given time. Conversely, channels which display rapid inactivation will have low R_{350} values. Slowed inactivation kinetics can lead to channels being open for longer durations and therefore allow more ions through the pore.

Tau values for activation and inactivation were used to compare the kinetics of *LCa$_v$2* channels. To find the tau values, the portion of the curve from the start of the inward current to peak, or from peak until the channels had inactivated, was isolated for analysis of activation or inactivation kinetics, respectively. These segments were then curve fit with a monoexponential equation for activation and a biexponential equation for inactivation using pClamp 10.0 software. The tau value represents the point at which two thirds of the

exponential curve (that was fit) has decayed. Therefore, higher values for the tau of activation represent whole-cell currents that reach peak from a closed state more rapidly than those with lower values; slower transition of the total population of cells from an activated state to an inactivated state will lead to increasing the tau of inactivation. The second tau value for inactivation was chosen for analysis as this represents the fast component of inactivation, which occurs in the first 100ms or so after peak is reached. Mean tau values ± SEM were then plotted in Origin 8.

2.12.4 Statistical Analysis

All data derived from patch clamp recording was statistically analyzed using one-way analysis of variation (ANOVA) tests freely available online at <http://www.danielsoper.com/statcalc/calc43.aspx> (Cohen *et al.*, 2003; Ferguson and Takane, 2005). Statistical significance was determined by *p*-values less than 0.05 (one symbol) or 0.005 (two symbols).

Chapter 3
Results

Alternative splicing has been reported for all $Ca_v\beta$ subunits and their splicing appears to be conserved in the N-terminus and HOOK domain when invertebrates (mollusks and squid), fish and mammals are compared. As seen in figure 3.1, the amino acid sequence similarity between invertebrate *Cavβ* subunits and all four mammalian $Ca_v\beta$ subunit genes is very low in the N-terminus and HOOK regions. The similarity in these regions is low because of extensive alternative splicing. These alternative splice isoforms have bearing on the function of $Ca_v\beta$ subunits, but the details of their roles in VGCC modulation are not clear because of the lack of accessible models for analyses. It is the goal of this project to isolate and evaluate $Ca_v\beta$ subunit splice isoforms in the pond snail *Lymnaea stagnalis*, an amenable model for molecular and electrophysiological study. Previously, a full length Lymnaea $Ca_v\beta$ subunit ($LCa_v\beta_A$; Genbank Accession # AF484087.1) has been reported, which forms part of a functional voltage-gated calcium channel complex when transfected in HEK 293T cells with the primary α_1, and auxiliary $\alpha_2\delta$ subunits (Spafford et al., 2004). The following chapter outlines the identification, cloning and characterization of two novel $Ca_v\beta$ subunit splice isoforms from *Lymnaea stagnalis*.

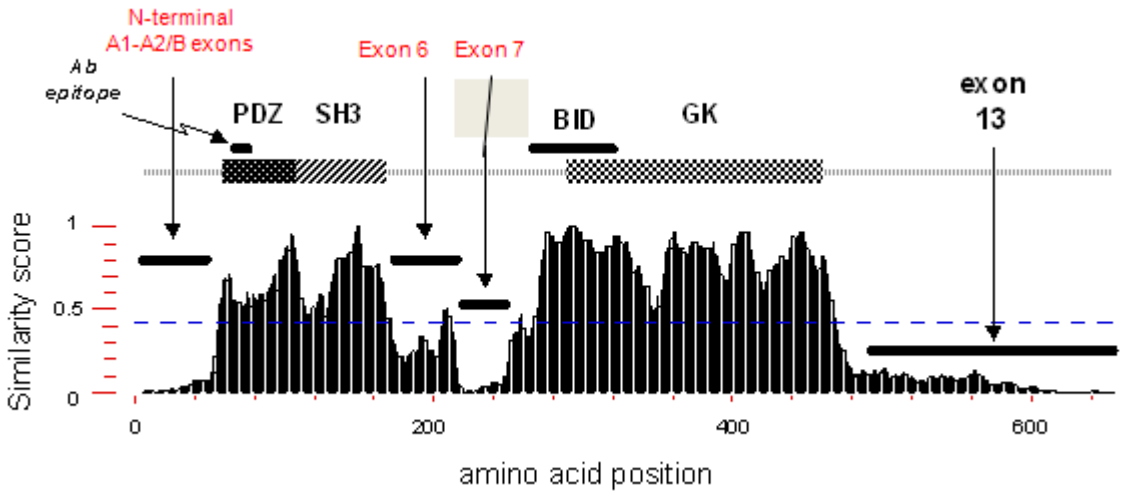

Figure 3.1: Running window of amino acid similarity among invertebrate and rat homologs. Note the highly conserved structural core of β subunits involving Src Homology 3 (SH3) and guanylate kinase (GK) domains. Highly divergent exons are present in the N-terminus, HOOK and C-terminal domains . Domain boundaries are assigned according to the rat β_3 gene (Birnbaumer *et al.*, 1998). A similarity score closer to one indicates that the amino acid sequences are closer in identity to one another at that location. GenBank (gi) sequences for analyses includes rat isoforms: 1b, 8393060; 2a, 16758716; 3, 1705686; 4, 423788; *Lymnaea stagnalis*, 29378325; *Loligo bleekeri* 19911801; *Drosophila melanogaster* 6646874; *C. elegans* 17506267; *Schistosoma mansoni* 15283999; *Cyanea capillata* 2654496. Alternatively spliced isoforms exist for regions of the N-terminus and exon 7of the HOOK domain. Adapted from Spafford, J.D. *et al.* (2004). *J. Biol. Chem.* 279, 39, 41157-41167.

3.1 Screening of cDNA Library

Many $Ca_v\beta$ subunit splice isoforms have previously been uncovered using degenerate primers to screen cDNA libraries. Using degenerate primers in the highly conserved SH3 region and anchoring universal primers EV2 and T77 on the vector, a parasitized cDNA library made from *Lymnaea* cerebral ganglia was screened and several products were identified. Several PCR products were produced that differed in size from the known isoform, $LCa_v\beta_A$, which would produce a product that is 326bp in length. The agarose gel of these products (from library fractions C, M, P, R, U, V, and W) can be seen in figure 3.2. After purification, there was only enough template remaining to sequence the products from fractions C, M, R, and W.

After analysis of the sequence, it was determined that the product from fractions R and W were truncated versions of $LCa_v\beta_A$, and fraction C did not sequence. However, the sequence from fraction M appeared to contain a novel N-terminus. This was determined by aligning the new sequence with the known sequence of $LCa_v\beta_A$ (figure 3.3), and noting that the sequence of the 3' end of the fragment was perfectly aligned, and then as the sequence reached the 5' end there was total divergence from the sequence of $LCa_v\beta_A$ in the final 111bp. At the 5' end of the 111bp there was also a start codon (ATG), indicating that a functional $LCa_v\beta$ subunit could be expressed from this sequence. This new N-terminal isoform was termed $LCa_v\beta_B$. Cloning of this novel N-terminus into the full-length $LCa_v\beta$ subunit was carried out in order to assess the functional differences between $LCa_v\beta$ subunit isoforms.

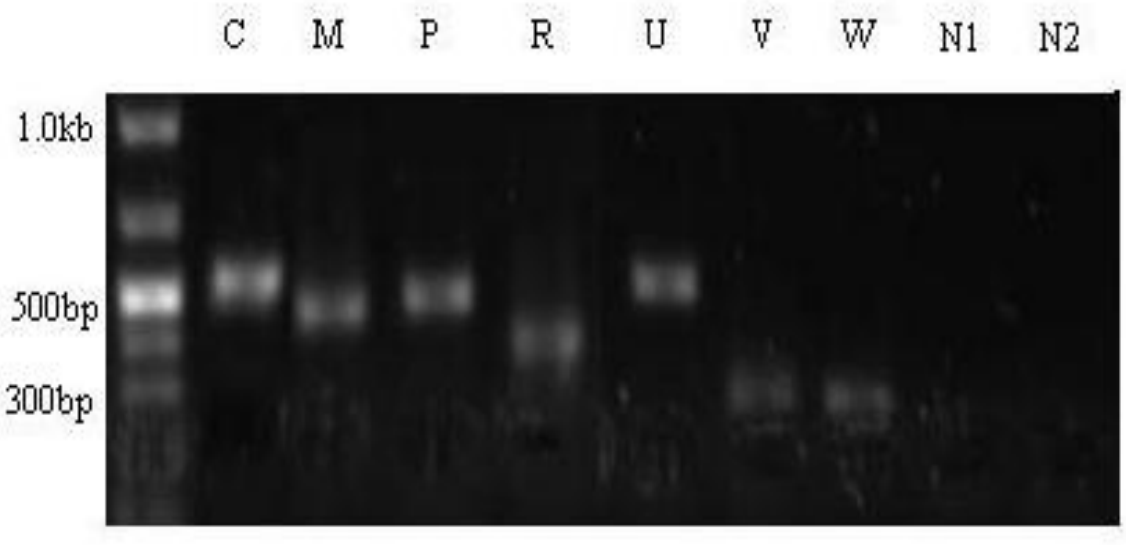

Figure 3.2: Results of cDNA library screening for novel $LCa_v\beta$ N-termini. Lanes N1 and N2 represent the negative control PCRs from the primary and secondary reactions, respectively. $LCa_v\beta_A$ would be expected to produce fragments of 326bp in length. The sample in lane M was sequenced and found to contain the novel N-terminus of $LCa_v\beta_B$.

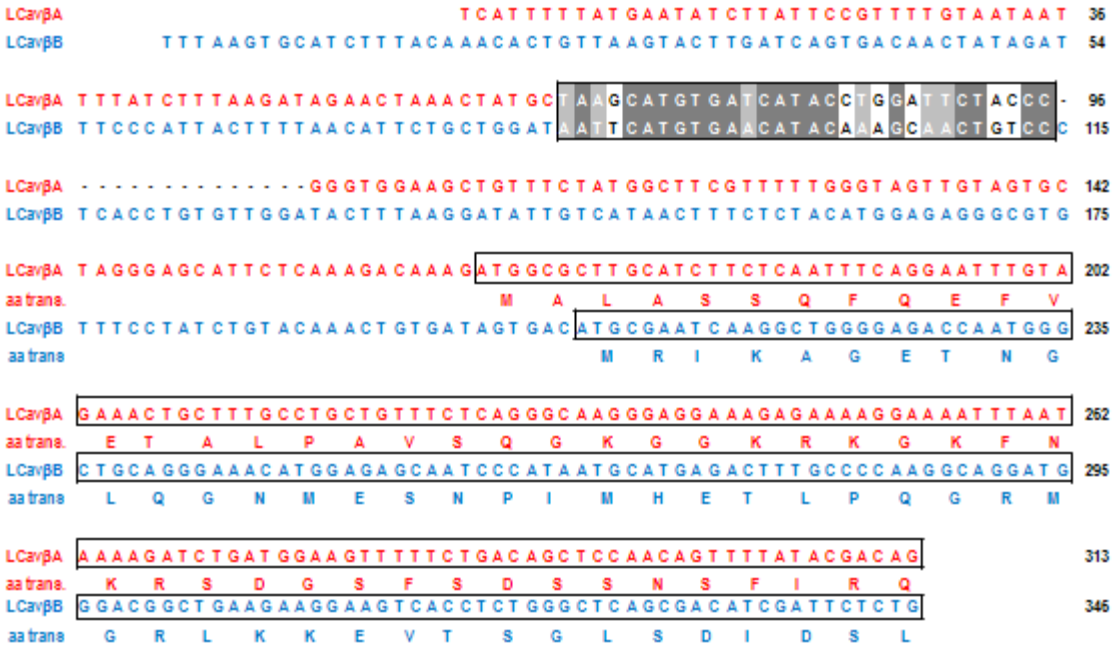

Figure 3.3: DNA sequence alignments of the unique N-terminal isoforms of *LCa*$_v$β subunits. Nucleotide and amino acid sequence alignment of the N-termini of *LCa*$_v$$\beta_A$ (red) and *LCa*$_v$$\beta_B$ (blue). Coding sequence is outlined by a black box. Identical DNA sequence are indicated by *dark outlined gray boxes* and similar ones by *lighter colored gray boxes.* Note that the only sequence shared between the two isoforms is a short 13 bp "CATGTGAwCATAC" motif in the 5' untranslated region, which may be a common upstream DNA regulatory element for *LCa*$_v$$\beta$ subunits. Downstream of the sequence shown above, until the HOOK region, there was 100% sequence identity at the nucleotide level.

3.2 Cloning of $LCa_v\beta_B$ into pMT2SX(R)

The N-terminus of $LCa_v\beta_B$ was amplified from fresh cDNA so that it could be cloned into a full-length $LCa_v\beta$ subunit in a mammalian expression vector. The digested product of the amplification, as well as $LCa_v\beta_A$-*pMT2SX(R)* vector can be seen in figure 3.4. The N-terminal fragment was 1014bp in length, while the PMT2SX(R) vector and C-terminus of the $LCa_v\beta$ subunit was 5.4kb in length. The correct clone of $LCa_v\beta_B$, was confirmed by restriction digestion with SalI and BlpI (as seen in figure 3.5) prior to sequencing, although a strange doubling of bands was noted. Sequencing of the clones revealed the presence of two $LCa_v\beta_B$ isoforms. Comparison of the sequence of the clones revealed that there is a 21bp insert present in the HOOK region of one $LCa_v\beta_B$ clone, but not the other. The coding sequence of $LCa_v\beta_B$ is shown in figure 3.6, where the novel N-terminus and the HOOK insert are shown in blue and red, respectively. The clones with, and without, the insert were called $LCa_v\beta_{B+}$ and $LCa_v\beta_{B-}$, respectively. $LCa_v\beta_A$ also contained the 21bp HOOK insert, and so it will be referred to as $LCa_v\beta_{A+}$.

3.3 Southern Blotting

There are four $Ca_v\beta$ subunit genes in vertebrates, and usually only one is found in invertebrates (although an exception is found in Schistosomes, where two different $Ca_v\beta$ subunit genes are found). As seen in figure 3.7, when a phylogeny of vertebrate and invertebrate $Ca_v\beta$ subunit genes is constructed, *Lymnaea* groups most closely with other

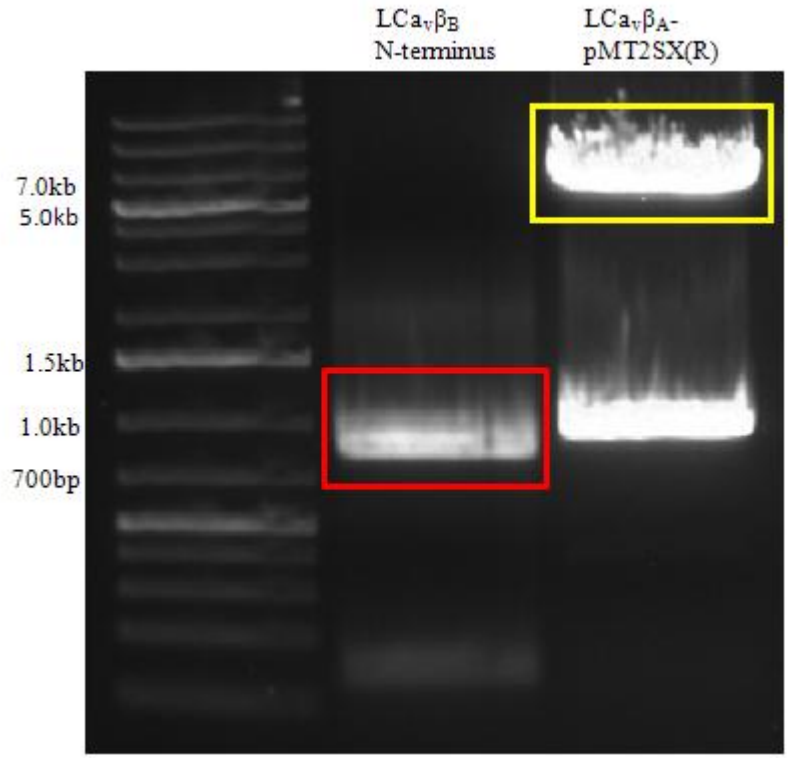

Figure 3.4: Fragments for cloning of *LCa$_v$β$_B$* into pMT2SX(R). All DNA fragments have been digested with NotI and BlpI to facilitate cloning. The middle lane (red box) contains the digested PCR fragment containing the N-terminus of *LCa$_v$β$_B$* (1.01kb). The right lane (yellow box) contains PMT2SX(R) and the C-terminus of *LCa$_v$β* (5.4kb).

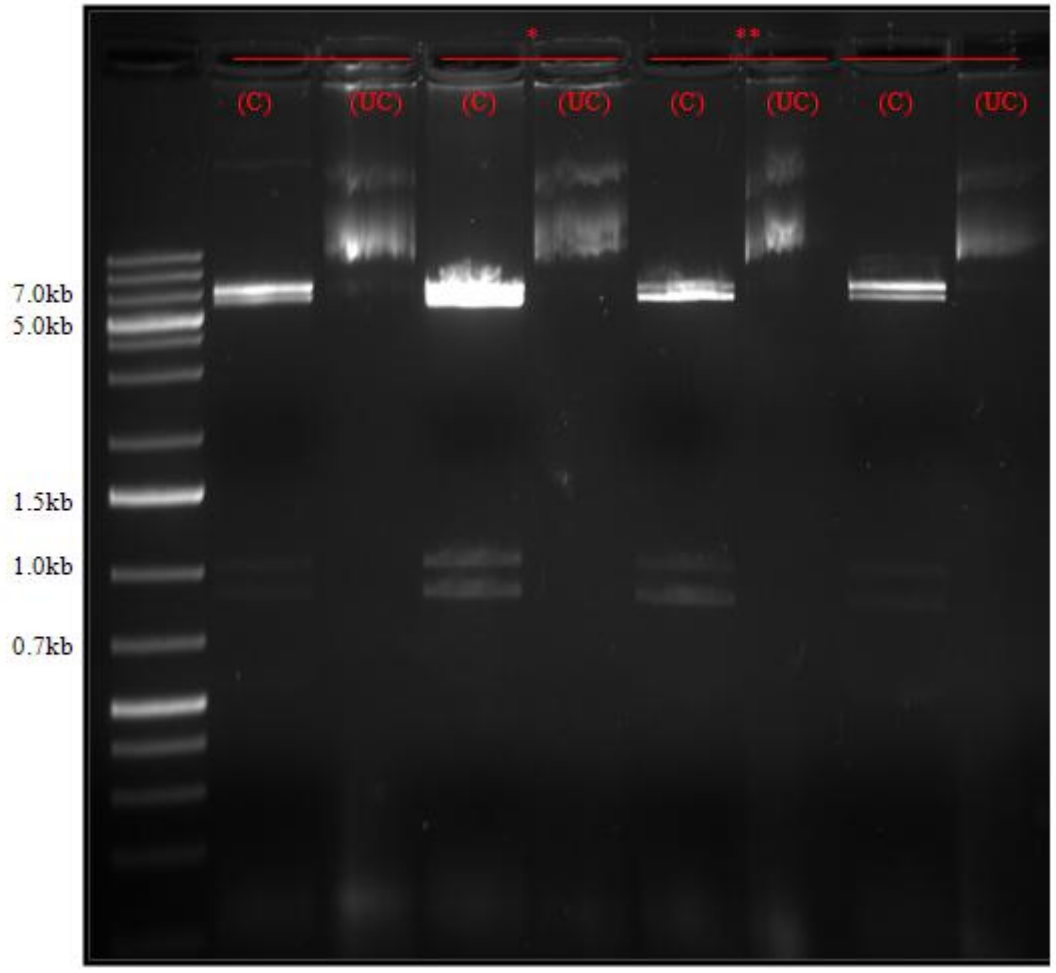

Figure 3.5: Confirmation of $LCa_v\beta_B$ clones by restriction digestion. Potential clones were digested with SalI and BlpI. Complete digestion of $LCa_v\beta_B$-*pMT2SX(R*) with these enzymes would be expected to produce two products of 1.0kb and 5.4kb in length. The doubling of bands seen above was not observed consistently and cannot be explained. Clones were also later confirmed by sequencing to be $LCa_v\beta_{B+}$ (*) and $LCa_v\beta_B$- (**). There are alternating lanes of digested (C) and undigested (UC) plasmid.

Figure 3.6: Complete coding sequence of *LCavβ_B*. The novel N-terminus of *LCavβ_B* is shown in blue, while the optional insert that is found in the HOOK region is underlined and highlighted in red. The optional HOOK insert is present in *LCavβ_{B+}* and *LCavβ_{A+}* but not *LCavβ_{B-}*.

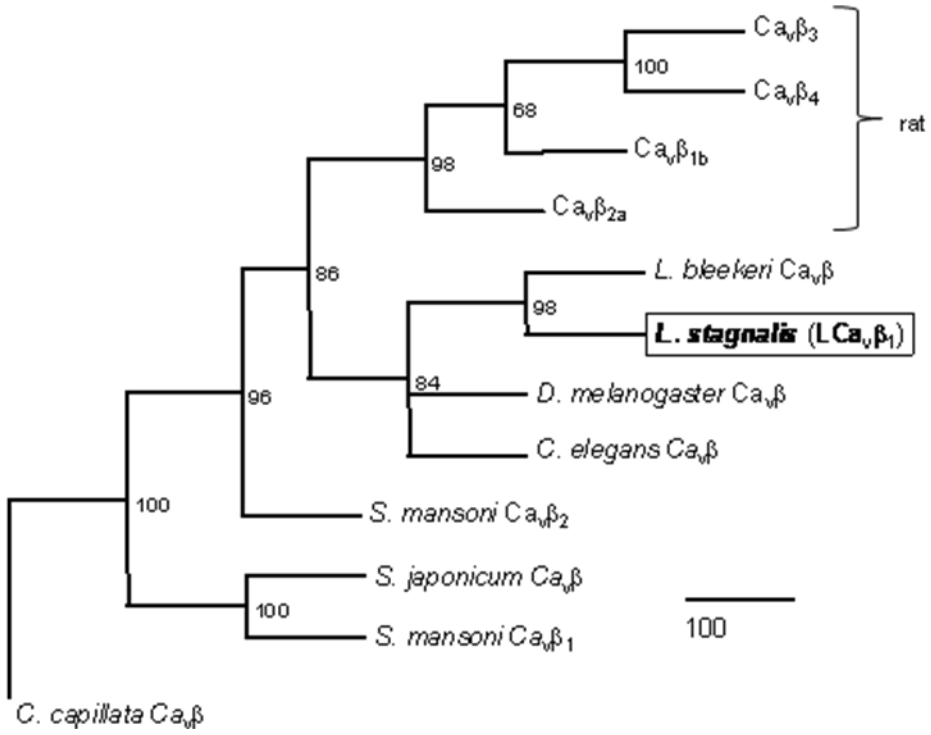

Figure 3.7: Phylogeny of invertebrate and rat $Ca_v\beta$ subunits. Protein sequences of $LCa_v\beta$ and other $Ca_v\beta$ subunit homologs were aligned and used to generate a consensus gene tree using the Branch-and-Bound algorithm. The gene tree was tested for robustness in 100 bootstraps which are displayed at the branch node. Modified from Spafford, J.D. *et al.* (2004). *J. Biol. Chem.* 279, 39, 41157-41167.

invertebrates like *Loligio* (squid) and *Drosophila*, while the four mammalian homologs are grouped together. In order to characterize the copy number and confirm that there is only a single $Ca_v\beta$ subunit homolog found in *Lymnaea*, Southern blotting experiments were carried out. First, small, unique fragments of each N-terminal sequence were successfully cloned into a pBluescriptSK(+) vector and the presence of the correct insert was confirmed by sequencing. Using these clones as template, DIG-labeled DNA probes were produced and purified as seen in figure 3.8. When compared to fragments amplified in the absence of DIG-labeled dUTP, the DIG-labeled probes appeared slightly heavier due to the presence of the DIG, which increases the molecular weight of the probe (figure 3.8).

Prior to restriction digestion, *Lymnaea* genomic DNA extracts were run on a gel to ensure that there was no (or little) degradation of the DNA and no RNA was present. As seen in figure 3.9, the DNA remained undegraded upon completion of the extraction and therefore was suitable for use in Southern blotting. This DNA was then fully digested with the chosen restriction enzymes as seen in figure 3.10. After transferring the restriction digests to positively-charged nylon membranes (which bind DNA), they were hybridized with the DIG-labeled DNA probes to produce the blots seen in figure 3.11. The blot of $LCa_v\beta_B$ (figure 3.11B) shows a single, dark band in each lane, indicating that this gene is a single-copy gene; however the blot of $LCa_v\beta_{A+}$ (figure 3.11A) was not so clear. Several attempts under various conditions were made to produce a clear Southern blot with no success. The blot of $LCa_v\beta_{A+}$ had two faint bands in each lane, possibly indicating the presence of an intron which divides the region that is recognized by the DIG-labeled probe. This is likely the case, given that mammalian $Ca_v\beta_1$ to $Ca_v\beta_4$ have an intron splicing the N-terminus of $Ca_v\beta_A$ isoforms (see

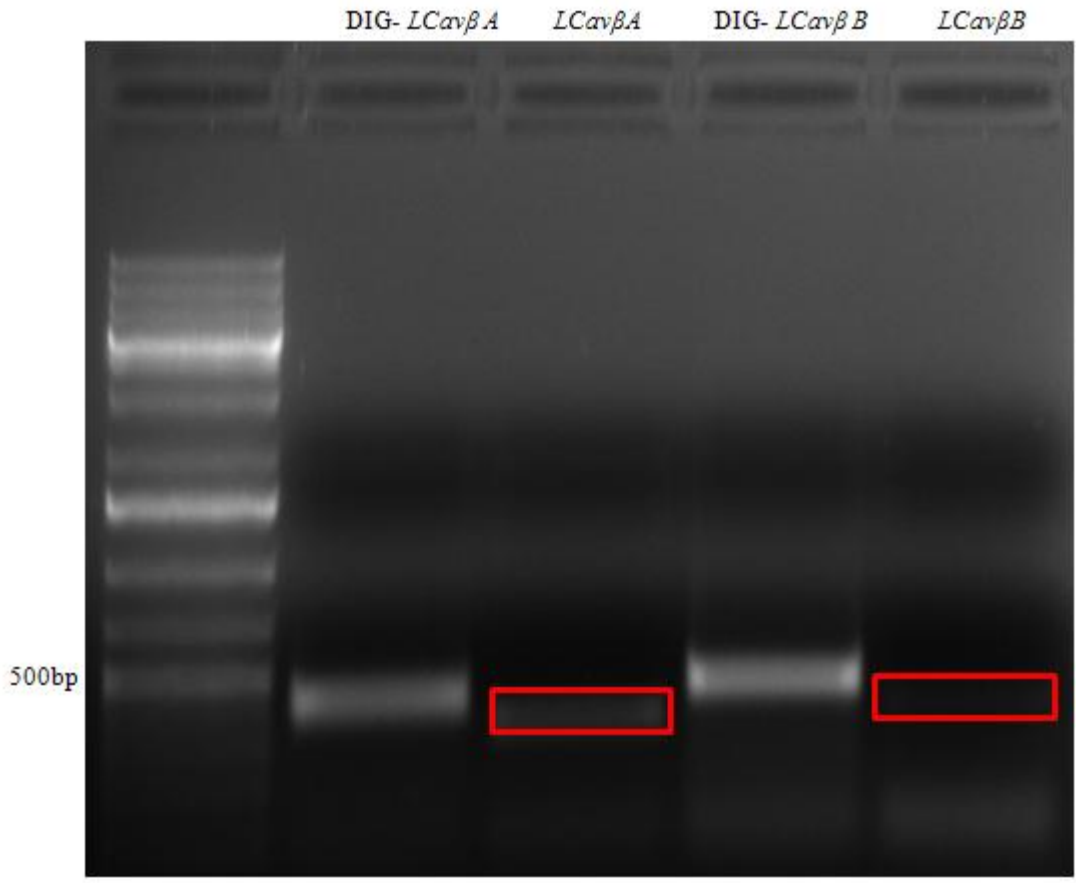

Figure 3.8: Synthesis of DIG-labeled DNA probes for Southern blotting of *LCavβ* subunit isoforms. The positions of positive control (non-DIG) reactions were highlighted with red boxes due to low yield. Note that the molecular weight of DIG-labelled DNA probes is slightly higher than positive controls due to the increased mass added by the incorporation of DIG-11-dUTP nucleotides.

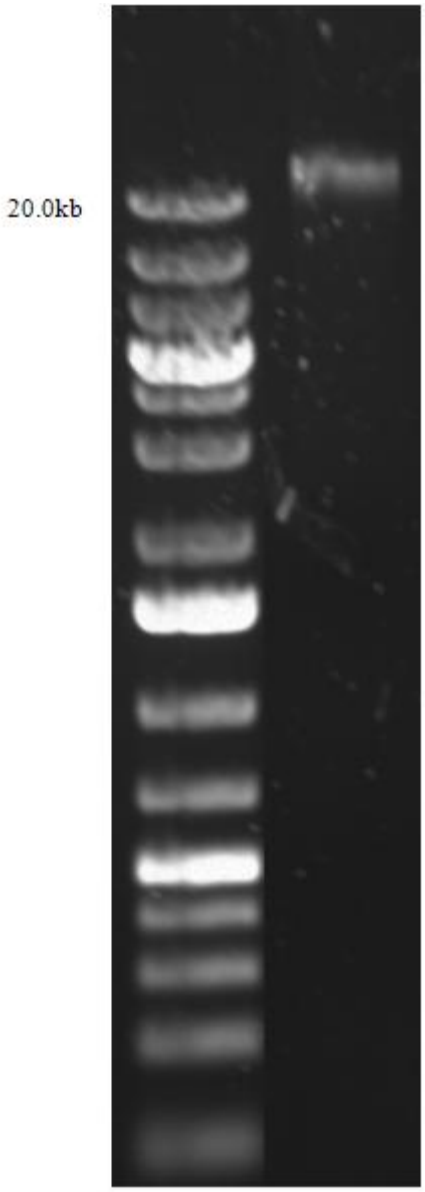

Figure 3.9: Uncut genomic DNA to be used for Southern blot analysis of LCa$_v$β. Note that the genomic DNA is undegraded and free of RNA after extraction from *Lymnaea stagnalis* tissue.

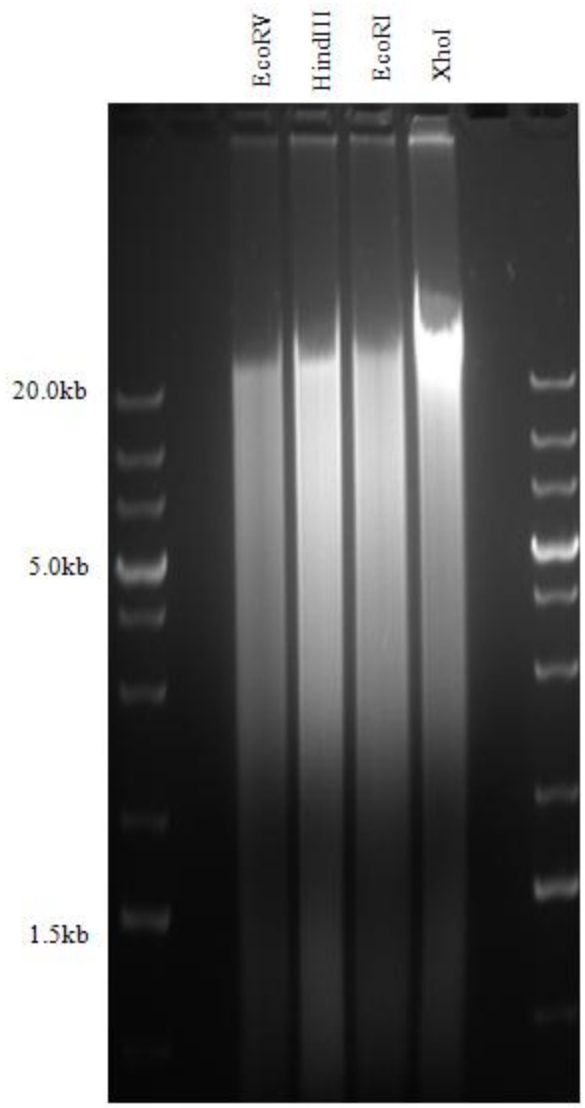

Figure 3.10: Digested genomic DNA for Southern blot anaylsis of *LCa$_v$β*. Extracted genomic DNA was fully digested with the restriction enzymes EcoRV, HindIII, EcoRI and XhoI.

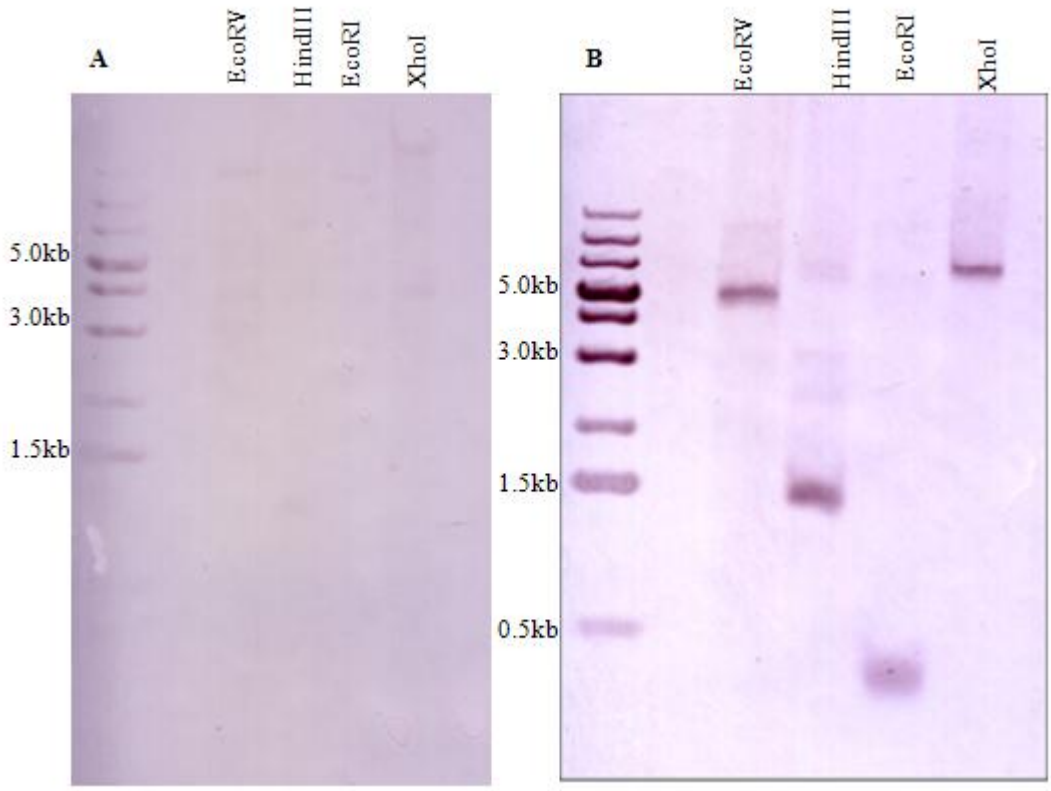

Figure 3.11: Southern blots of *LCavβ*. (A) Southern blot of $LCav\beta_{A+}$ shows multiple faint bands in each lane of the blot. The double banding is caused by the presence of an intron which divides the N-terminus of $LCav\beta_{A+}$ between two exons. (B) Southern blot of $LCav\beta_{B+}$ shows discreet single bands in each lane, consistent with a single-copy gene.

section 3.4 and figure 3.15). To further investigate the genomic structure of the *LCavβ* subunit, genomic sequencing of the N-terminus was carried out.

3.4 Genomic Analysis of the Lymnaea $Ca_v\beta$ Subunit

In order to characterize the genomic structure and evolution of the *LCa$_v$β* subunit, several attempts were made to sequence the genomic region between the N-terminal exons. A PCR product of approximately 3.0kb in length was produced using genomic DNA as the template and primers which target the C-terminal end of the B exon (called end-LBetaBexon) and the N-terminal end of the conserved SH3 domain (CBSB2) shared by both *LCa$_v$β$_A$* and *LCa$_v$β$_B$* (figure 3.12). This product was then cloned into the pCR XL-TOPO vector (figure 3.13) and sequenced, leading to the proposed genomic structure illustrated in figure 3.14A. Sequencing of the cloned fragment revealed the presence of three exons (labelled B, C and D in figure 3.14B and C), separated by two introns. Just upstream of the CBSB2 primer site, the SH3 domain is divided by a 2263bp intron that is bounded by putative donor (5'-GTAAAG) and acceptor (5'-TTTCAG) sites to facilitate splicing. Exon C (39amino acids), which is common to both N-terminal *LCa$_v$β* subunit variants, can be found upstream of this intron preceded by a 516bp intron. Again, putative donor (5'-GTAATA) and acceptor (5'-ACACAG) sites were located in this 516bp intron indicating that splicing was indeed possible in this region. Finally, as the sequence continues upstream the distal portion of the unique N-terminus found in *LCa$_v$β$_B$* is reached (this will be referred to as exon B). No sequence was obtained upstream of this region.

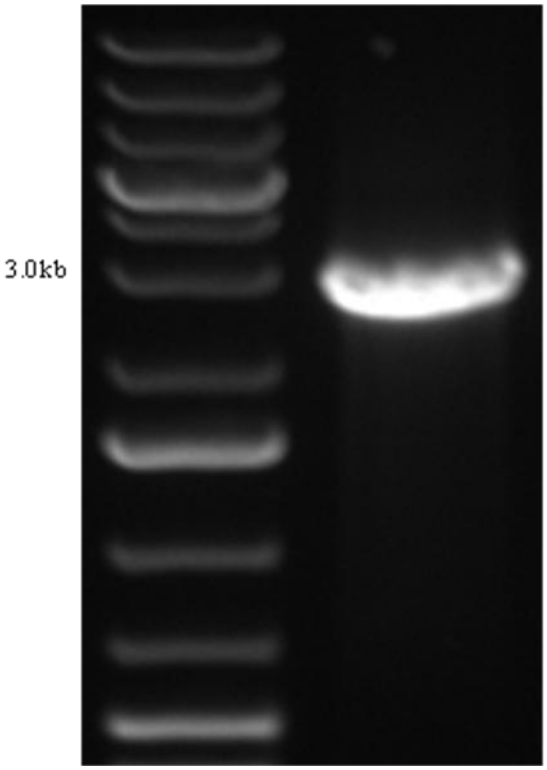

Figure 3.12: Secondary genomic PCR of $LCa_v\beta$ N-terminus. Primers CBSB2 and end-LBetaBexon were employed to produce a secondary PCR product of approximately 3.0kb in length from a genomic DNA template. Negative control reactions (data not shown) failed to produce any detectable products as expected.

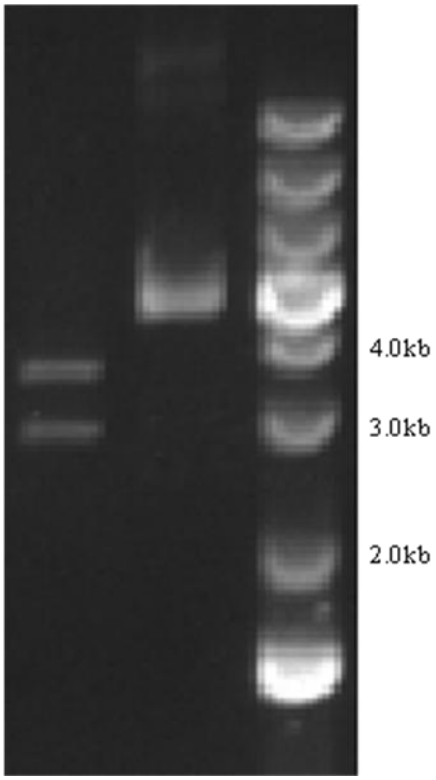

Figure 3.13: Cloning of *LCa$_v\beta$* N-terminal genomic fragment. Plasmids raised in CopyCutter cells were isolated and digested with EcoRI (left lane), removing the *LCa$_v\beta$* genomic fragment (3.0kb) from the pCR XL-TOPO vector (3.5kb; undigested in centre lane).

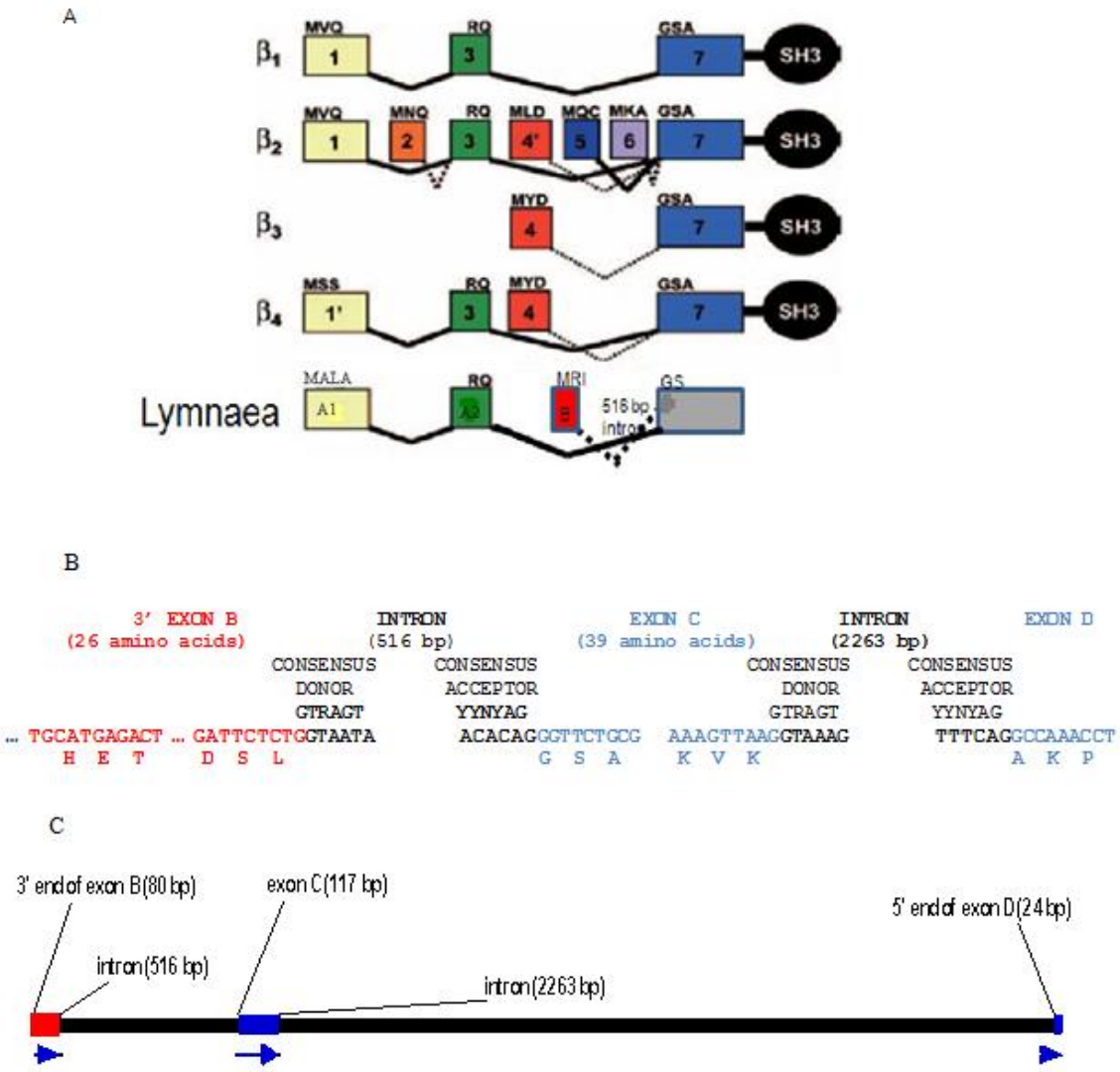

Figure 3.14: Proposed genomic structure of the *LCa$_v$β* subunit N-terminus mimics the genomic structure of mammalian *Ca$_v$β* subunits. (A) The proposed genomic structure of the *LCa$_v$β N-terminus* resembles that of mammalian *Ca$_v$β2 and Ca$_v$β4* genes. Both *LCa$_v$β2* and *LCa$_v$β4* contain two exons (homologous to putative exons A1 and A2, yellow and green) encoding homologs of *LCa$_v$βA* , followed by single short N-terminal exons (red, blue or purple) which do not resemble one another. A conserved exon (blue; beginning GSA…) is found in all *Ca$_v$β* subunits follows. Modified from Vendel, A.C. *et al.* (2006). *Protein Sci.* 15, 2, 378-383. (B) Introns (black) between exons B (red) and C (blue), and C and D (blue) contain donor and acceptor sites to facilitate splicing of these exons. (C) Schematic representation of intron structure of the N-terminus of *LCa$_v$β*.

Given these findings, and in comparison to what is observed in mammals, fish and other invertebrates (figure 3.15), we propose that the N-terminal exon of $LCa_v\beta_A$ is upstream of the exon B sequence, and not part of a separate gene. This is supported by the fact that there was no divergence in the nucleotide sequence between $LCa_v\beta_A$ and $LCa_v\beta_B$ outside of the N-terminus and HOOK regions. All of the $LCa_v\beta_B$ clones made from cDNA were sequenced in the reverse direction with the primer *BlpIbb,* which covered the N-terminus, SH3, and HOOK domains (approximately 1kb downstream from the N-terminus). The sequence was then compared to the known sequence of $LCa_v\beta_A$. In exon C and downstream regions, no sequence divergence was noted between $LCa_v\beta_A$ and $LCa_v\beta_B$, with the exception of the optional seven amino acid insert in the HOOK region. If the N-termini of $LCa_v\beta_A$ and $LCa_v\beta_B$ were products of different genes, it is likely that some divergence of downstream sequence at the nucleotide level would have taken place by random mutation.

The genomic structure of other $Ca_v\beta$ subunit genes were compared in an alignment of the N-terminus of $LCa_v\beta_A$ and $LCa_v\beta_B$ with several invertebrate and vertebrate $Ca_v\beta$ subunit homologs (figure 3.15). It was immediately clear that there are homologs of both $LCa_v\beta_A$ and $LCa_v\beta_B$ found in another mollusc, *Aplysia californica*. Also, the N-terminal amino acid sequence of $LCa_v\beta_A$ was conserved to a higher degree among all species, while the sequence of $LCa_v\beta_B$ seemed to have diverged from vertebrate $Ca_v\beta$ subunits to a greater extent. The N-terminus of $LCa_v\beta_A$, in fact, appeared to be constructed from two exons based on comparison with the vertebrate homologs (these will be referred to as exons A1 and A2). Exon A1 did not show a high degree of conservation, with exons varying in length and composition between species; however, this exon always ended in a glutamine residue that was conserved

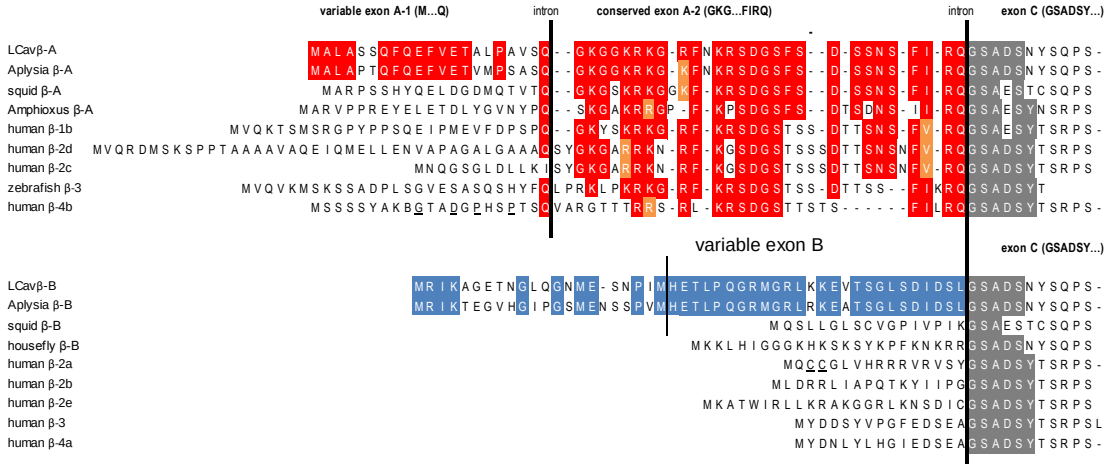

Figure 3.15: Amino acid alignment of N-terminus of invertebrate and vertebrate *LCa$_v$β* subunits.

Conserved residues are highlighted in red, blue or grey for exons A1/A2, B or C, respectively. Thick black lines represent exon boundaries, while the thin black line in molluscan *Ca$_v$β$_B$* represents the starting point of the known N-terminal genomic sequence. Underlining represents palmitoylation sites. Note that the amino acid composition of exons A1 and B are highly variable between moluscs and non-molluscs, while exons A2 and C are more highly conserved among invertebrates and vertebrates. GenBank accession numbers of the aligned sequences can be found in table 2.2.

among all species. Exon A2 contained several regions rich in charged amino acids (lysine, argenine and aspartic acid) that were highly conserved among molluscs, mammals and fish perhaps suggesting that this region may be of physiological significance. It was also interesting to see that homologs of exons A1 and A2 could be found in all vertebrate $Ca_v\beta$ subunit genes ($Ca_v\beta_1$, $LCa_v\beta_2$, $Ca_v\beta_3$ and $Ca_v\beta_4$). Strangely, homologs of exons A1 and A2 are present in zebrafish $Ca_v\beta_3$, however, in mammals these exons appeared to have been lost in the $Ca_v\beta_3$ gene, leading to the hypothesis that the loss of the $Ca_v\beta_A$ N-terminus in $Ca_v\beta_3$ occurred after the divergence of mammalian and fish $Ca_v\beta$ subunits.

When we compared the protein sequence of $LCa_v\beta_B$ to other molluscan and vertebrate $Ca_v\beta$ genes (figure 3.15), it was evident that snails like *Lymnaea* and *Aplysia* contained a much longer N-terminus than non-molluscs including squid (*Loligo)*, another invertebrate. In squid, fish and mammals the N-terminus of the $LCa_v\beta_B$ homologs were contained in a single exon. Consistent with what is found in mammals, the single discreet bands observed in the Southern blot of $LCa_v\beta_B$ (figure 3.11B) suggests that there is no intron dividing exon B in molluscs. Although not found in the cDNA library, shorter isoforms of $LCa_v\beta_B$ were possible as methionine residues were found in the N-terminus at positions 15, 21 and 30. These residues could potentially serve as start codons for the production of shorter variants of $LCa_v\beta_B$ producing N-termini that would be 32, 26 and 17 residues long, respectively (figure 3.15). These truncated variants would have been similar in length to most non-molluscan homologs, which varied from 15 to 24 amino acids. Contrary to the relatively high degree of conservation that was observed in the N-terminus of $Ca_v\beta_A$ homologs among

species, there was surprisingly little conservation observed between molluscan $Ca_v\beta_B$ and isoforms found in other species.

Aside from the N-terminal region, $LCa_v\beta$ also contained alternative splicing in the HOOK region. In order to study the patterns of evolutionary conservation found in this domain, an amino acid alignment of the invertebrate, mammalian and fish HOOK regions was constructed (figure 3.16). The alignment of the HOOK region revealed some interesting patterns of conservation, leading to the hypothesis that that there may have been a primordial form of the HOOK domain shared among invertebrates, mammals and fish. As seen in figure 3.16, the HOOK region is encoded by exons 6 and 7. Exon 6 does not show a high degree of conservation and, not surprisingly, it was noted that in this region conservation was found mostly within closely-related species- the invertebrates (*Lymnaea* and *Loligo*) seem to group together, as do vertebrate $Ca_v\beta_1$ and $Ca_v\beta_2$ genes, while $Ca_v\beta_3$ and $Ca_v\beta_4$ appear to be unique. The length of exon 6 was found to be quite variable, but was always serine-rich and always ended in a -TPPXX motif were X= T, P, S or A (except in zebrafish $Ca_v\beta_4$).

The second exon of the HOOK region, exon 7, is alternatively spliced and can be highly variable in length (figure 3.16). In vertebrates (fish and mammals), exon 7 is formed from one of three mutually exclusive exons termed 7A, 7B or 7C (figure 3.16; Foell et al., 2004). Depending on which exon is expressed, the size of the HOOK region will differ substantially. Long isoforms, of 45 or 52 amino acids in human $Ca_v\beta_{1a}$ or $Ca_v\beta_{2d}$, respectively, are formed by the inclusion of exon 7A, which ends with the motif -PFFKK that is conserved in all species studied. In a unique variant of human $Ca_v\beta_2$, exon7C (21 residues long) is included in place of exon 7A or 7B, leading to a moderately sized HOOK region.

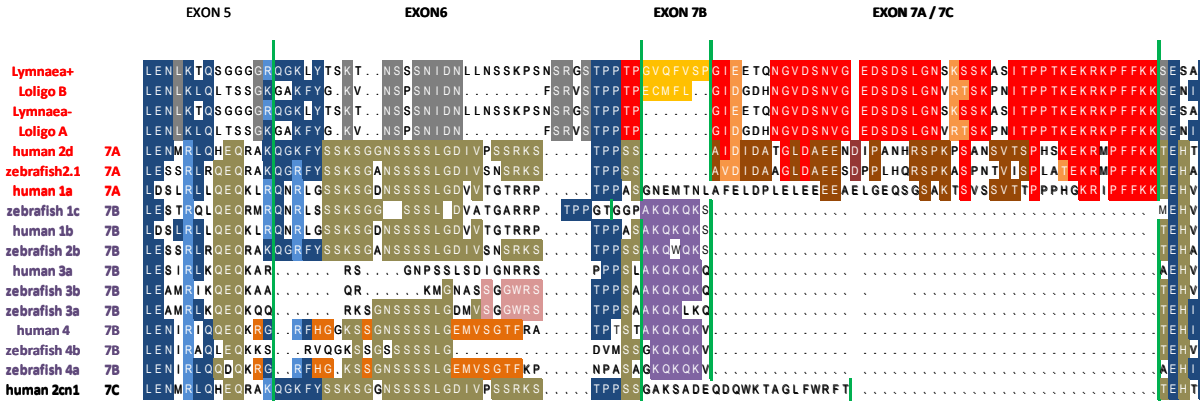

Figure 3.16: Amino acid alignment of HOOK region of invertebrate and vertebrate *LCa$_v$β* subunits. Conserved residues are highlighted and grouped by colour according to amino acid similarity. Note the conserved -PFFKK motif at the end of exon 7A, and the consistent size and location of exon 7B (although the sequence differs between invertebrates and vertebrates). Taken together these patterns of conservation suggest that exon 7A was likely present in the ancestral *Ca$_v$β* subunit which evolved to form the invertebrate and vertebrate *Ca$_v$β* subunits. Exon 7B was likely formed by a process of convergent evolution due to sequence divergence. GenBank accession numbers of the aligned sequences can be found in table 2.2.

Finally, in all four vertebrate $Ca_v\beta$ subunits, short isoforms are created when exon 7B (AKQKQKX) is included in place of exon7A or exon 7C. Interestingly, splicing of exon 7 was also observed in invertebrates, although exons 7A, 7B or 7C do not appear to be mutually exclusive, as they are in fish and mammals (figure 3.16).

The HOOK region of molluscan and squid $Ca_v\beta$ subunits contain exons equivalent to 7A and 7B (figure 3.16). Exon 7A (which ends in –PFFKK) was conserved in invertebrates, mammalian $Ca_v\beta_1$ and $Ca_v\beta_2$ and zebrafish $Ca_v\beta_{2.1}$, but appears to have been lost in mammalian and zebrafish $Ca_v\beta_3$ and $Ca_v\beta_4$ genes. Based on this observation, it is hypothesized that exon 7A was contained in a primordial $Ca_v\beta$ subunit from which all others have evolved. In mammalian $Ca_v\beta$ subunits, exons 7A and 7B of the HOOK region were mutually exclusive, unlike in invertebrates like *Lymnaea* and *Loligo,* where exon 7A was found to be constitutively expressed, while the short exon 7B was optional. Exon 7B was only present (upstream of exon 7A) in $LCa_v\beta_{A+}$, $LCa_v\beta_{B+}$ and $LoCa_v\beta_{1B}$ isoforms, but not in $LCa_v\beta_{B-}$ or $LoCa_v\beta_{1A}$ subunits. In $LCa_v\beta_{A+}$ and $LCa_v\beta_{B+}$, this exon (GVQFVSP) was identical in position and length but differed in amino acid composition from the vertebrate sequence of exon 7B; while in squid the optional exon (ECMFL) was in the same position but only five amino acids in length. The fact that the position, but not the sequence, of exon 7B is conserved points to the likelihood that the formation of these optional exons was driven by a process of convergent evolution after the divergence between molluscs, squid and vertebrates.

During this process of convergent evolution, the HOOK domain insertions found in each species would have arisen independently by random mutation causing alterations to the

length of the HOOK domain. These changes in length were beneficial as they allowed for modulation of channel gating, and therefore were conserved in several species although they arose separately. Following this line of reasoning, it could be hypothesized that the ancestor of vertebrates evolved a separate, short isoform containing exon 7B (not found in invertebrates) that was found in all four $Ca_v\beta$ subunit genes (AKQKQKX), while invertebrates evolved entirely different mutations in the exact same region independently. This hypothesis explains why invertebrates have evolved an optional exon instead of mutually exclusive exon splicing as in vertebrates. This pattern of alternative splicing was interesting, because studies have implicated these regions in the modulation of channel biophysics in both squid (Kimura and Kubo, 2003) and mammals (Richards et al., 2007). How the presence of these inserts will affect the electrophysiology of $LCa_v\beta$ remains to be determined.

3.5 Western Blotting of $LCa_v\beta_{A+}$ and $LCa_v\beta_{B+}$

Before analyzing how the trafficking and biophysics of LCa_v1 and LCa_v2 were influenced by $LCa_v\beta$ subunit expression, it was crucial to show that these proteins could be expressed heterologously in HEK 293T cells. In order to accomplish this task, Western blotting was carried out using lysate from HEK 293T cells transfected with $LCa_v\beta_{A+}$, $LCa_v\beta_{B+}$ or no DNA (mock transfection), as seen in figure 3.17. In lanes containing lysate from transfected cells, single bands of relatively similar intensity could be seen at approximately 60kDa. No bands were seen in the lane which contained lysate from the mock-transfected cells. This corresponded with the expected sizes of $LCa_v\beta_{A+}$ and $LCa_v\beta_{B+}$, which were 62.81kDa and

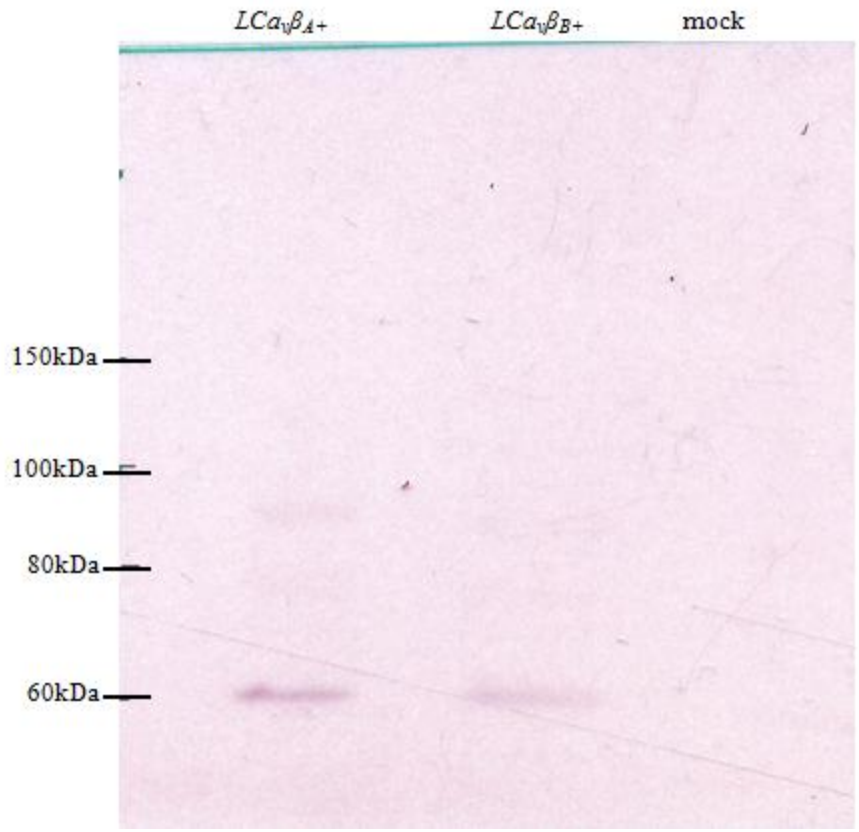

Figure 3.17: Western blot of *$LCa_v\beta$* subunits. $LCa_v\beta_{A+}$ and $LCa_v\beta_{B+}$ were expressed in HEK 293T cells and lysed after five days of expression. $LCa_v\beta_{A+}$ and $LCa_v\beta_{B+}$ were detected by a rabbit anti- $LCa_v\beta$ antibody and a secondary antibody coupled to horseradish peroxidase. Cells that were transfected with $LCa_v\beta_{A+}$ or $LCa_v\beta_{B+}$ show expression of an appropriately sized protein (~60kDa), whereas mock-transfected cells do not, indicating that HEK cells do not express endogenous $Ca_v\beta$ subunits.

62.63kDa, respectively. The lack of banding in the mock transfection sample indicated that there was no significant expression of endogenous $Ca_v\beta$ subunit that possesses epitopes similar to $LCa_v\beta$ in HEK 293T cells.

3.6 *Antibody Staining of $LCa_v\beta$*

In order to visualize the cellular localization of LCa_v1, it was successfully cloned into a pEGFP-C1vector with an N-terminal fusion of EGFP in reading frame. A clone for the generation of EGFP-LCa_v2 was constructed previously in our laboratory in a similar fashion by Adriano Senatore. In order to confirm that the correct insert was present, restriction digestion was performed as seen in figure 3.18. These digests verified that both LCa_v1 and LCa_v2 were present in their respective clones, and so these constructs were transfected into MSR cells in combination with various $LCa_v\beta$ subunit isoforms. These cells would be used in the fluorescent labeling of $LCa_v\beta$ subunits with antibodies, for the purpose of determining their subcellular distribution with respect to the α_1 subunit.

The results of staining MSR cells with a specific antibody generated against $LCa_v\beta$ subunit (which recognizes an epitope common to both $LCa_v\beta_{A+}$ and $LCa_v\beta_{B+}$) were rather inconclusive. Background staining remained high even under the most stringent conditions. Despite the high background, it was clear that some cells bore higher antibody staining (above background levels). This was in contrast to the untransfected control cells, where cells were all stained with equal intensity (figures 3.19 and 3.20). The images shown in figures 3.19 and 3.20 are representative of 10 to 12 images taken for each dataset.

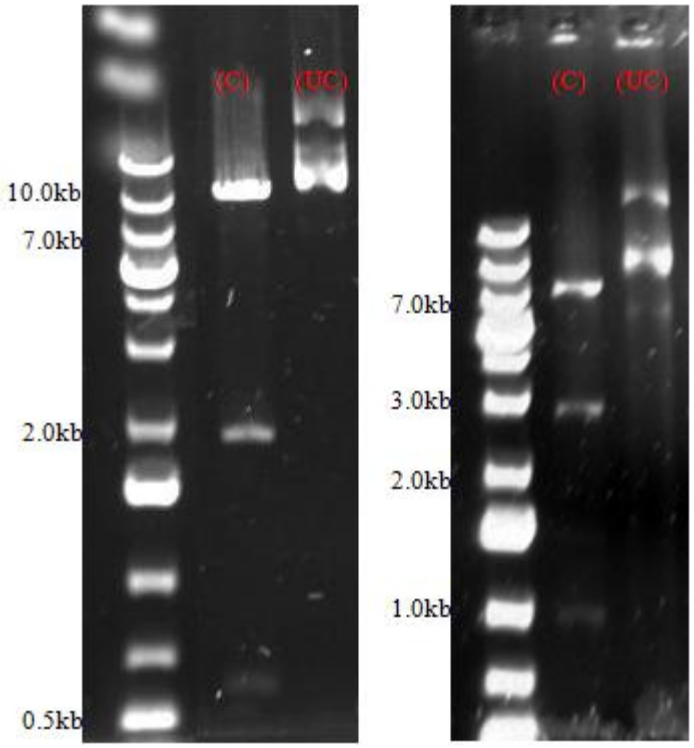

Figure 3.18: Restriction digestion of *LCa$_v$1*-pEGFP-C1 and *LCa$_v$2*-pEGFP-C1. The identity of clones were confirmed by digestion with BamHI. Expected fragment sizes (*LCa$_v$1*-pEGFP-C1: 8.8kb, 1.8kb, 582bp; *LCa$_v$2*-pEGFP-C1: 7.3kb, 2.8kb, 984bp) were produced, indicating that the clones are correct. Digested (C) and undigested (UC) samples are displayed.

Antibody staining for *LCa$_v$1* when co-expressed with *LCa$_v$β*$_{A+}$ or *LCa$_v$β*$_{B+}$ or in the absence of *LCa$_v$β*, is depicted in figure 3.19. When *LCa$_v$β* is not present, EGFP (linked to *LCa$_v$1*) is distributed diffusely throughout the cell, and only minimal red background is seen in all cells. For cells transfected with both *LCa$_v$β*$_{A+}$ and *LCa$_v$β*$_{B+}$, it was observed that *LCa$_v$1* was still fairly evenly distributed throughout the cell, although there appeared to be slightly more intense staining around, and near, the membrane. The distribution of both *LCa$_v$β*$_{A+}$ and *LCa$_v$β*$_{B+}$, were also concentrated nearer to the membrane, although there is still some cytoplasmic staining above background levels. Some cells in both instances, however, seem to be stained equally throughout the cell. Representative antibody staining for *LCa$_v$2* is shown in figure 3.20 when co-transfected with *LCavβ*$_{A+}$, *LCavβ*$_{B+}$ or neither. Some cells again seemed to contain equal distribution of *LCa$_v$β* subunit (red) and *LCa$_v$2* (green) fluorescence throughout the cell. This was true all the time in cells lacking *LCa$_v$β*, but again, in cells which contained either *LCa$_v$β*$_{A+}$ or *LCa$_v$β*$_{B+}$, many cells were stained more heavily around the membrane.

It has been shown in mammals that *Ca$_v$β* subunits assist in the membrane trafficking of the primary α_1 subunit (Neuhuber *et al*., 1998; Raghib *et al.*, 2001; Colecraft *et al.*, 2002), but does the same effect occur for *Lymnaea* channels expressed *in vitro*? These results presented in figures 3.19 and 3.20 indicated that when *LCa$_v$β* subunits were expressed with either *LCa$_v$1* or *LCa$_v$2*, we see a rise in membrane insertion of the α_1 subunit, and the *LCa$_v$β* subunits seem to be colocalized, to some degree, with the *α_1* subunit. *LCa$_v$β* subunits are expected to be found in the cytoplasm also because they are not membrane bound unless associated with calcium channels. The α_1 subunits, however, are transmembrane proteins and

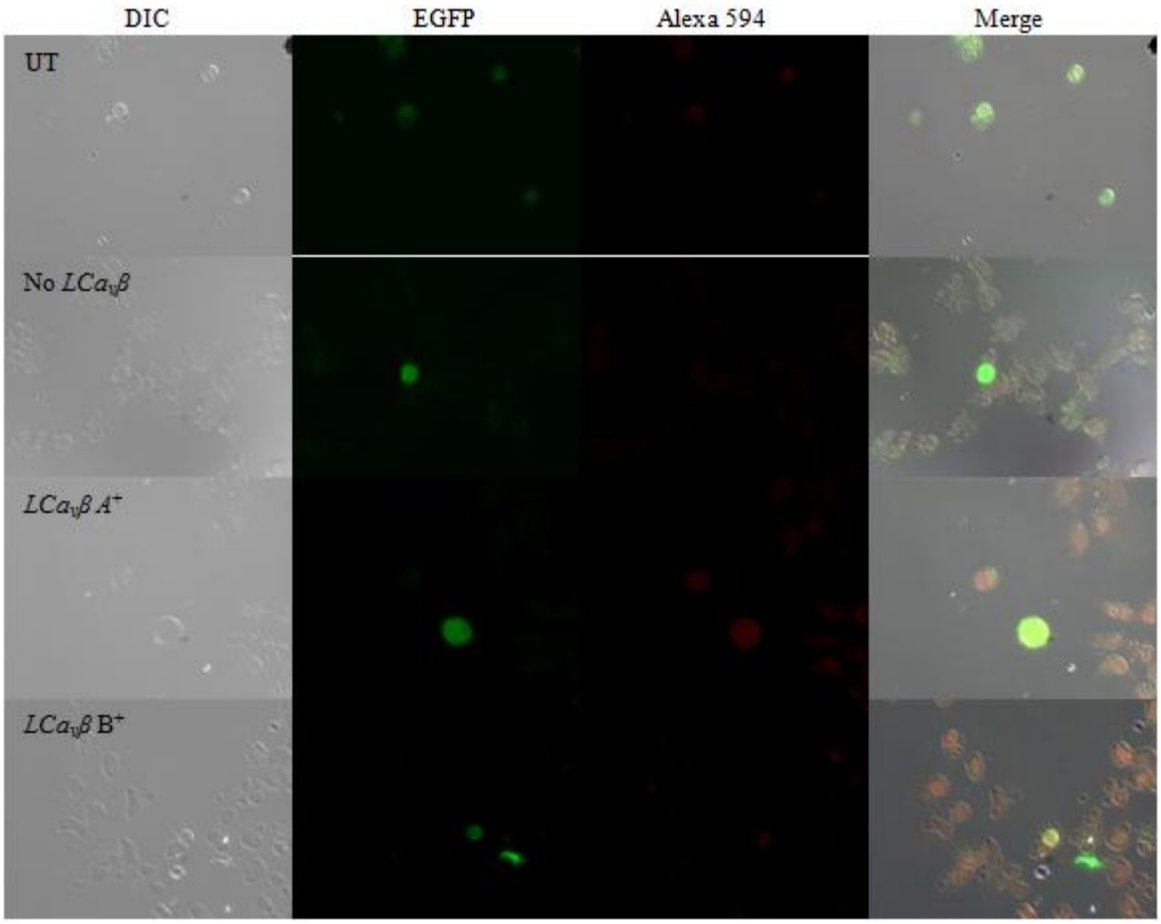

Figure 3.19: Localization of *LCa_v1*-EGFP and *$LCa_v\beta$* in transfected GripTite 293 MSR cells.

Untransfected (UT) control cells are shown in the top row. *LCa_v1* was directly tagged with EGFP (green), and *$LCa_v\beta$* was labeled with anti- *$LCa_v\beta$* antibody that was detected with an AlexaFlour594-conjugated secondary antibody (red). Images displayed are representative of 10 to 12 images.

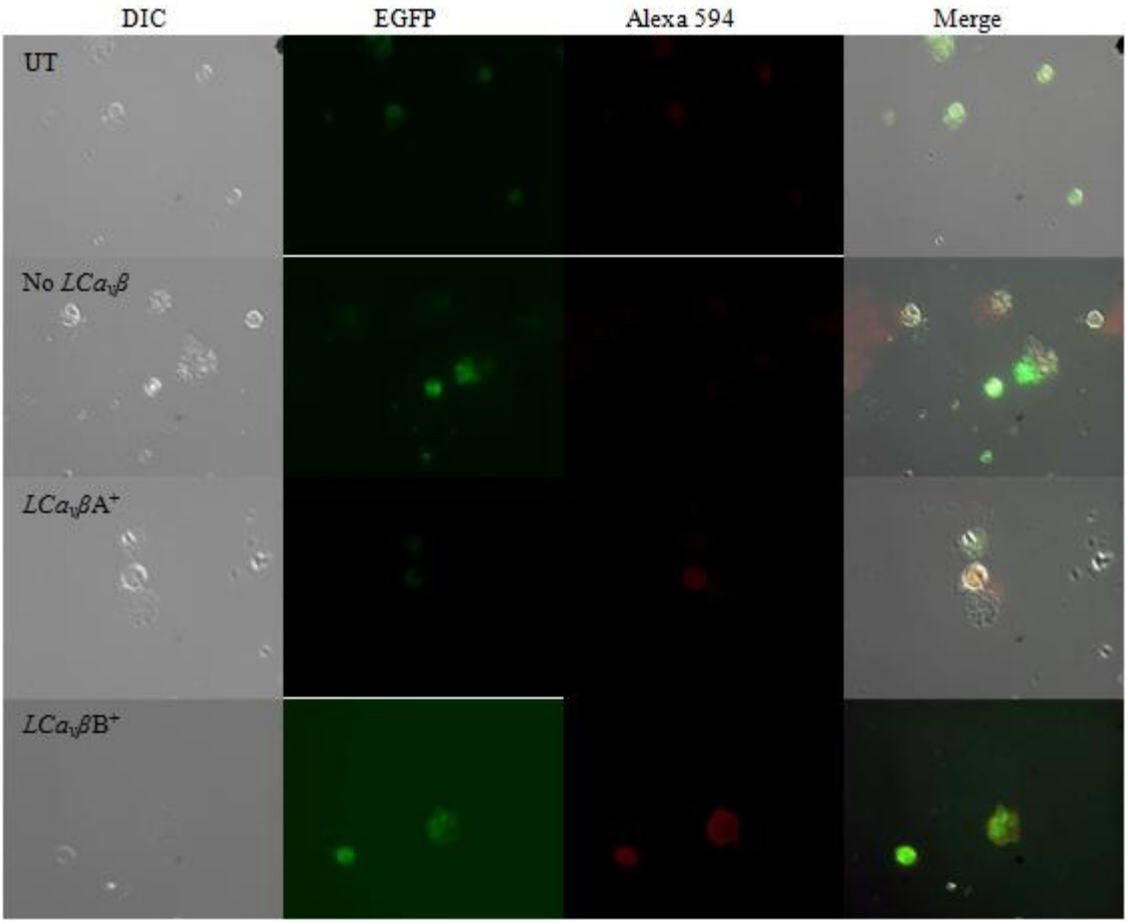

Figure 3.20: Localization of LCa_v2-EGFP and $LCa_v\beta$ in transfected GripTite 293 MSR cells.

Untransfected (UT) control cells are shown in the top row. LCa_v2 was directly tagged with EGFP (green), and $LCa_v\beta$ was labeled with anti- $LCa_v\beta$ antibody that was detected with an AlexaFlour594-conjugated secondary antibody (red). Images displayed are representative of 10 to 12 images

Table 3.1: Summary of *LCa$_v$1* electrophysiology results. Data is given as mean±SEM.

Electrophysiology		*LCa$_v$β$_{A+}$*	n	*LCa$_v$β$_{B+}$*	n	*LCa$_v$β$_{B-}$*	n
G$_{max}$ (pS)		0.0515±0.0117	7	0.0824±0.0222	24	0.0386±0.0353	5
E$_{rev}$ (mV)		55.19±1.45§		51.67±0.663$^{\#}$		50.35±2.63	
Activation	V$_{0.5}$(mV)	2.07±1.05§		0.475±0.0501$^{\#\P\P}$		3.55±1.07§§	
	K$_a$	7.09±0.19		6.77±0.133		6.96±0.174	
Inactivation	V$_{0.5}$(mV)	¯12.84±4.56	2	¯20.74±2.18	5	¯18.10±0.723	3
	K$_i$	11.82±0.499§		8.42±0.578$^{\#}$		8.76±0.830	
Peak Current (pA)		-111.01±17.99¶	7	-230.54±44.74	24	-178.28±11.69$^{\#}$	5
Kinetics at ¯10mV	t$_{peak}$(ms)	61.24±9.50		66.12±9.08	18	64.72±9.06	
	R$_{350}$	0.284±0.0929§		0.479±0.036$^{\#}$		0.533±0.0530	
Kinetics at 0mV	t$_{peak}$(ms)	64.86±12.22		51.31±5.56		65.64±11.20	
	R$_{350}$	0.557±0.0476¶		0.607±0.0179¶		0.701±0.0251$^{\#\S}$	
Kinetics at 10mV	t$_{peak}$(ms)	37.29±3.42		37.16±4.97		56.70±16.94	
	R$_{350}$	0.655±0.0428		0.608±0.0273¶		0.741±0.0522§	
Kinetics at 20mV	t$_{peak}$(ms)	38.66±5.24§		26.35±3.09$^{\#\P}$		47.46±8.82§	
	R$_{350}$	0.599±0.0424		0.549±0.0350		0.680±0.0777	
Kinetics at 30mV	t$_{peak}$(ms)	24.94±5.63		23.32±2.38¶		37.70±8.44§	
	R$_{350}$	0.465±0.0381		0.423±0.0459		0.571±0.102	

One Way ANOVA vs. *LCa$_v$β$_{A+}$*: #p<0.05, ##p<0.005
One Way ANOVA vs. *LCa$_v$β$_{B+}$*: §p<0.05, §§p<0.005
One Way ANOVA vs. *LCa$_v$β$_{B-}$*: ¶p<0.05, ¶¶p<0.005

therefore should be strictly localized to the membrane. This suggested that the *LCa$_v$β* subunits were complexing with the α_1 subunit at the cell membrane, but their role in the membrane trafficking of *LCa$_v$1* and *LCa$_v$2* remains unclear.

3.7 Electrophysiology

The modulatory effects of the novel *LCa$_v$β* subunits (*LCa$_v$β$_{B+}$ and LCa$_v$β$_{B-}$*) on snail *LCa$_v$1* and *LCa$_v$2* channels expressed heterologously in HEK 293T cells were assessed using whole-cell voltage clamping experiments. A summary of all electrophysiological data for *LCa$_v$1*and *LCa$_v$2* is presented in tables 3.1 and 3.2, respectively. In an attempt to graphically summarize

Table 3.2: Summary of *LCa$_v$2* electrophysiology results. Data is given as mean±SEM.

Electrophysiology		no *LCa$_v\beta$*	n	*LCa$_v\beta_{A+}$*	n	*LCa$_v\beta_{B+}$*	N	*LCa$_v\beta_{B-}$*	n
G_{max} (pS)		0.0546± 0.0148§	5	0.0303± 0.00229	9	0.0288± 0.00216*	8	0.0454± 0.00899	7
E_{rev} (mV)		56.27± 1.15$^{\#\#\S\P}$		67.18± 2.02**¶	10	65.55± 2.70*		61.00± 0.921$^{*\#}$	
Activation	$V_{0.5}$	18.04± 5.35		12.30± 0.96		12.07± 1.21		9.95± 1.07	
	K_a	8.12±0.80$^{\#\S\P\P}$		6.74±0.27*		6.49±0.30*		6.13±0.30**	
Inactivation	$V_{0.5}$	¯32.34±6.76	4	¯25.23±1.32§	7	¯33.12±4.20$^{\#}$	4	¯29.16±2.57	4
	K_i	10.54±1.21¶¶		9.60±1.33¶		9.82±1.15¶		5.62±0.21$^{**\#\S}$	
Peak Current (pA)		-56.93±13.94¶¶	5	-160.10±34.62¶	10	-260.49±116.05	8	-289.09±46.85$^{**\#}$	7
Kinetics at 0mV	Tau act	5.49±1.63	9	2.75±0.46	7	4.90±1.77	6	2.38±0.77	5
	Tau inact	33.85± 9.83		51.24± 19.21	8	51.82± 14.39	7	86.38± 26.55	7
Kinetics at 10mV	Tau act	1.66±0.24$^{\#\S}$		1.75±0.17*		1.25±0.17*		1.74±0.24	5
	Tau inact	66.37± 10.80		79.03± 17.69		57.76± 7.55		88.90± 13.85	7
Kinetics at 20mV	Tau act	1.46±0.28		1.08±0.05		1.17±0.06		1.32±0.15	5
	Tau inact	37.20± 3.51$^{\#\P\P}$		74.91± 17.48*		45.83± 4.60¶		79.95± 12.61**§	7
Kinetics at 30mV	Tau act	1.09±0.16		0.92±0.05		1.00±0.11		1.05±0.17	5
	Tau inact	34.87± 3.88$^{\#\P\P}$		60.55± 6.52*¶		44.92± 5.07¶¶		105.48± 15.84$^{**\#\S\S}$	7
Kinetics at 40mV	Tau act	0.89±0.12		0.96±0.21		0.82±0.10		1.00±0.27	5
	Tau inact	40.58±7.61$^{\#\P\P}$		67.92±9.74*§		42.79±6.97$^{\#\P\P}$		97.55±12.93**§§	7

One Way ANOVA vs. no *LCa$_v\beta$*: *p<0.05, **p<0.005
One Way ANOVA vs. *LCa$_v\beta_{A+}$*: #p<0.05, ##p<0.005
One Way ANOVA vs. *LCa$_v\beta_{B+}$*: §p<0.05, §§p<0.005
One Way ANOVA vs. *LCa$_v\beta_{B-}$*: ¶p<0.05, ¶¶p<0.005

the modulatory effects of *LCa$_v\beta$* subunits on calcium channel kinetics, representative traces of *LCa$_v$1* and *LCa$_v$2* (normalized to peak) can be seen in figures 3.21 and 3.22, respectively. It should be noted that there is no data for *LCa$_v$1* in the absence of *LCa$_v\beta$* subunits. Although more than 150 patches were made on cells from multiple transfections, no *LCa$_v$1* currents were ever produced in the absence of *LCa$_v\beta$* subunits. This suggests that the *Ca$_v\beta$* subunit is critical for *LCa$_v$1* trafficking *in vitro*. The discussion of results below will highlight the

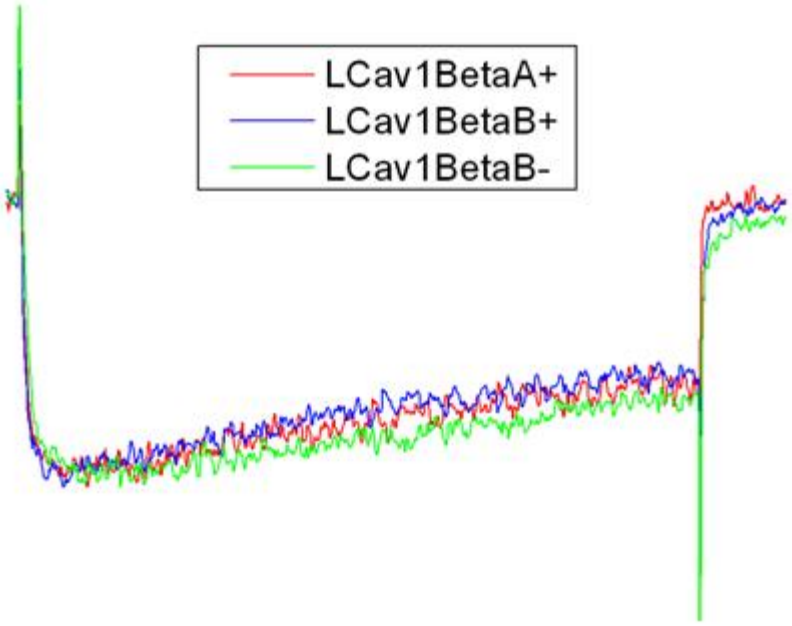

Figure 3.21: Representative traces of *LCa$_v$1*. Traces were recorded in the presence of $LCa_v\beta_{A+}$, $LCa_v\beta_{B+}$ or $LCa_v\beta_{B-}$ subunits at a test potential of 10mV for 450ms. Traces have been normalized to peak and then overlapped to highlight differences in overall channel activity. Note that inactivation decay is retarded by $LCa_v\beta_{B-}$ expression.

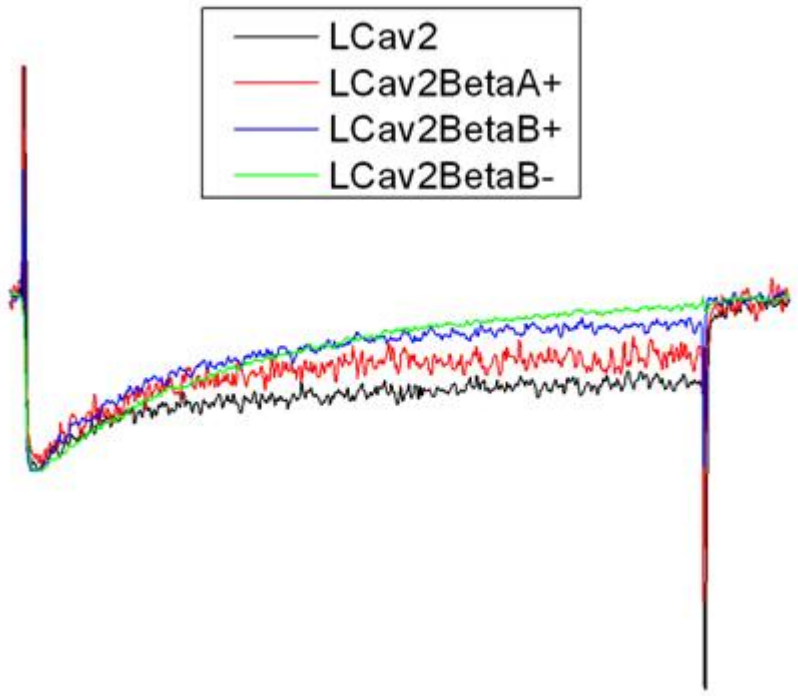

Figure 3.22: Representative traces of *LCa$_v$2*. Traces were recorded in the presence of $LCa_v\beta_{A+}$, $LCa_v\beta_{B+}$ or $LCa_v\beta_{B-}$ subunits at a test potential of 30mV for 450ms. Traces have been normalized to peak and then overlapped to highlight differences in overall channel activity.

electrophysiological properties imparted by differential $LCa_v\beta$ subunit expression and the physiological significance of these effects.

3.7.1 Current-Voltage Relationships and Peak Current Amplitude

Peak currents from LCa_v1 and LCa_v2 were measured from a holding potential of -100 mV to voltage steps in a range of -50 mV to +50 mV in 10mV increments. These current-voltage relationships reflect the voltage-sensitivity of channels to opening in response to a depolarizing stimulus like an action potential. Illustrated in figure 3.23, it is evident that neither $LCa_v\beta_{A+}$, $LCa_v\beta_{B+}$, nor $LCa_v\beta_{B-}$ significantly shifted the current-voltage curves of LCa_v1. The IV curves for LCa_v2 (figure 3.24) revealed only slight deviations in the current-voltage relationship involving slight hyperpolarizing shifts induced by $Ca_v\beta$ subunit expression. A hyperpolarizing shift (to the left) indicates that there is a greater probability of channel opening at lower (more hyperpolarized) voltages. In other words, more channels will be recruited to open in response to smaller depolarizations caused by the arrival of action potentials at the axon terminal. In effect, this would allow for the influx of Ca^{2+} into the cell to occur more rapidly since less stimulation would be required to activate channels.

Maximal peak currents from -50 mV to +50 mV were used to infer the effect of $LCa_v\beta$ subunit expression on the current density of LCa_v1 and LCa_v2. Since the maximal current size is dependent on the number of functional channels, it can be used to infer how many channels are being trafficked to the membrane. In mammalian systems, $Ca_v\beta$ subunits have been shown to increase the current density, which is thought to be accomplished by

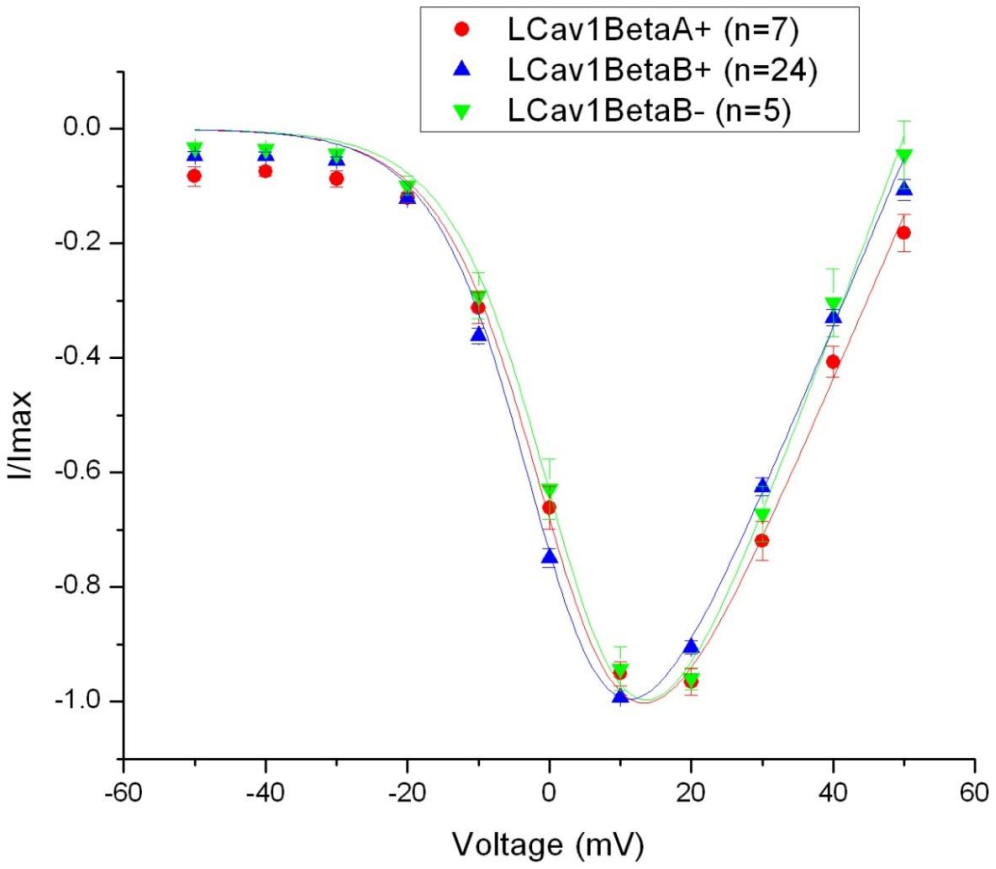

Figure 3.23: Current-Voltage relationship of *LCa$_v$1*. Comparison of *LCav1* whole-cell current-voltage relationship when co-expressed with *LCa$_v\beta_{A+}$*, *LCa$_v\beta_{B+}$* or *LCa$_v\beta_{B-}$* subunits. No significant changes were noted. Curves have been fitted using the OhmicBoltzmann equation and data points represent mean±SEM.

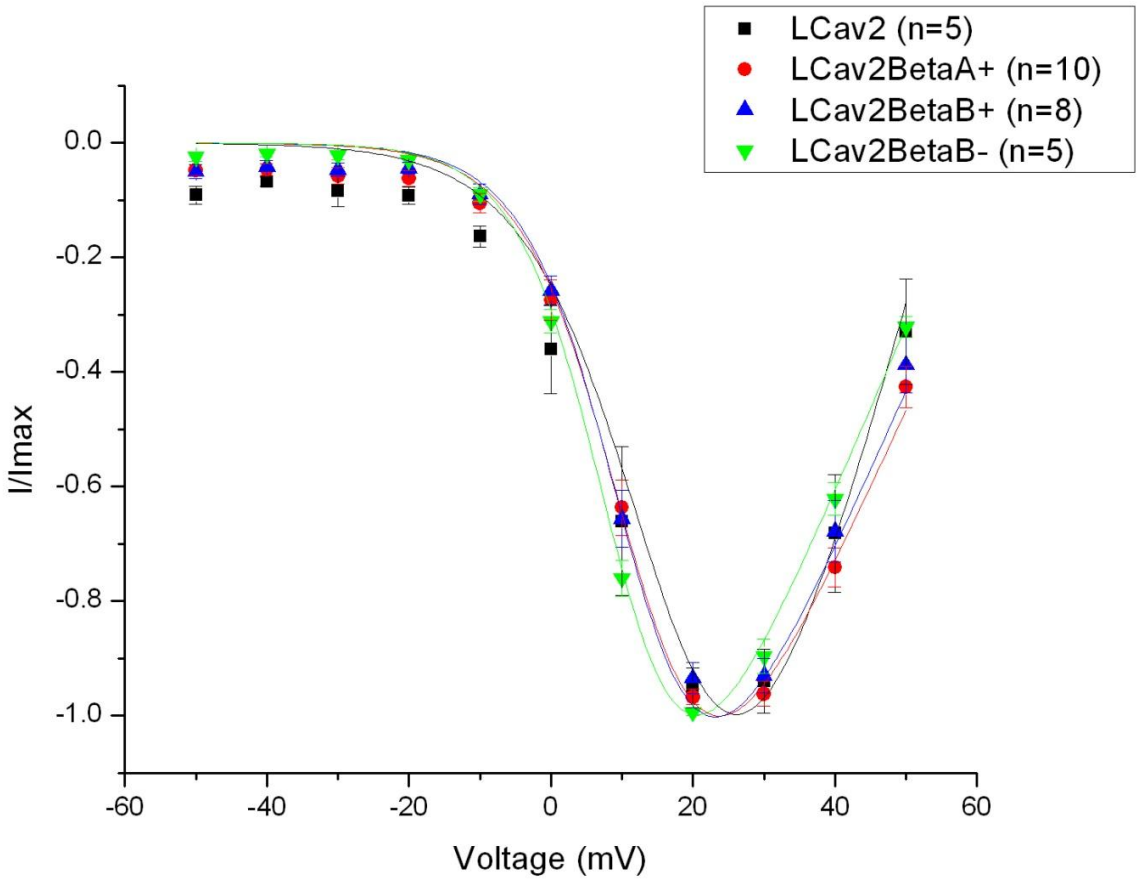

Figure 3.24: Current-Voltage relationship of *LCa$_v$2*. Comparison of *LCa$_v$2* whole-cell current-voltage relationship when co-expressed with *LCa$_v\beta_{A+}$*, *LCa$_v\beta_{B+}$* or *LCa$_v\beta_{B-}$* or no *LCa$_v\beta$* subunit. Curves have been fitted using the OhmicBoltzmann equation and data points represent mean±SEM.

assisting in the assembly and membrane trafficking of the α_1 subunit. The data from each current-voltage recording (regardless of the voltage) was used to construct the box plots of peak current amplitude for *LCa$_v$1* and *LCa$_v$2* in figures 3.25A and 3.26A, respectively. As both figures illustrate, there were some significant changes in the amplitude of the peak current for both *LCa$_v$1* and *LCa$_v$2* induced by the expression of *Ca$_v\beta$* subunits. The co expression of *LCa$_v\beta_{A+}$* resulted in lower *LCa$_v$1* current amplitude (-111.01±17.99 pA) when compared to either *LCa$_v\beta_{B-}$* (-178.28±11.69 pA; *p=0.018*) or *LCa$_v\beta_{B+}$* (-230.54±44.74 pA; not statistically significant). In figure 3.26, it can be seen that *LCa$_v\beta_{B-}$* caused an increase in the peak current of *LCa$_v$2* (to -289.09±46.85 pA) as compared to no *LCa$_v\beta$* subunit (-56.93±13.94 pA; *p=0.002*) or *LCa$_v\beta_{A+}$* (-160.10±34.62 pA; *p=0.039*). Although the expression of *LCa$_v$2* with *LCa$_v\beta_{B+}$* resulted in an average peak current of -260.49±116.05 pA, it did not result in any statistically significant differences due to the high level of variability between cells.

The current through an ion channel is a function of the conductance and driving force. The driving force is a function of the membrane potential minus the reversal potential for that ion, and is greatest at low potentials when the difference between membrane and reversal potentials is greatest. However, at these low potentials, the calcium channels are not conducting or gating. Whole-cell conductance is a function of the number of open channels, which increases with depolarization. The amplitude of the currents in the IV curves were therefore influenced by both driving force and conductance, but when this data is transformed by the Boltzmann equation (as during the construction of activation curves) the effects of driving force are removed. In voltage-clamp experiments the membrane potential is

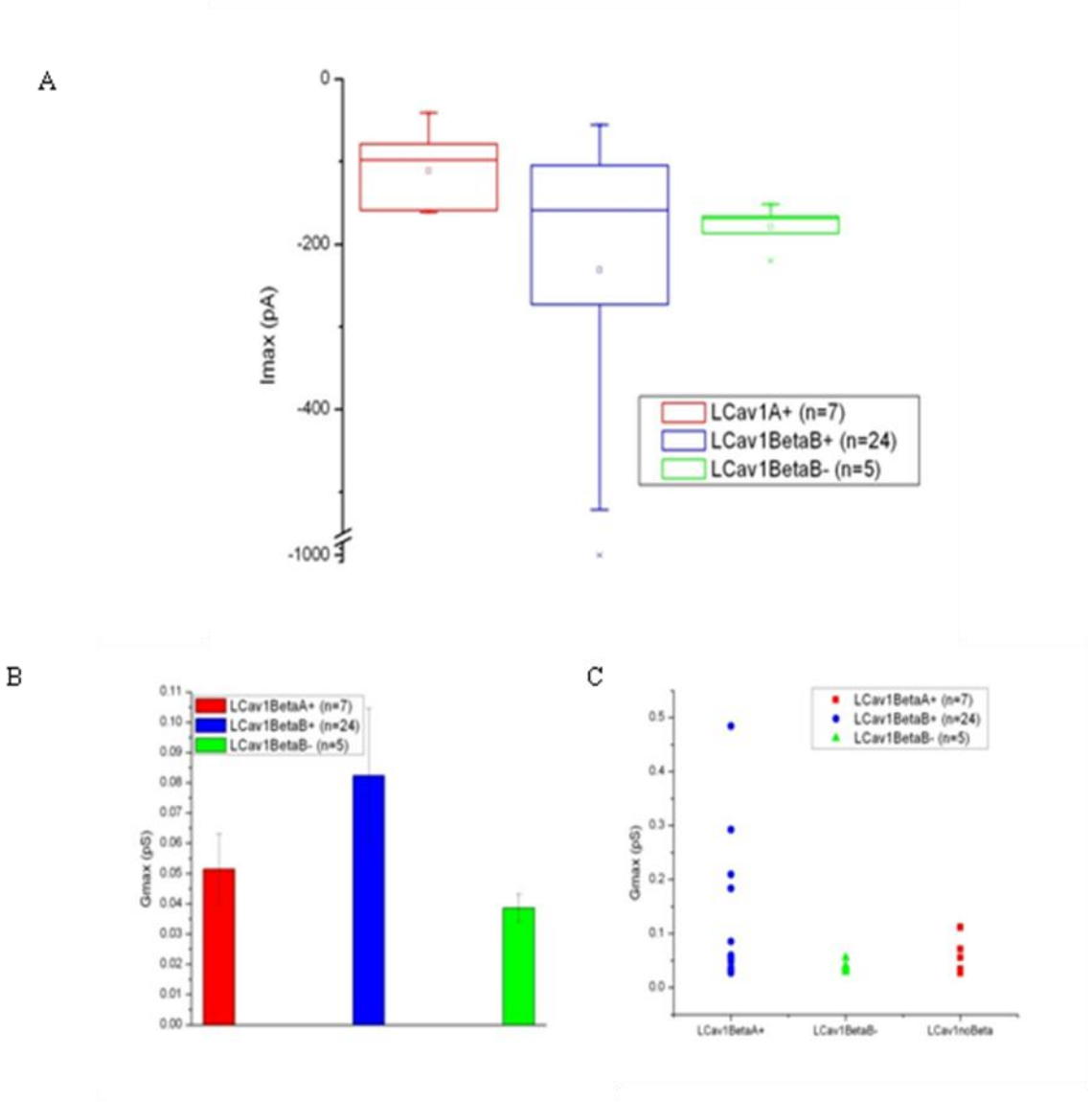

Figure 3.25: Peak current amplitude and conductance of *LCa$_v$1*. (A) Box plots depicting peak current amplitude when *LCa$_v$1* was co-expressed with either *LCa$_v$β$_{A+}$*, *LCa$_v$β$_{B+}$* or *LCa$_v$β$_B$-*. No currents were obtained in the absence of *LCa$_v$β* suggesting that *LCa$_v$β* may be required for membrane expression of functional *LCa$_v$1* channels. (B) Bar chart depicting the average maximal conductance values when *LCa$_v$1* was co-expressed with *LCa$_v$β$_{A+}$*, *LCa$_v$β$_{B+}$* or *LCa$_v$β$_B$-*. No changes in conductance were statistically significant (C) Scatter of individual values used in (B). Data in (A) and (B) represent mean±SEM.

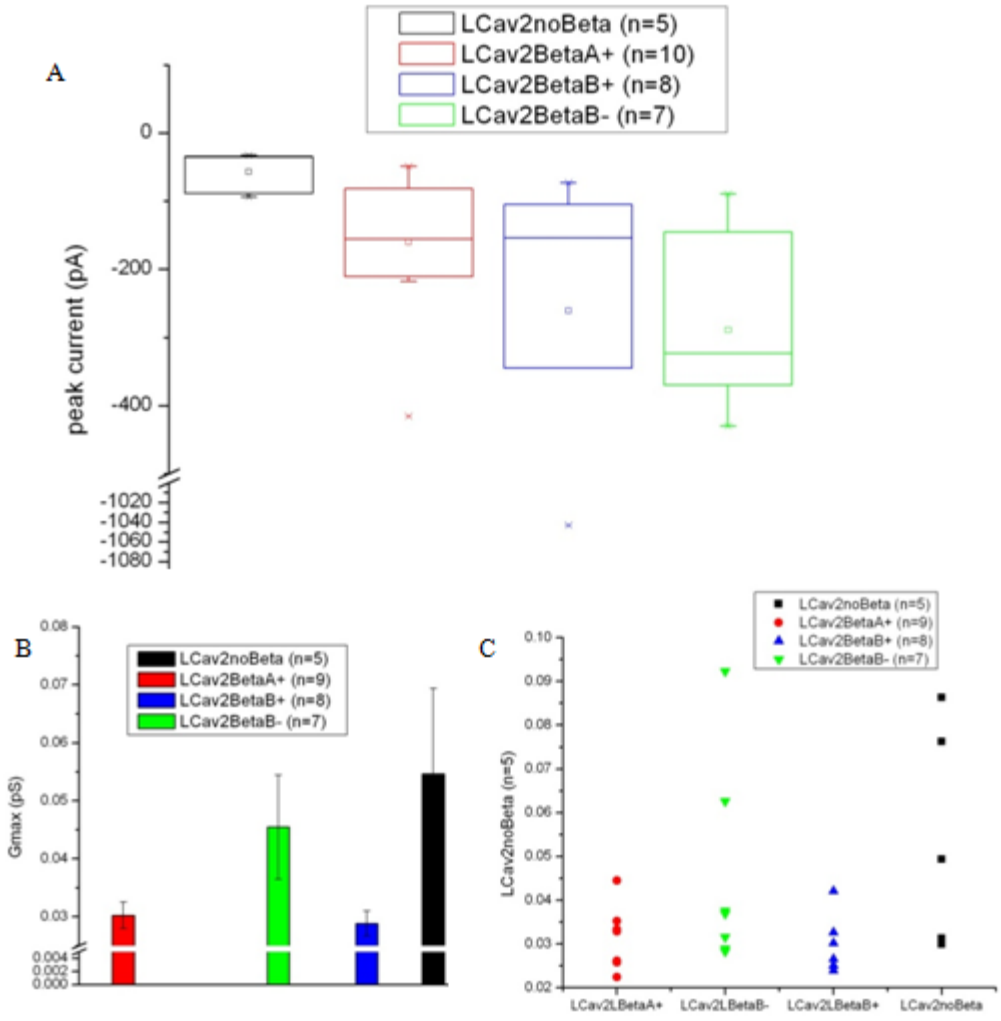

Figure 3.26: Peak current amplitude and conductance of *LCa$_v$2*. (A) Box plots depicting peak current amplitude when *LCa$_v$2* was co-expressed with either *LCa$_v\beta_{A+}$*, *LCa$_v\beta_{B+}$* , *LCa$_v\beta_{B-}$* or no *LCa$_v\beta$* subunit. Although peak current generally increased with *LCa$_v\beta$* expression, only *LCa$_v\beta_{B-}$* was significantly larger than no *LCa$_v\beta$* and *LCa$_v\beta_{A+}$* (B) Bar chart depicting the average maximal conductance values when *LCa$_v$2* was co-expressed with *LCa$_v\beta_{A+}$*, *LCa$_v\beta_{B+}$* , *LCa$_v\beta_{B-}$* or no *LCa$_v\beta$*. *LCa$_v\beta_{B+}$* expression resulted in lowered conductance of *LCa$_v$2*. (C) Scatter of individual values used in (B). Data in (A) and (B) represent mean±SEM.

constant, and so the whole-cell conductance values are therefore representative of the rate of ion flow into the cell through a single open channel multiplied by the number of recruited channels that are open. As figure 3.25 shows, there were no significant differences in maximal *LCa$_v$1* conductance as a result of *LCa$_v$β* subunit expression. The maximal conductance of *LCa$_v$2* (0.0546±0.0148 pS), however, was lowered by *LCa$_v$β* subunit expression (figure 3.26), although the only statistically significant decrease was caused by the expression of *LCa$_v$β*$_{B+}$ (0.0288±0.00216 pS). In physiological terms, this decrease in conductance would lessen the amount of Ca^{2+} gated into the cell upon the arrival of an action potential, effectively dampening the release of neurotransmitters and other second-messenger effects induced by Ca^{2+} influx.

3.7.2 Voltage-Dependence of Activation

The current-voltage relationship data was subjected to a Boltzmann transformation and curve fit to produce the activation curves of *LCa$_v$1* and *LCa$_v$2*. These curves describe the fraction of channels that have opened (become activated) from the resting (closed) state upon depolarization to a given voltage. In studies of mammalian VGCCs expressed in HEK 293T cells, *Ca$_v$β* subunits were found to generally cause a slight hyperpolarization of the voltage-dependence of activation (Yasuda et al., 2004). Small, but statistically significant differences were seen in the half-activation potential ($V_{0.5}$) of *LCa$_v$1* (figure 3.27, table 3.1), which represents the potential at which 50% of the channels present in the cell have become activated from the closed state. The expression of *LCa$_v$β*$_{B+}$ caused a hyperpolarizing shift in

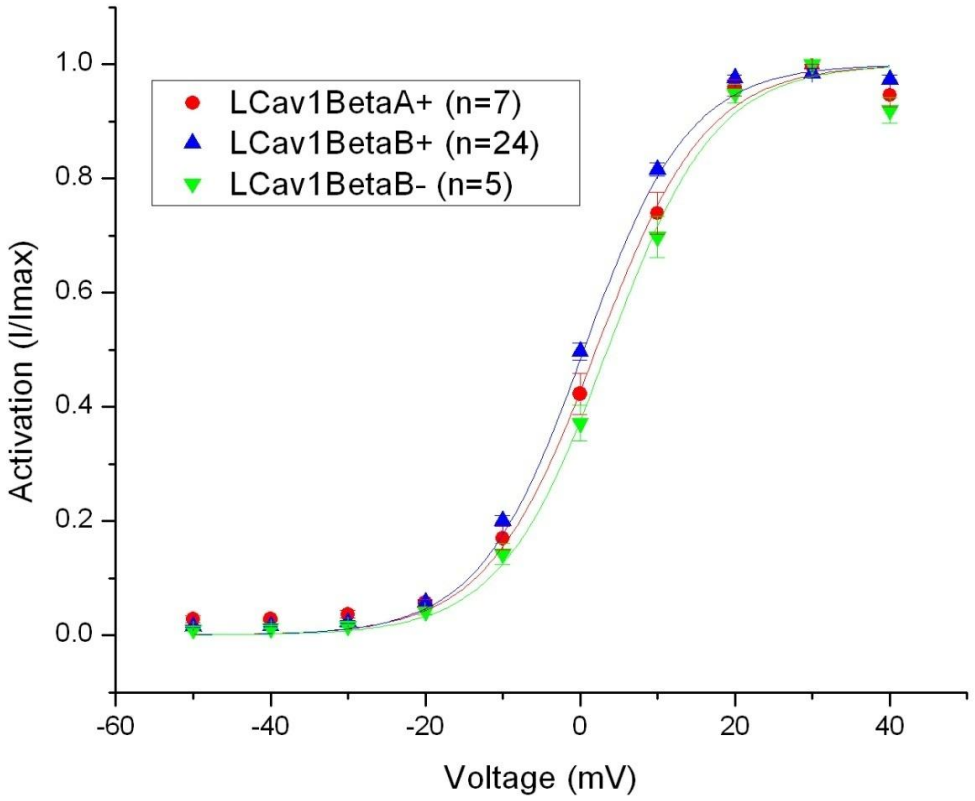

Figure 3.27: Activation curve of *LCa$_v$1*. Effect of *LCa$_v$β* subunit isoforms on activation of *LCa$_v$1* channels expressed in HEK 293T cells obtained by whole-cell patch clamp recording. Curves have been fitted with the Boltzmann equation and data points represent mean±SEM. Note that a small hyperpolarizing shift has been induced by the expression of *LCa$_v$β$_{B+}$*.

the half-activation potential to 0.475±0.0501mV as compared with 2.07±1.05mV (*p=0.007*) and 3.55±1.07mV (*p=0.000*) for $LCa_v\beta_{A+}$ and $LCa_v\beta_{B-}$, respectively. In physiological terms, this translates to more calcium entry into the cells at lower voltage thresholds, potentially leading to easier excitability of tissues expressing the $LCa_v\beta_{B+}$ isoform. The hyperpolarizing shifts seen here are a hallmark feature of $Ca_v\beta$ subunit modulation and are also observed mammalian channels.

Although no significant shifts in half-activation potential of the activation curve of *LCav2* were noted, a hyperpolarizing effect was caused by a steepening of the slope of the activation curve (K_a), as illustrated in figure 3.28. The co-expression of any *LCavβ* isoform with *LCav2* caused a significant decrease in K_a for all *LCavβ* subunit isoforms when compared to channels expressed in the absence of *LCavβ* subunits ($LCa_v\beta_{A+}$: *p=0.010*; $LCa_v\beta_{B+}$: *p=0.006*; $LCa_v\beta_{B-}$: *p=0.002*). No significant differences in activation between the various *LCavβ* subunits were observed. Steepening of the curve indicates that the voltage-sensing machinery has become more sensitive to voltage changes, such that the same depolarization causes greater conductance changes. These shifts in the voltage dependence of activation, in effect, increase the sensitivity of the calcium channel complex to a depolarizing stimulus such as an action potential. Under these conditions of increased voltage-sensitivity to depolarization, physiological process initiated by calcium influx, such as neurotransmitter release or muscle contraction, will occur more readily since less depolarization of the cell membrane is needed.

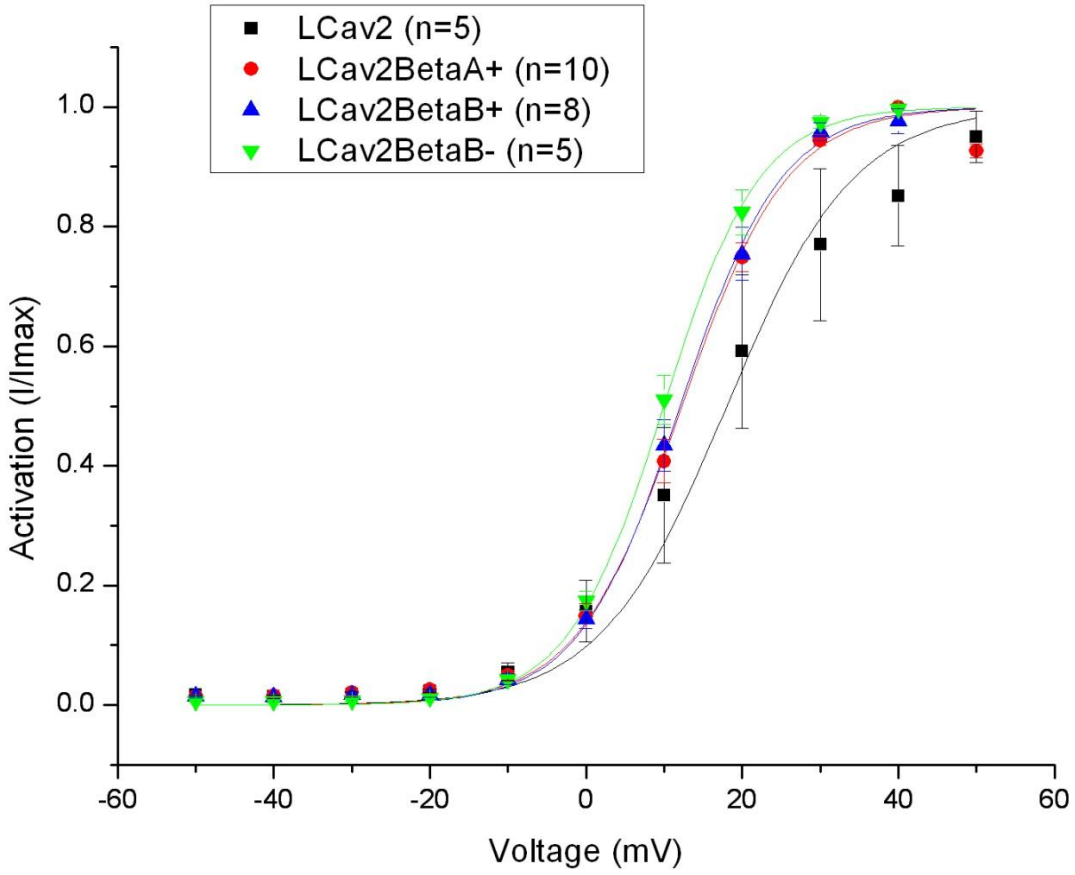

Figure 3.28: Activation curve of *LCa$_v$2*. Effect of *LCa$_v\beta$* subunit isoforms on activation of *LCa$_v$2* channels expressed in HEK 293T cells obtained by whole-cell patch clamp recording. Curves have been fitted with the Boltzmann equation and data points represent mean±SEM. Note that expression of *LCa$_v\beta_{A+}$*, *LCa$_v\beta_{B+}$* and *LCa$_v\beta_{B}$*- always resulted in a hyperpolarization of the curve due to a decrease (steepening) of K_a.

3.7.3 Steady-State Inactivation

A steady-state inactivation curve measures the fraction of channels that have switched from the activated state to the inactivated (refractory) state at a given voltage. In order to assess the effect of $LCa_v\beta$ subunit expression on the steady state-inactivation of LCa_v1 and LCa_v2, a brief depolarizing step to peak (10mV for LCa_v1; 30mV for LCa_v2) was taken, followed by a long conditioning pulse in the voltage range of -100mV to 20mV (increasing by 10mV each sweep). This conditioning pulse lasted until channels were fully inactivated at peak potential (up to 15 seconds). After the long conditioning pulse, which induced inactivation in a subset of the population of channels, a second brief step to peak was taken to assess the fraction of channels that are inactivated by sustained depolarization to a given potential.

Steady-state inactivation analysis of LCa_v1 (figure 3.29) revealed no significant shifts in the half-inactivation potentials, although the standard error values were quite large (Table 3.1). The half-inactivation potential is the voltage at which 50% of channels in a given population have reverted from the open state to an inactivated, refractory state and cannot be opened regardless of the depolarizing stimulus. When the slope of the inactivation curve (K_i) was compared there was a significant difference ($p=0.019$) noted between $LCa_v\beta_{A+}$ (11.82±0.499) and $LCa_v\beta_{B+}$ (8.42±0.578). Although the K_i of $LCa_v\beta_{B-}$ was 8.76±0.830, it was not statistically different from $LCa_v\beta_{A+}$ ($p=0.122$). These changes in K_i indicate that when $LCa_v\beta_{A+}$ was expressed, the steady-state inactivation of LCa_v1 was altered in such a way that the inactivation of channels was less sensitive to increases in membrane potential, allowing channels to remain open longer thereby increasing Ca^{2+} influx into the cell.

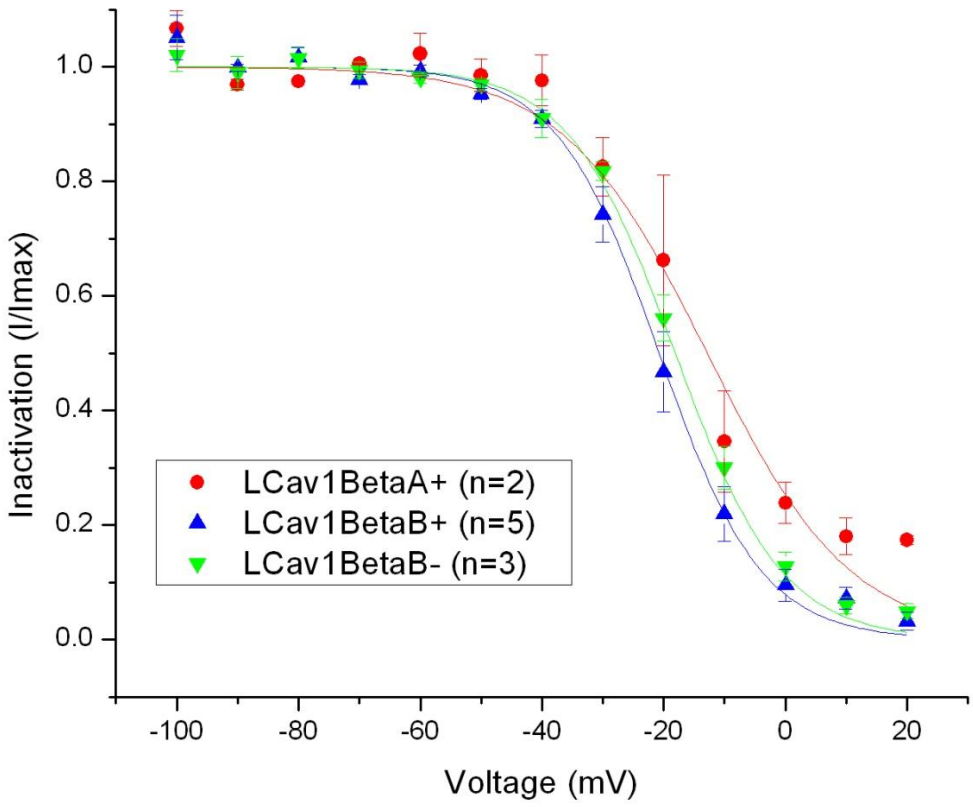

Figure 3.29: Steady-state inactivation curves of *LCav1*. Effect of $LCa_v\beta$ subunit isoforms on steady-state inactivation of LCa_v1 channels expressed in HEK 293T cells. Data was obtained by whole-cell patch clamp recording and curves have been fitted with the Boltzmann equation . Data points represent mean±SEM. Co-expression of $LCav\beta_{A+}$ produced a depolarizing shift due to an increase in K_i.

Analysis of the effect of $LCa_v\beta$ subunit expression on the steady-state inactivation of LCa_v2 has produced some interesting results, as seen in figure 3.30. Most notably, the slope of the inactivation curve is drastically steepened when $LCa_v\beta_{B-}$ is co-expressed with LCa_v2, in comparison to no $LCa_v\beta$ subunit ($p=0.004$), $LCa_v\beta_{A+}$ ($p=0.042$) or $LCa_v\beta_{B+}$ ($p=0.011$). This signifies that the steady-state inactivation of LCa_v2 was delayed in the presence of $LCa_v\beta_{B-}$, and then occurred more rapidly as compared to other $LCa_v\beta$ subunit isoforms indicating an increase in the voltage-sensitivity of inactivation. When the half-inactivation potentials were compared, some differences were noted (Table 3.1). However, the only statistically significant difference was the shift from -25.23±1.32mV to -33.12±4.20mV ($p=0.049$) when we compare the co-expression of LCa_v2 with $LCa_v\beta_{A+}$ and $LCa_v\beta_{B+}$, respectively. Although similar differences were observed in other datasets, they were not statistically significant, and so it appears as though the expression of $LCa_v\beta_{A+}$ caused channels to delay entry into the refractory state until greater levels of depolarization are reached. The effects induced by the expression of $LCa_v\beta_{A+}$ would allow LCa_v2 channels to remain open longer thereby increasing total Ca^{2+} influx into the cell. Ordinarily, sustained influx of Ca^{2+} is halted by channel inactivation. The refractory state of the channels keeps the levels of free Ca^{2+} in the cytosol from elevating to toxic levels. Physiologically, a longer duration of Ca^{2+} influx will allow for downstream processes affected by Ca^{2+}, such as muscle contraction or neurotransmitter release, to be sustained for a longer time period.

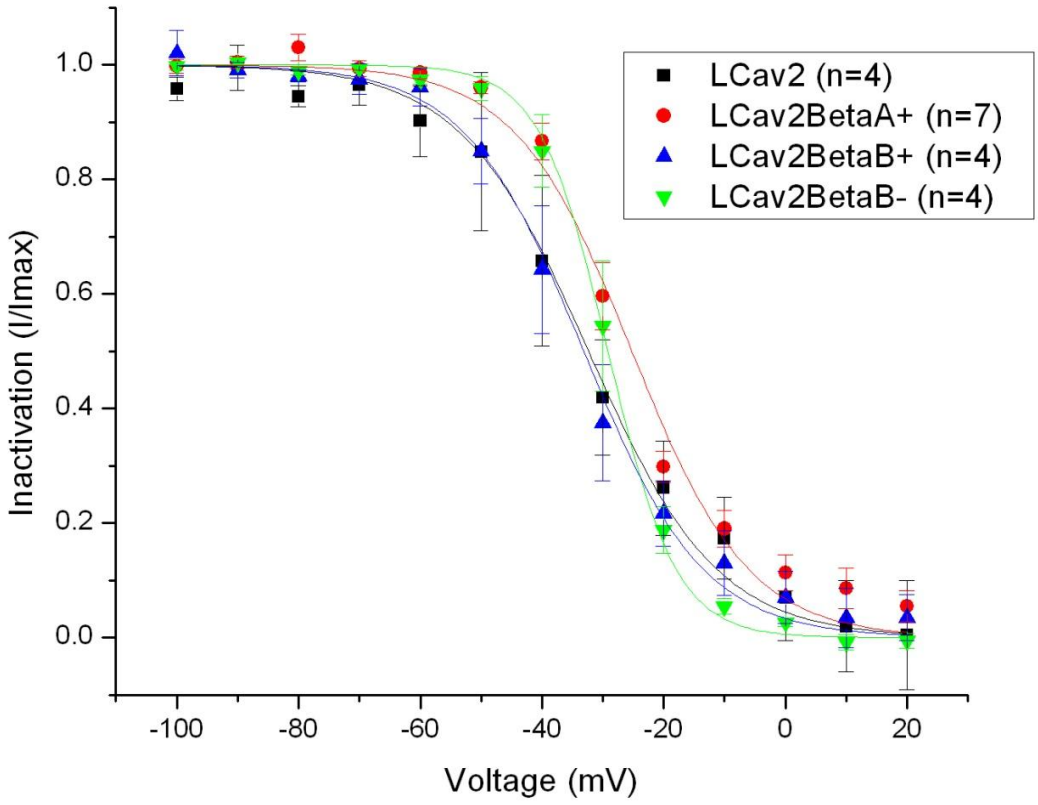

Figure 3.30: Steady-state inactivation curves of *LCa$_v$2.* Effect of *LCa$_v$β* subunit isoforms on steady-state inactivation of *LCa$_v$2* channels expressed in HEK 293T cells. Data was obtained by whole-cell patch clamp recording and curves have been fitted with the Boltzmann equation . Data points represent mean±SEM. Co-expression of *LCavβ$_{A+}$* produced a depolarizing shift due to an increase in the half-inactivation potential, while co-expression of *LCavβ$_{B-}$* resulted in drastic decreases in the slope of the inactivation curve.

3.7.4 Gating Kinetics

Finally, it was important to examine the kinetics of activation and inactivation. Activation kinetics describe the speed with which a population of channels open after receiving a depolarizing stimulus and can be measured several ways. The activation kinetics of LCa_v1 were measured as the time to reach peak (in ms) after the application of a depolarizing stimulus, while the tau values of activation were calculated for LCa_v2. Tau values represent the point in time when two thirds of channels present in a cell have opened. In both cases, larger values indicate an increased latency period between depolarization and activation due to conformational changes which must occur in the α_1 subunit. Activation was found to be voltage dependent, so values were measured at test pulses of different voltages. In mammals, the expression of $Ca_v\beta$ subunits was found to speed up activation kinetics in some cases.

When the effects of $LCa_v\beta$ subunit expression on activation kinetics of LCa_v1 were compared, few significant differences were noted as illustrated in figure 3.31. The expression of the $LCa_v\beta_{B-}$ subunit resulted in an increase in the time to peak current, as compared to $LCa_v\beta_{B+}$, when cells were depolarized to 20mV and 30mV. At 20mV, the time to peak current increased from 26.35±3.09ms in the presence of $LCa_v\beta_{B+}$ to 47.46±8.82ms when $LCa_v\beta_{B-}$ was expressed ($p=0.009$). Similarly, at 30mV, the time to peak had increased ($p=0.031$) from 23.32±2.38ms (when $LCa_v\beta_{B+}$was expressed) to 37.70±8.44ms when exon 7B was removed (as in $LCa_v\beta_{B-}$). The time to activation was also considerably slower in the presence of $LCa_v\beta_{A+}$ (38.66±5.24ms) as compared to $LCa_v\beta_{B+}$ ($p=0.049$),but not $LCa_v\beta_{B-}$. It is evident by comparison of $LCa_v\beta_{B+}$ and $LCa_v\beta_{B-}$ that the seven amino acid insert in the HOOK region (exon 7B) results in more rapid activation of LCa_v1. Physiologically, more

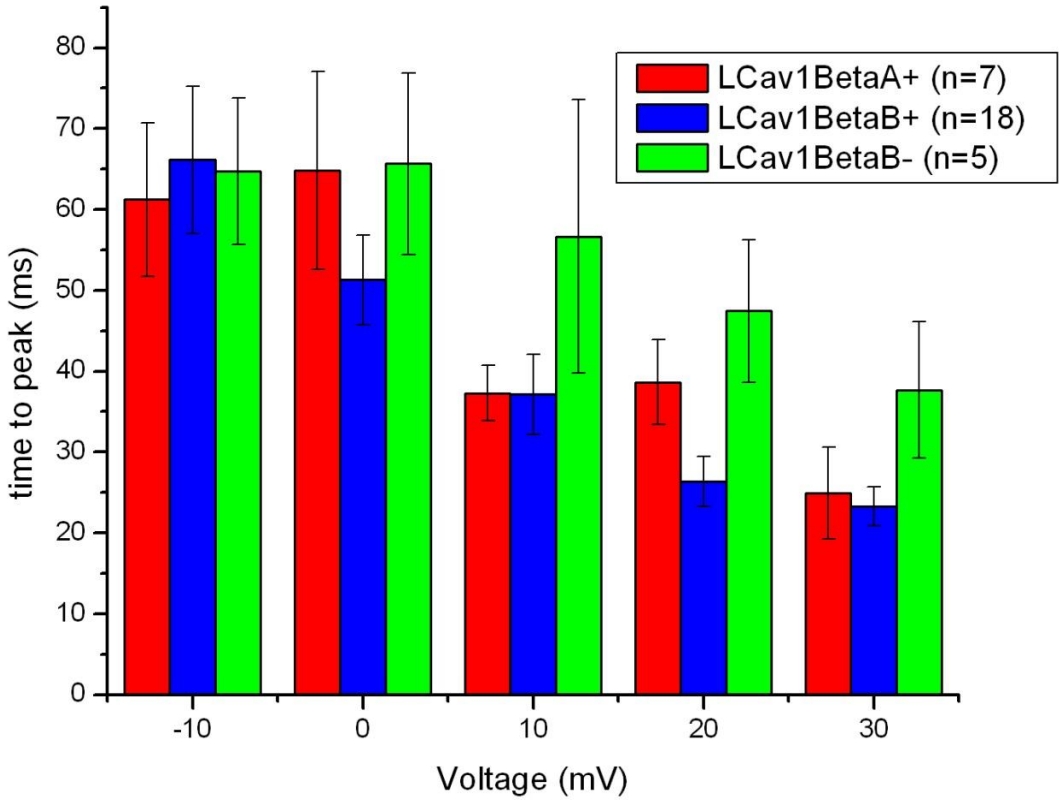

Figure 3.31: Activation kinetics of *LCa$_v$1.* Effects of *LCa$_v$β* expression on the time to peak (ms) is plotted as a measure of latency to channel opening. Bars represent mean±SEM. When the kinetics imparted by *LCa$_v$β$_{B+}$* and *LCa$_v$β$_{B-}$* were compared, it was observed that the presence of exon 7B (in *LCa$_v$β$_{B+}$*) mediated an increase in the speed of channel activation following depolarization to 20mV and 30mV.

rapid activation means that there will be increased Ca^{2+} influx as channels are able to open quicker, leading to more rapid coupling of electrical and chemical signals such as the arrival of an action potential at a nerve terminal and neurotransmitter exocytosis or muscle contraction.

The kinetics of *LCa$_v$2* activation were not significantly altered by the coexpression of *LCa$_v$β* subunits. The only exception is that the tau of activation at 10mV (figure 3.32) was slightly raised and lowered, respectively, when *LCa$_v$β$_{A+}$*or *LCa$_v$β$_{B+}$* were expressed. As compared to a tau of activation of 1.66±0.24ms in the absence of *LCavβ* subunits, it increased to 1.75±0.17ms with *LCa$_v$β$_{A+}$* (*p=0.049*) and decreased to 1.25±0.17ms with *LCa$_v$β$_{B+}$* (*p=0.040*). Perhaps the reciprocal effects of *LCa$_v$β$_{A+}$* and *LCa$_v$β$_{B+}$* are physiologically relevant as they could act in concert to effectively fine-tune electrochemical coupling mechanisms, however, this is unclear as the expression of *LCa$_v$β$_{B-}$* had no effect on the tau of activation.

Similar to activation kinetics, inactivation kinetics can be quantified several ways. Due to the extremely slow inactivation of *LCa$_v$1*, the rate of inactivation was measured by determining the fraction of current that remained 350ms after reaching peak (R_{350}). Since the inactivation of *LCa$_v$2* was more rapid, the inactivation decay could be fit with an exponential curve that allowed for the determination of the tau of inactivation, which is a parameter that represents the time after peak when approximately two thirds of all channels in a cell have entered the inactivated state. In either case, the larger the R_{350} or tau, the slower the inactivation kinetics (channels are delaying the transition from the open state to the refractory state). The inactivation is voltage dependent, so the R_{350} and tau values can be measured at

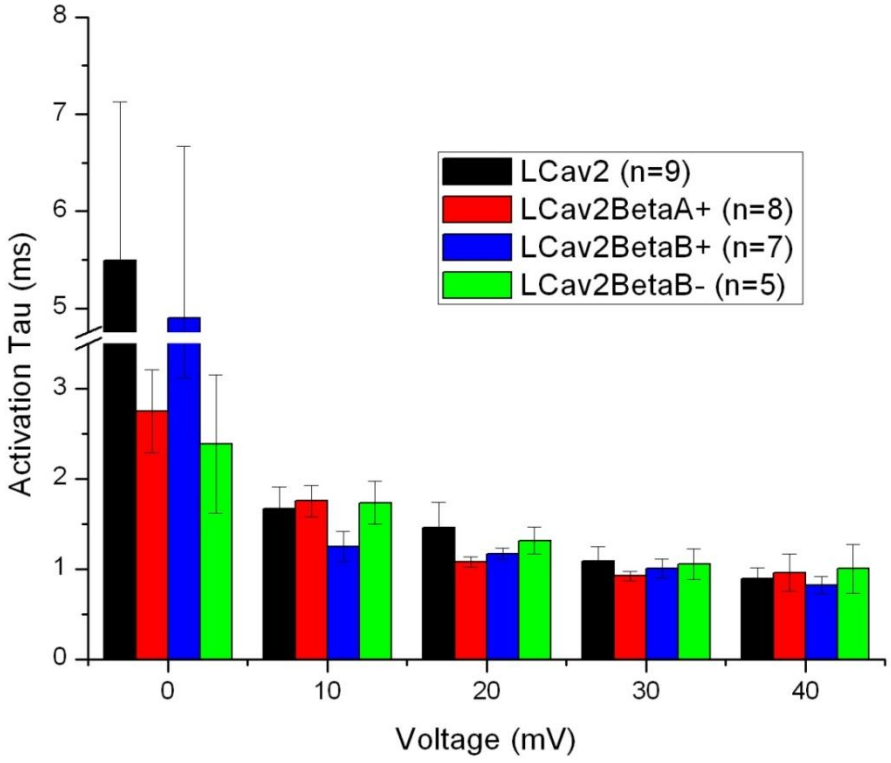

Figure 3.32: Activation kinetics of *LCa_v2*. Effects of *$LCa_v\beta$* expression on the tau of activation are plotted as a measure of latency to channel opening. Bars represent mean±SEM. No significant difference in activation of *LCa_v2* were observed as a result of differential *$LCa_v\beta$* expression.

test pulses of different voltages. In mammals, $Ca_v\beta$ subunit expression has varying effects on the kinetics of inactivation, with $Ca_v\beta_{2a}$ slowing it while the other three $Ca_v\beta$ subunits either accelerate it or have no effect (Yasuda et al., 2004).

The inactivation kinetics of LCa_v1 seemed to be affected by $LCa_v\beta$ subunit expression, especially in the range of -10 to 10mV. The R_{350} plot seen in figure 3.33 shows that when LCa_v1 is expressed with $LCa_v\beta_{B-}$, the inactivation is slowed as compared to $LCa_v\beta_{A+}$ or $LCa_v\beta_{B+}$. These differences were significant when cells were depolarized to 0mV, as compared to $LCa_v\beta_{A+}$ ($p=0.039$) and $LCa_v\beta_{B+}$ ($p=0.018$), whereas at 10mV it is only different from $LCa_v\beta_{B+}$ ($p=0.034$). One interesting finding is that, at -10mV, the R_{350} is increased by the expression of $LCa_v\beta_{B+}$ or $LCa_v\beta_{B-}$ (as compared to $LCa_v\beta_{A+}$), although the only statistically significant difference was with $LCa_v\beta_{B+}$ ($p=0.025$). Based on these observations it appears as though the removal of exon 7B from the HOOK region has resulted in delayed inactivation of LCa_v1, which would allow for sustained calcium influx into the cell over long periods of depolarization.

At voltage ranges around and slightly above peak, there were several interesting changes in the tau of inactivation for LCa_v2 induced by the differential expression of $LCa_v\beta$ subunits (figure 3.34). Interestingly, the tau of inactivation is always highest when LCa_v2 is coexpressed with $LCa_v\beta_{B-}$. At voltages of 20mV, 30mV and 40 mV, these differences are statistically significant as compared to cells not expressing $LCa_v\beta$ ($p=0.003, 0.000, 0.001$) and $LCa_v\beta_{B+}$ ($p=0.030, 0.005, 0.005$). $LCa_v\beta_{A+}$ was only significantly different at 30mV ($p=0.026$) with a tau of inactivation that was higher than that of no $LCa_v\beta$ and $LCa_v\beta_{B+}$. This data suggests that perhaps the HOOK region insertion causes a quickening of inactivation in

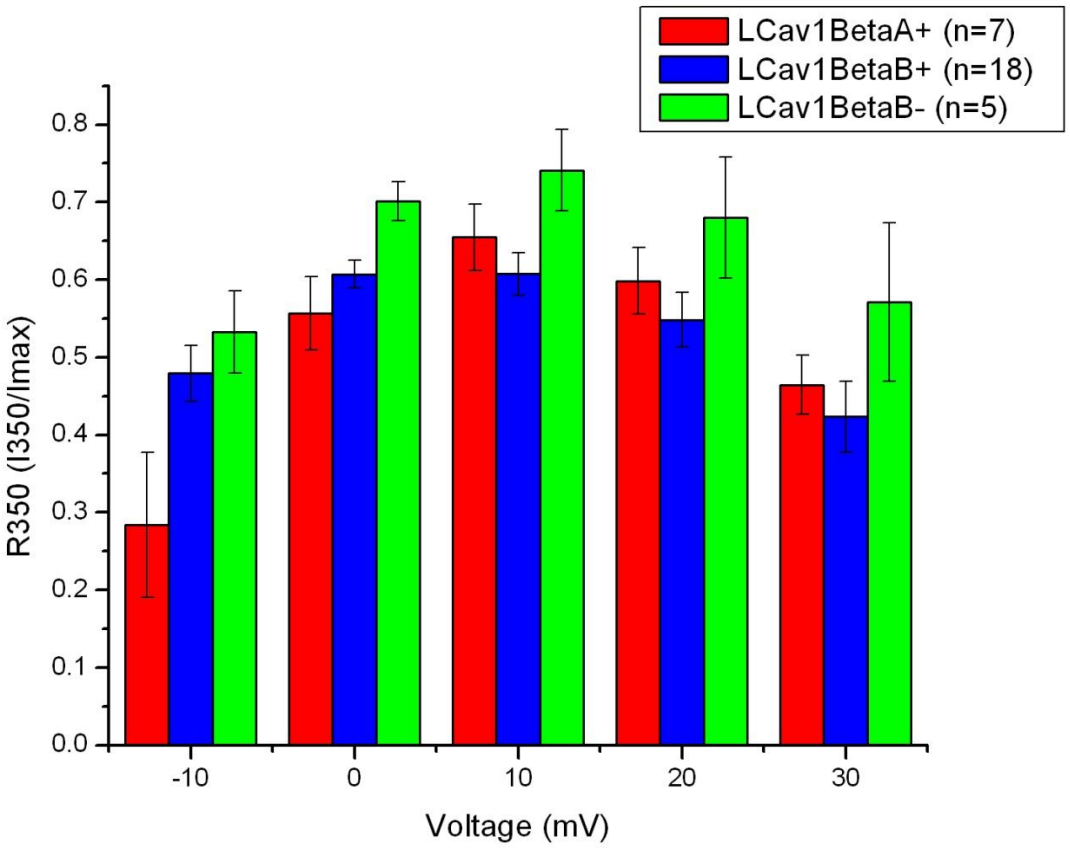

Figure 3.33: Inactivation kinetics of *LCa$_v$1*. R_{350} values are plotted as a representation of the ability of *LCa$_v\beta_{A+}$*, *LCa$_v\beta_{B+}$* and *LCa$_v\beta_{B}$-* to modulate the the speed with which whole-cell inactivation decay occurs. Bars represent mean±SEM. In the voltage range around peak (0 and 10mV), co-expression of *LCa$_v\beta_{B}$-* appears to mediate a decrease in inactivation decay as compared to other isoforms.

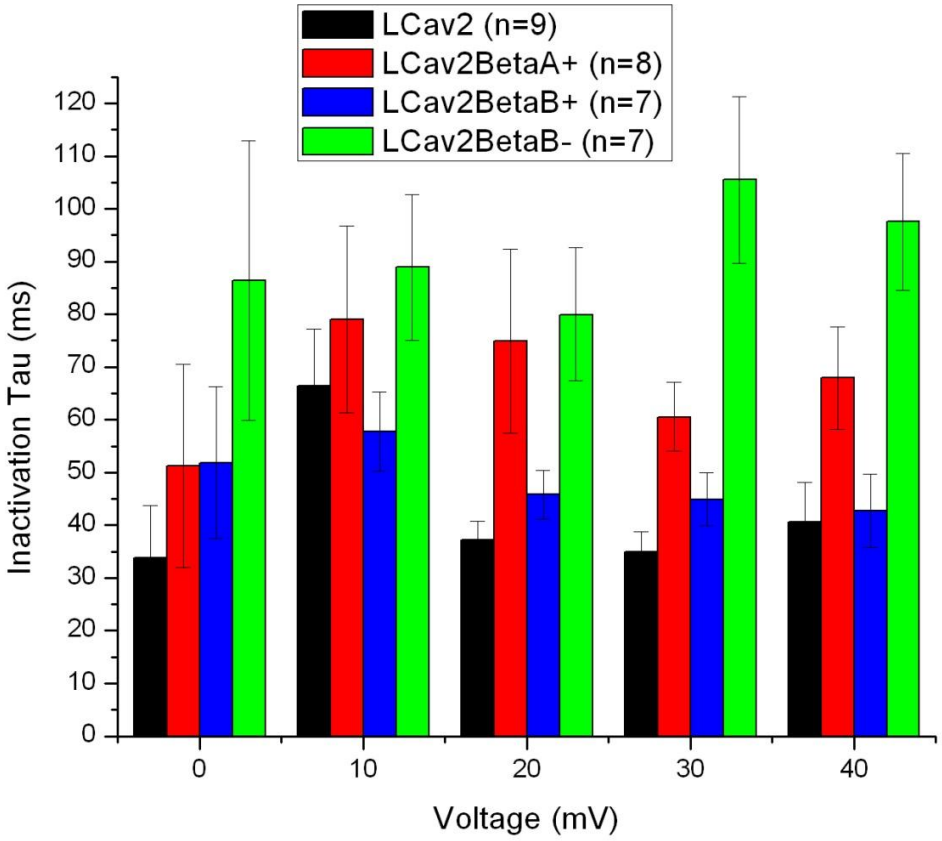

Figure 3.34: Inactivation kinetics of *LCa$_v$2*. Tau values for the fast component of inactivation are plotted as a representation of the ability of *LCa$_v\beta_{A+}$*, *LCa$_v\beta_{B+}$* and *LCa$_v\beta_{B}$-* to modulate the speed with which whole-cell inactivation decay occurs. Bars represent mean±SEM. Inactivation of *LCa$_v$2* was severely attenuated by the co-expression of *LCa$_v\beta_{B}$-* and, to a lesser extent by *LCa$_v\beta_{A+}$*.

LCa$_v$2 channels, similar to the phenomenon that was observed for *LCa$_v$1*. It was also noted that, at the same voltage range, expression of *LCa$_v$β*$_{A+}$ also caused a slowing of inactivation as compared to no *LCa$_v$β* and *LCa$_v$β*$_{B+}$. It seems as though the *LCa$_v$β* subunit isoforms slow inactivation kinetics to some extent, and that the HOOK region may be instrumental in the modulation of inactivation properties. Delaying the inactivation of the calcium channels can have several physiologically relevant effects, due to the overall increase in Ca^{2+} influx that results. Increased Ca^{2+} influx will lead to an increase in activities like muscle contractility or neurotransmission which are initiated by the entry of Ca^{2+}.

Chapter 4
Discussion

It has been the goal of this project to address the manner in which *$Ca_v\beta$* subunits differentially regulate the expression and activity of HVA calcium channels in *Lymnaea stagnalis*. Several interesting findings have been presented in this study which help to elucidate the role of *$LCa_v\beta$* subunits in the modulation of *LCa_v1* and *LCa_v2* expression and biophysics. First, it has been shown that alternative splicing of the *$LCa_v\beta$* subunit does occur in the N-terminus and HOOK regions and that this is acommon feature of all *$Ca_v\beta$* subunits. Next, it has been shown that the invertebrate *$LCa_v\beta$* subunits can be expressed heterologously in mammalian cell culture, and that co-expression of *$LCa_v\beta$* subunits with *LCa_v1* or *LCa_v2* can produce physiological effects *in vitro.* Co-expression of *$LCa_v\beta$* subunits has enhanced the membrane trafficking of functional α_1 subunits and modulated their biophysical properties. Taken together, this work has broadened our understanding of the physiology of voltage-gated calcium channels in the simple model organism *Lymnaea*, in an attempt to further our understanding of the function of *$Ca_v\beta$* subunits.

4.1 Alternative Splicing of the N-terminus and HOOK Region Is a Common Feature of $Ca_v\beta$ Subunits

It had often been theorized that alternative splicing played a large role in the *$Ca_v\beta$* subunit modulation of invertebrate calcium channels since they contain only a single homolog of the

four genes that encode $Ca_v\beta$ subunits in mammals (Spafford *et al.*, 2004). Studies have shown that while the core MAGUK-like structure of the $Ca_v\beta$ subunit SH3 and GK domains remained highly conserved among all $Ca_v\beta$ subunits, the HOOK region and N-terminus can be highly variable (figure 3.1) and are often subjected to alternative splicing (Vendel *et al.*, 2006; Chen *et al.*, 2004; Foell *et al.*, 2004; Helton and Horne, 2002; Hanlon *et al.*, 1999). As it has been shown here, there were multiple splice isoforms present in $LCa_v\beta$- two of which were cloned and characterized in this study. Screening of *Lymnaea* cDNA revealed the presence of $LCa_v\beta_{B+}$ and $LCa_v\beta_{B-}$, in which a mutually exclusive N-terminus has replaced that found in $LCa_v\beta_{A+}$. This finding was significant since it had been previously shown that alternative splicing of the N-terminus could be found in invertebrate $Ca_v\beta$ subunits (Kimura and Kubo, 2003; Moroz *et al.*, 2006) as well as mammalian $Ca_v\beta_2$ and $Ca_v\beta_4$ subunits (Colecraft *et al.*, 2002; Helton and Horne, 2002; Takahashi *et al.*, 2003; Foell *et al.*, 2004; Vendel *et al.*, 2006).

These alternate splice isoforms were found to have differential expression patterns and the ability to modulate the biophysical properties of both Ca_v1 and Ca_v2 channels. For instance, Helton and Horne (2002) were able to demonstrate that alternative splicing in the A-domain of the N-terminus of $Ca_v\beta_4$ produced two mutually exclusive isoforms- $Ca_v\beta_{4a}$ and $Ca_v\beta_{4b}$, whose N-termini are substantially different in length. The length of the N-terminus in $Ca_v\beta_{4a}$ was 49 amino acid residues, whereas that of $Ca_v\beta_{4b}$ was a mere 15 amino acids in length as seen tables 4.1 and 4.2 (found at the end of this chapter). From an electrophysiological perspective, it was shown that $Ca_v\beta_{4a}$ and $Ca_v\beta_{4b}$ have differential effects on the voltage-dependencies of activation and inactivation, as well as the inactivation

kinetics of $Ca_v2.2$ channels, but not $Ca_v1.2$ (Helton and Horne, 2002). In addition to this finding, it was also found that the expression patterns of $Ca_v\beta_{4a}$ and $Ca_v\beta_{4b}$ in the cerebellum were non-overlaping. It was observed that $Ca_v\beta_{4a}$ and $Ca_v\beta_{4b}$ were localized to different layers and subcellular locations in the cerebellum- $Ca_v\beta_{4a}$ was preferentially expressed at synapses in the molecular layer, while $Ca_v\beta_{4b}$ is expressed in the Purkinje cell bodies and other cells that cross the molecular layer (Vendel *et al.*, 2006). Furthermore, it has been shown that each of the five N-terminal splice variants of $Ca_v\beta_2$ impart different gating properties to $Ca_v1.2$ channels when expressed in HEK cells (Takahashi *et al.*, 2003). Some isoforms of $Ca_v\beta_2$ ($Ca_v\beta_{2a}$ and $Ca_v\beta_{2e}$) contain palmitoylation sites in the N-terminus (Chien *et al.*, 1996), while others ($Ca_v\beta_{2b}$, $Ca_v\beta_{2c}$ and $Ca_v\beta_{2d}$) do not. Palmitoylation of the N-terminus allowed the $Ca_v\beta$ subunit to become anchored in the cell membrane and drastically alter the peak ionic current (Chien *et al.*, 1996) and induce slower inactivation kinetics (Takahashi *et al.*, 2003). Based on these previous findings, it was not surprising that alternative splicing was also present in the N-terminal A-domain of $LCa_v\beta$.

Serendipitously, alternative splicing was also discovered in the HOOK region of $LCav\beta$. Exon 7 of $LCa_v\beta_{A+}$ and $LCa_v\beta_{B+}$ was found to contain an optional seven amino acid insert (exon 7B; GVQFVSP), which was not present in $LCa_v\beta_{B-}$ (see figures 3.6 and 3.16). Alternative splicing has also been noted in the HOOK region (exon 7) in both squid (*Loligo*) $Ca_v\beta$ subunits (Kimura and Kubo, 2003) and mammalian $Ca_v\beta_1$ (Powers *et al.*, 1992) and $Ca_v\beta_2$ (Takahashi *et al.*, 2003) subunits, as well as zebrafish $Ca_v\beta_2$ (Zhou *et al.*, 2008). In squid, exon 7B consists of a five amino acid insert (ECMFL) that is optional and may or may not be expressed with the long exon 7A; however, in mammals and fish exons 7A and 7B are

mutually exclusive, leading to "long" and "short" isoforms which encode either exon 7A or 7B, respectively (figure 3.16). Alternative splicing of the HOOK region was a promising target for investigation as it has been directly implicated in the modulation of inactivation kinetics of calcium channels (Richards *et al.*, 2007).

When $Ca_v\beta_{1b}$ and $Ca_v\beta_{2a}$ were mutated such that the entire HOOK region had been deleted, Richards *et al.* (2007) found that the inactivation kinetics of *Cav2.2* currents were enhanced, resulting in faster whole-cell inactivation decay. The N-terminus, SH3 and GK domains were found not to be involved in this alteration of inactivation kinetics through the use of strategically truncated mutant controls (Richards *et al.*, 2007). In *Lymnaea*, it is likely that alternative splicing may be responsible for channel type-specific regulation since they do not have the genetic diversity seen in mammals, but rather contain only a single homolog of the four mammalian $Ca_v\beta$ subunit genes. In the field of neuroscience, characterization of the functional and structural significance of alternative splicing events, such as these, remains a challenge.

4.2 Genomic Structure of Lymnaea $Ca_v\beta$ Subunit is Conserved in Vertebrates

In order to ensure that there was in fact only a single gene coding for $LCa_v\beta$, Southern blotting analysis was carried out with limited success. Previous studies had indicated the presence of only a single gene as multiple rounds of PCR screening (Spafford *et al.*, 2004) did not reveal additional $LCa_v\beta$ subunit genes. Using $LCa_v\beta_B$ N-terminus as a probe, it

appears as only a single copy in a Southern blot hybridrization experiment (figure 3.11B). It remains unclear, however, if $LCa_v\beta_A$ is truly a single-copy gene as Southern blotting failed to produce definitive proof (figure 3.11A). Although several attempts were made to troubleshoot the Southern blotting of $LCa_v\beta_A$, in each attempt the result was the same- two faint bands were produced in each lane. This could be caused by two possible situations: either the gene is not a single-copy gene, or there is an intron present which divides the sequence epitope that is recognized by the DIG-labeled probe. Of these two possibilities, the latter is more likely based on the previous findings of other groups (Spafford *et al.*, 2004) and the fact that both bands visualized on the blot of $LCa_v\beta_A$ were of roughly equal intensity, yet not as intense as those on the blot for $LCa_v\beta_B$. Since the bands were of approximately equal intensity, it could be argued that an intron may be present because the DIG signal was divided between the two fragments of DNA. Since the percent GC composition and size of the DIG-labeled probes for both $LCa_v\beta_A$ and $LCa_v\beta_B$ was comparable, it would also have been expected that both probes would hybridize equally well, producing bands of comparable intensity given that all other factors were the same. Finally, when the blots of $LCa_v\beta_A$ and $LCa_v\beta_B$ are compared, it was evident that the position of one of the bands produced by $LCa_v\beta_A$ correlated roughly with the band seen in the blot of $LCa_v\beta_B$. This had suggested, again, that both probes were binding to the same fragment (containing the single-copy gene), yet $LCa_v\beta_A$ was also binding to another fragment which perhaps was on the other side of a restriction site (which divided the $LCa_v\beta_A$ hybridization site in two). For these reasons, it was inferred that *Lymnaea* contains only a singleton homolog of the $Ca_v\beta$ subunit.

In an attempt to confirm that both $LCa_v\beta_A$ and $LCa_v\beta_B$ are alternative splice isoforms of a single $LCa_v\beta$ gene, genomic sequencing of the N-terminus was subsequently carried out. Introns separating exon B and C, and C and D were found to be 516 and 2263bp in length, respectively, and were bounded by consensus donor and acceptor sites to facilitate spliceosome activity (figure 3.14 B and C). Similar genomic structure is conserved in the N-terminus of mammalian (figure 3.14A) and teleost $Ca_v\beta_2$ and $Ca_v\beta_4$ genes (Birnbaumer *et al.*, 1998; Foell *et al.*, 2004; Vendel *et al.*, 2006, Ebert *et al.*, 2008a; Ebert *et al.*, 2008b). As illustrated in figure 3.14A, alternative splicing in the N-terminus of $Ca_v\beta_2$ and $Ca_v\beta_4$ is common, and results in at least two mutually exclusive N-terminal domains which themselves were products of either two exons or a single exon. Based on these findings and the results of Southern blotting (figure 3.11), it can be concluded that the splicing pattern observed in mammalian $Ca_v\beta_2$ and $Ca_v\beta_4$ genes is conserved in *Lymnaea*, such that the N-terminus of $LCa_v\beta_A$ (MALA….FIRQ) is coded for by two exons upstream of a single B exon that encodes the N-terminus of $LCa_v\beta_B$ (MRIK….IDSL). This consistent pattern of conservation suggests that invertebrate and vertebrate $Ca_v\beta$ subunits have arisen from a common ancestral protein.

Several studies have noted that the N-terminus of $Ca_v\beta$ subunit genes contain some of the longest known introns in both humans and fish. In humans, these introns can range from 90 to 125kb in length in $Ca_v\beta_2$ and $Ca_v\beta_4$ (Ebert *et al.*, 2008a,b), although the average human intron size is only 3.7kb and less than one-quarter of introns in the human genome are greater than 2.6kb (Sakharkar *et al.*, 2004; Hong *et al.*, 2006). Likewise, the N-terminal introns of teleost fish (zebrafish and pufferfish) are also significantly larger than average, ranking them

among the largest of all fish introns (Ebert *et al.*, 2008a,b; Aparicio *et al.*, 2002). Several other tetrapod $Ca_v\beta$ subunits were also found to contain disproportionately large introns in the N-terminus of their $Ca_v\beta$ subunits (Ebert *et al.*, 2008a,b). Could the conservation of these large introns be due to the presence of important regulatory elements that control isoform expression and alternative-splicing of the N-terminus? Cis-regulatory elements contained within non-coding (intron) sequence have been shown to influence mRNA metabolism and processing in several fundamental ways, including modulation of transcription rate (by controlling accessibility to DNA and polyadenylation), nuclear export, translation and degradation of mRNA transcripts (Le Hir *et al.*, 2003; Nott *et al.*, 2003). Therefore, conservation of large intron size in the N-terminus may be due to the presence of important cis-regulatory elements found within them. These elements may take part in the modulation of isoform expression at both the transcriptional and translational levels, allowing an organism to spatially and temporally regulate $Ca_v\beta$ subunit expression.

It has been shown that the HOOK region of the $Ca_v\beta$ subunits of invertebrates, mammals and fish are alternatively spliced in similar manners (see section 4.1), although it seems as though splicing patterns suggest that divergence of invertebrate and vertebrate $Ca_v\beta$ subunit isoforms in the HOOK domain occurred after the split between these two groups occurred millions of years ago. The HOOK domain of $Ca_v\beta$ consists of exons 6 and 7, and exon 7 can be divided into exons 7A, 7B and 7C which may expressed in different configuration (figure 3.16). All organisms included in this study were found to contain exon 6, which was moderately conserved among species (figure 3.1), however the patterns of splicing in exon 7 were not consistent between invertebrates and vertebrates. The

invertebrates *Lymnaea* and *Loligo* contained exon 7A, and sometimes contained an optional, short exon just upstream (exon 7B). Vertebrates, however, contained either exon 7A or 7B, but not both (i.e. they were mutually exclusive). Also, the amino acid composition of exon 7B differed drastically between *Lymnaea*, squid and vertebrates, although the size of exon 7B was always short (seven amino acids in *Lymnaea* and vertebrates, five in squid; figure 3.16). Given these facts, it is likely that sequence divergence within the HOOK region did not occur in an ancestral $Ca_v\beta$ subunit, but rather after the split between molluscs, squid and vertebrates. The commonalities found in the loci and size and putative functions of exon 7B has lead to the hypothesis that these exons may have been the result of convergent evolution since the sequence of theis exon differs between molluscs, squid and vertebrates. In the process of convergent evolution, the independent formation of exon 7B in molluscs, squid and mammals was driven by the ability of random mutations in the HOOK region to impart new modulatory effects on HVA VGCCs. These modulatory effects, in turn, would have been beneficial as it would allow for fine-tuning of channel gating activity, and so these independently-evolved isoforms of exon 7B remain today in the genomes of molluscs, squid, fish and mammals.

4.3 *Lymnaea $Ca_v\beta$ Subunits Enhance Peak Current Amplitude and Assist in Membrane Trafficking of LCa_v1 and LCa_v2*

It was previously known that HEK cells could express $LCa_v\beta_{A+}$ (Spafford *et al.*, 2004), but would it express $LCa_v\beta_{B+}$ as well, if at all? Prior to assessing the role of $LCa_v\beta_{A+}$, $LCa_v\beta_{B+}$

and $LCa_v\beta_{B-}$ in the membrane trafficking of LCa_v1 and LCa_v2, Western blotting was used to validate the expression of $LCa_v\beta$ proteins in cultured HEK cells (figure 3.17). It was determined that both $LCa_v\beta_{A+}$ and $LCa_v\beta_{B+}$ are expressed in HEK cells that have been transfected with these plasmids, however, in mock transfected cells no proteins were detected by the rabbit anti-$LCa_v\beta$ antibody. This indicates that there is, in fact, transcription, translation and expression of the $LCa_v\beta$ proteins in HEK cells that have been transfected, and that no endogenous HEK cell proteins are recognized by the anti-$LCa_v\beta$ antibody. The lack of endogenous $Ca_v\beta$ subunit expression is important as it ensures that any modulation of channel biophysics is indeed caused by the $LCa_v\beta$ subunit isoform in question. Therefore, it was suitable to have used cultured, transfected HEK cells for fluorescent imaging and electrophysiological analysis of $LCa_v\beta$ induced modulation of LCa_v1 and LCa_v2.

It has been previously reported that co-expression of mammalian $Ca_v\beta$ subunits with mammalian HVA calcium channels resulted in a drastic increase in the whole-cell peak current amplitude when expressed in cell culture. It has been postulated by several groups that the observed enhancement of peak current amplitude was due to a "chaperoning" role of $Ca_v\beta$ subunits in the membrane trafficking of the primary α_1 subunit to the membrane (Chien *et al.*, 1995; Yamaguchi *et al.*, 1998; Gao *et al.*, 1999; Brice *et al.*, 1997). In order to rule out changes in the level of α_1 expression as the cause of current enhancement, immunolabelling experiments were employed. With both Ca_v1 and Ca_v2 channels, the α_1 subunit exhibited perinuclear staining of the cytoplasm in the absence of $LCa_v\beta$ subunit expression. Likewise, when expressed in the absence of other VGCC subunits, $Ca_v\beta$ subunits (except the palmitoylated $Ca_v\beta_{2a}$) were diffusely localized to the cytoplasm. In all cases, the co-

expression of *Ca_v1* or *Ca_v2* with any *$Ca_v\beta$* subunit led to an increase in the membrane localization of the α_1 and *$Ca_v\beta$* subunits, which appeared to cluster together (Chien *et al.*, 1995; Yamaguchi *et al.*, 1998; Gao *et al.*, 1999; Brice *et al.*, 1997). As further evidence that *$Ca_v\beta$* subunits may act as a "chaperone" in the trafficking of α_1 subunits to the membrane, it was observed that when *Xenopus* oocytes were pre-treated (prior to expression of calcium channels) with vacuolar-type H^+-ATPase (V-ATPase) inhibitor, which impairs intracellular transportation by acidifying vacuoles, both the enhancement of peak current amplitude and localization of α_1 to the membrane were abolished (Yamaguchi *et al.*, 1998). This evidence clearly implicates *$Ca_v\beta$* subunits in the intracellular transport of calcium channel α_1 subunits to the cell surface, but is this the case for invertebrates like *Lymnaea*?

As illustrated in figure 3.26, the average peak current of *LCa_v2* was enhanced when the α_1 subunit was co-expressed with any of the three *$LCa_v\beta$* isoforms, although the increases were only statistically significant for *$LCa_v\beta_{B-}$*, due to large variability and low repeat values in the other datasets (leading to a large standard error). Co-expression of *$LCa_v\beta_{B-}$*, also resulted in an average peak current for *LCa_v2* that was larger than that for *$LCa_v\beta_{A+}$* (figure 3.26). As for *LCa_v1*, it was difficult to determine if *$LCa_v\beta$* subunit expression enhanced membrane trafficking (and therefore peak current amplitude) because no *LCa_v1* currents were recorded in the absence of *$LCa_v\beta$* subunits. Could it be that perhaps there were no currents recorded because *LCa_v1* was not being inserted into the membrane in the absence of an *$LCa_v\beta$* subunit chaperone? The fact that currents in excess of 100pA were consistently produced when *LCa_v1* was co-expressed with *$LCa_v\beta_{A+}$*, *$LCa_v\beta_{B+}$* or *$LCa_v\beta_{B-}$* (figure 3.25) lends credibility to this hypothesis. To further investigate the role of *$LCa_v\beta$* subunits in

membrane trafficking, fluorescent labeling of α_1 and *LCa$_v\beta$* subunits expressed in HEK 293T cells was preformed.

Although the anti-*LCa$_v\beta$* antibody showed a high degree of specificity in Western blot analysis, there was some degree of background staining present when fluorescent antibody staining experiments were carried out. HEK 293T cells were transfected with either *LCa$_v$1* or *LCa$_v$2* channels that have been fused to EGFP at the N-terminus and *LCa$_v\beta$* subunits were localized by means of an *LCa$_v\beta$* subunit-specific antibody that can be detected with a secondary antibody conjugated to AlexaFluor594. As seen in the upper row of figures 3.19 and 3.20, untransfected cells were consistently stained at low levels when imaged for EGFP (green) and AlexaFlour594 (red). When transfected cells were imaged with the fluorescent microscope, it was evident that some cells were more intensely stained than others. Cells with fluorescence above background levels indicated positively transfected cells because the higher levels of fluorescence are a result of EGFP-fused channel (green) expression or *LCa$_v\beta$* (red) expression detected by fluorescent (secondary) antibodies in these cells. Thus it was possible to distinguish true signal from background fluorescence.

Among cells transfected with either *LCa$_v$1* or *LCa$_v$2*, some differences related to *LCa$_v\beta$* subunit expression became evident. In the absence of any *LCa$_v\beta$*, both EGFP-*LCa$_v$1* and -*LCa$_v$2* were always distributed diffusely throughout the cell, as seen in the second row of figure 3.19 and 3.20, respectively. This is comparable to what has been observed for mammalian *Ca$_v$1* and *Ca$_v$2* channels in the absence of *Ca$_v\beta$* subunit expression (Chien *et al.*, 1995; Yamaguchi *et al.*, 1998; Gao *et al.*, 1999; Brice *et al.*, 1997), and so it appears that in the absence of *LCa$_v\beta$* expression both *LCa$_v$1* and *LCa$_v$2* fail to insert in the cell membrane.

Membrane trafficking of both *LCa$_v$1* and *LCa$_v$2* appeared to have been restored by the expression of either *LCa$_v$β$_{A+}$* or *LCa$_v$β$_{B+}$* (*LCa$_v$β$_{B-}$* was not tested). As seen in the bottom two lines of figures 3.19 and 3.20, the majority of cells showed at least a partial co-localization of *LCa$_v$1* and *LCa$_v$2*, respectively, with either *LCa$_v$β* isoform at the cell membrane. In many of these instances, however, there remained a significant amount of EGFP-*LCa$_v$1* or –*LCa$_v$2* in the cytoplasm and it was often difficult to determine if channels were significantly localized in the membrane. On the other hand, the *LCa$_v$β* subunit staining with AlexaFlour594 clearly revealed higher levels of membrane localization when transfected with *LCa$_v$1* or *LCa$_v$2*. Again, this is consistent with previous reports that have noted co-localization of mammalian α_1 and *Ca$_v$β* subunits when they are co-expressed (Chien *et al.*, 1995; Yamaguchi *et al.*, 1998; Gao *et al.*, 1999; Brice *et al.*, 1997), except for the diffuse perinuclear staining of α_1 which remained in the cytoplasm. Earlier studies that have also shown that *LCa$_v$2* and *LCa$_v$β$_{A+}$* do indeed co-localize at the cell membrane when co-expressed in HEK cells (Spafford *et al.*, 2004). The fact that there is no difference between *LCa$_v$β$_{A+}$* and *LCa$_v$β$_{B+}$* was not surprising, given the fact that the hydrophobic groove found in the GK domain has been implicated as the major determinant of trafficking of α_1 (Chen *et al.*, 2004; Bichet *et al.*, 2000), and the GK domains of *LCa$_v$β$_A$+* and *LCa$_v$β$_{B+}$* are identical. Although there were no apparent differences in membrane trafficking of *LCa$_v$1* or *LCa$_v$2* due to changes in *LCa$_v$β* expression, differences in whole-cell peak current of both channels were induced by differentially expressing the various *LCa$_v$β* isoforms.

4.4 Lymnaea $Ca_v\beta$ Subunits Subtly Modulate the Voltage-Dependencies of Activation and Inactivation

It has long been reported that $Ca_v\beta$ subunits can regulate the biophysical properties of HVA calcium channels, including their voltage-dependencies of activation and inactivation. Not surprisingly, this was true of $LCa_v\beta$ subunits as well, although the modulatory effects seem to be quite subtle. Although it is well-established that mammalian $Ca_v\beta$ subunits modulate channel gating, the degree to which these parameters are altered, however, may depend on the expression system used. Some studies have found enhanced $Ca_v\beta$ subunit modulation of channel gating when *Xenopus* oocytes are used for heterologous expression of channel complexes as compared to mammalian systems such as HEK 293T or COS-7 cells (Yasusda *et al.*, 2004). In order to minimize the quantitative differences resulting from artifacts of the expression system, only qualitative differences will be highlighted when possible. Tables 4.1 and 4.2 summarize the qualitative effects of $Ca_v\beta$ subunit modulation on L-type and non-L-type HVA calcium channels, respectively, from several invertebrate and vertebrate species.

All of the $LCa_v\beta$ subunit isoforms, expressed here in HEK cells, appeared to have clear, but subtle effects on the voltage-dependencies of activation and inactivation of LCa_v2. As illustrated in figure 3.28, a hyperpolarizing shift in the voltage-dependency of activation was caused by the co-expression of $LCa_v\beta_{A+}$, $LCa_v\beta_{B+}$ or $LCa_v\beta_{B-}$, due to a steepening of the slope of the activation curve (K_a). The half-activation potentials of LCa_v2, although not statistically significant, differed by five to ten millivolts depending on which $LCa_v\beta$ isoform was expressed. This is consistent with what has been reported previously when mammalian $Ca_v\beta$ subunits have been expressed in HEK 293T cells. Representatives of all four

mammalian $Ca_v\beta$ subunits, $Ca_v\beta_{1b}$, $Ca_v\beta_{2a}$, $Ca_v\beta_3$, $Ca_v\beta_{4a}$ and $Ca_v\beta_{4b}$, have been reported to decrease (steepen) the slope of the activation curve of *LCa_v2* (Helton and Horne, 2003; Yasuda *et al.*, 2004). The alteration of the slope usually resulted in a hyperpolarizing shift that was less than 5mV in magnitude (except in the case of $Ca_v\beta_{4a}$, in which no shift resulted). Previous reports have suggested that $LCa_v\beta_{A+}$ had no effect on the voltage-dependence of activation for *LCa_v2*, contradictory to what was observed here (Spafford *et al.*, 2004). Perhaps the hyperpolarization of the activation curve is caused by specific determinants located in the N-terminus of the α_1 subunit, as the aforementioned study utilized a chimeric *LCa_v2* channel which contained the N-terminus from rat *$Ca_v2.1$*.

Physiologically, hyperpolarizing shifts in the voltage-dependence of activation results in a population of channels which have increased sensitivity to depolarizing stimuli. By modulating the expression of $Ca_v\beta$ subunits in a given cell or at a particular synapse, an organism can fine-tune their physiological response to a given stimulus. For example, in some instances an organism may want to strengthen the coupling between a neuronal signal and its physical response, as in the arrival of an action potential and muscle contraction seen in excitation-contraction coupling. One mechanism by which this coupling could occur more rapidly is to allow the entry of Ca^{2+} into the cell with less depolarization (leading to the observed hyperpolarizing shift). Hyperpolarizing the voltage-dependence of activation effectively lowers the threshold of depolarization that is required for activation.

Modulation of steady-state inactivation has been a hallmark of $Ca_v\beta$ subunit expression, and it appears that this holds true for *Lymnaea* subunits to some extent. It was evident from figure 3.30 that the N-terminus and HOOK region were having an influence on

the steady-state inactivation of *LCa$_v$2*. In the absence of exon 7B (GVQFVSP), the slope of the inactivation curve (K_i) was drastically decreased (table 3.2) compared to all other datasets, indicating that steady-state inactivation was delayed until cells were exposed to more depolarized membrane potentials. Under these conditions, the transition of *LCa$_v$2* channels from open (activated) to inactivated would be delayed until the membrane was depolarized to a greater extent. Upon reaching the threshold for inactivation, however, the population of channels would achieve inactivation more rapidly because there were no alterations to the half-inactivation potential induced by *LCa$_v\beta_{B-}$* expression.

Aside from the HOOK region, it also appeared that the N-terminus may alter the steady-state inactivation properties of *LCa$_v$2*. Small, depolarizing shifts in the half-inactivation potential of *LCa$_v$2* were observed when co-expressed with *LCa$_v\beta_{A+}$*, as seen in figure 3.30, and ranged from 4 to 8mV in magnitude, although these shifts were only significant when compared to *LCa$_v\beta_{B+}$* (table 3.2). In mammalian systems, steady-state inactivation of *Ca$_v$2* channels can be shifted in either a hyperpolarizing or depolarizing direction depending on which *Ca$_v\beta$* subunit gene or isoform is expressed (table 4.2). In general, mammalian *Ca$_v\beta_{1b}$*, *Ca$_v\beta_3$* and *Ca$_v\beta_{4b}$* were reported to induce small hyperpolarizing shifts in the half-inactivation potential of *Cav2* without alteration of the slope of the inactivation curve, K_i (except for *Ca$_v\beta_{1b}$* which resulted in a slight decrease in the slope) (Yasuda *et al.*, 2004). On the other hand, it is well-documented that *Ca$_v\beta_{2a}$* expression results in a large depolarization of the steady-state inactivation curve due to palmitoylation of its N-terminus, and does not allow for full inactivation of all channels within a given population (Yasuda *et al.*, 2004). *Ca$_v\beta_{4a}$* was found to have no effect on the steady-state inactivation of

Ca_v2. Interestingly, both squid *$Ca_v\beta$* subunits (*$LoCa_vBeta_{1a}$* and *$LoCa_vBeta_{1b}$*) were also found to depolarize the steady-state inactivation curves of *Ca_v2* channels, and similar to *$Ca_v\beta_{2a}$*, they also did not allow for full inactivation of all channels in a given population although they do not contain palmitoylation motifs in their N-termini (Kimura and Kubo, 2003).

Depolarization of the steady-state inactivation curve of *LCa_v2* by expression of *$LCa_v\beta_{A+}$* could potentially have meaningful physiological ramifications. Depolarizing shifts in the steady-state inactivation curve indicates that within a given population of channels, any one channel is more likely to be open at a given potential. For example, a right shift of the steady-state inactivation curve extends the range of depolarization a channel is able to tolerate prior to reverting to a refractory state allowing for increased calcium influx into the cytoplasm. In a sense, shifts of this nature act to "desensitize" a population of channels to inhibition by repeated stimuli (such as a train of action potentials) which maintain higher-than-normal levels of depolarization. In the absence of *$Ca_v\beta$* subunits which depolarize the voltage-dependence of inactivation, channels would more readily become refractory to opening, effectively limiting the duration of the downstream physiological response (including neurotransmitter secretion and muscle contraction).

The lack of *LCa_v1* recording data in the absence of *$Ca_v\beta$* subunits did not allow for a direct comparison of *$LCa_v\beta$* subunit modulation, since there was no basis for comparison. Despite this fact, some differences in the voltage-dependencies of activation and inactivation were noted between *LCa_v1* channel complexes containing different *$LCa_v\beta$* subunit isoforms. It was noted that the half-activation potential of *LCa_v1* was hyperpolarized by the expression

of $LCa_v\beta_{B+}$, as compared to either $LCa_v\beta_{A+}$ or $LCa_v\beta_{B-}$. Although the shift was statistically significant, it is unlikely to be of physiological significance since the magnitude of the shift was less than 3mV (figure 3.27 and table 3.1). As for the steady-state inactivation of *LCa_v1*, it was noted that the expression of $LCa_v\beta_{A+}$ increased the average half-inactivation potential of *LCa_v1* by 6 to 8mV. Although these differences were not statistically significant, there was a significant increase in the slope of the inactivation curve (K_i) of *LCa_v1* when it was co-expressed with $LCa_v\beta_{A+}$ as compared to either $LCa_v\beta_B$ isoform. This decrease in the steepness of the curve has created the appearance of a hyperpolarizing shift although the changes in half-inactivation differences were not statistically significant. As with *LCa_v2*, depolarization of the voltage-dependence of inactivation will allow for greater calcium influx over extended periods of depolarization, in effect "desensitizing" the population of channels to inhibition by a prolonged stimulus.

In the absence of a no $Ca_v\beta$ subunit control, it has been exceedingly difficult to try and elucidate the modulatory effects of $LCa_v\beta$ subunits on *LCa_v1* as it has often been observed that mammalian L-type (*Ca_v1*) channels are often modulated by $Ca_v\beta$ subunits in an isoform-specific manner. For example, in mammalian systems $Ca_v\beta_{1a}$, $Ca_v\beta_{2a}$, $Ca_v\beta_3$ and $Ca_v\beta_{4b}$ all shift the half-activation potentials in a hyperpolarizing direction, but yet $Ca_v\beta_{1b}$, $Ca_v\beta_{2b}$ and $Ca_v\beta_{4a}$ do not induce any shifts. In addition, the slope of the activation curve was decreased when *LCa_v1* was co-expressed with $Ca_v\beta_{1b}$, $Ca_v\beta_{4a}$ and $Ca_v\beta_{4b}$, but not in the presence of other $Ca_v\beta$ subunits (Jangsangthong *et al.*, 2009; Yasuda *et al.*, 2004; Takahashi *et al.*, 2003; Helton and Horne, 2002). Similarly, when the $Ca_v\beta$ subunit modulation of the steady-state inactivation of *Cav1.2* was studied, it was found that mammalian $Ca_v\beta_{1a}$, $Ca_v\beta_{1b}$,

$Ca_v\beta_3$ and $Ca_v\beta_{4b}$ induced hyperpolarizing shifts in the half-inactivation potential ranging from 5 to 12mV in magnitude while $Ca_v\beta_{2a}$ induced a 7mV depolarizing shift, and $Ca_v\beta_{2b}$ and $Ca_v\beta_{4a}$ had no effect (Jangsangthong *et al.*, 2009; Yasuda *et al.*, 2004, Helton and Horne, 2002). Since mammalian $Ca_v\beta$ subunits do not modulate L-type calcium channels in predictable and consistent ways, it has not been possible to attribute differences observed in the voltage-dependencies of activation and inactivation of LCa_v1 to specific $LCa_v\beta$ subunit isoforms.

4.5 The N-terminus and HOOK Regions of the $Ca_v\beta$ Subunit Modulate Channel Kinetics

Perhaps the most characteristic feature of $Ca_v\beta$ subunits is their ability to mediate calcium channel kinetics. VGCCs can exist in three functional states- open, closed or inactivated- and the speed with which channels transition between these states can be modulated by $Ca_v\beta$ subunits in mammals (Jones, 1998). Likewise, invertebrate $Ca_v\beta$ subunits appear to modulate the kinetics of both LCa_v1 and LCa_v2, and evidence suggests that both the N-terminus and HOOK regions contain important determinants of this effect.

The HOOK region is involved in modulating the kinetics of LCa_v2 inactivation as seen in figure 3.34. When the exon 7B (GVQFVSP) was removed from the HOOK region, the tau of inactivation increased (table 3.2), which indicated a delay in channel inactivation. The role of the HOOK region is evident when we compare $LCa_v\beta_{B+}$ and $LCa_v\beta_B$-, since they only differed by the seven amino acids encoded by exon 7B. $LCa_v\beta_{A+}$ also increased the tau

of inactivation as compared to the absence of $LCa_v\beta$ subunit and $LCa_v\beta_{B+}$ (although the latter differences were not statistically significant at all tested potentials, see table 3.2). This is comparable to previous research that had reported slowed inactivation kinetics when LCa_v2 was co-expressed with $LCa_v\beta_{A+}$ (Spafford *et al.*, 2004). Therefore, it seems that both the N-terminus and HOOK region act to modulate inactivation kinetics of LCa_v2, with both exons A1 and A2 as well as exon 7B (GVQFVSP) slowing inactivation. Similar trends were observed in the modulation of $Ca_v2.3$ channels by squid $Ca_v\beta$ subunits, $LoCa_vBeta_{1a}$ and $LoCa_vBeta_{1b}$, which both caused a slowing of inactivation kinetics (Kimura and Kubo, 2003). Mammalian $Ca_v\beta$ subunits are known to both enhance and inhibit the inactivation kinetics of $Ca_v2.2$ (table 4.2). Inactivation was significantly sped up by $Ca_v\beta_3$, and to a lesser extent by $Ca_v\beta_{1b}$, whereas $Ca_v\beta_{2a}$ slowed inactivation drastically (Yasuda *et al.*, 2004). $Ca_v\beta_{4b}$ had no effect on inactivation kinetics of $Ca_v2.2$, while $Ca_v\beta_{4a}$ induced an increase in rate of inactivation kinetics (Helton and Horne, 2002; Yasuda *et al.*, 2004). Due to the numerous differences between individual $Ca_v\beta$ subunit isoforms it has been difficult to pinpoint the exact structural determinants of the observed modulatory effects.

Figure 3.34 clearly illustrates that the removal of exon 7B (GVQFVSP) from the HOOK region of $LCa_v\beta_B$ resulted in slower inactivation kinetics of LCa_v2. Published reports investigating mammalian $Ca_v\beta$ subunits have suggested the opposite effect is occurring. Mutagenesis studies had found that the removal of the entire HOOK region from human $Ca_v\beta_{1b}$ and $Ca_v\beta_{2a}$ subunits resulted in more rapid inactivation kinetics of human $Ca_v2.2$ channels expressed *in vitro* (Richards *et al.*, 2007). In squid, both $LoCa_vBeta_{1a}$ and $LoCa_vBeta_{1b}$ mediated slowing of $Ca_v2.3$ inactivation, although inactivation was delayed to a

greater extent by *LoCa$_v$Beta$_{1b}$*, which contains exon 7B (Kimura and Kubo, 2003). It seems that exon 7B of invertebrate *Ca$_v\beta$* subunits may be responsible, at least in part, for the slower inactivation kinetics observed for *Ca$_v$2* channels. In vertebrates, exon 7A (long) and 7B (short) are mutually exclusive to each other and appear to have opposing effects on *Ca$_v$2* inactivation kinetics (table 4.2). Isoforms containing the long exon 7A mediate slowed inactivation kinetics, whereas those expressing the shorter exon 7B tend to modulate more rapid inactivation of *Ca$_v$2* channels. Perhaps then, it is not the actual structure of the HOOK region that is important in modulating inactivation kinetics, but rather its length and the positioning of exon 7B that are important. This hypothesis is supported by the fact that the exact position of exon 7B has been conserved across vertebrate and invertebrate species, although the sequence has not. There does not appear to be any correlation between the length or structure of the *Ca$_v\beta$* subunit N-terminus and its observed effects on *Ca$_v$2* channel kinetics (table 4.2).

When the kinetics of *LCa$_v$1* (expressed with the three *LCa$_v\beta$* isoforms) were compared, it was determined that the GVQFVSP insert in the HOOK region (exon 7B) was also influential in the modulation of L-type calcium channels. The removal of exon 7B resulted in slower activation (figure 3.31) and inactivation (figure 3.33), although the differences were not always statistically significant (Table 3.1). The observed differences between *LCa$_v\beta_{B-}$* and the other *LCa$_v\beta$* subunit isoforms were found to increase as the membrane potential was increased. This suggested that the removal of exon 7B in the HOOK region is responsible for slowing the kinetics of activation and inactivation of *LCa$_v$1*. No differences in *LCa$_v$1* kinetics were consistently observed between *LCa$_v\beta_{A+}$* and *LCa$_v\beta_{B+}$*,

which differ only in the structure of the N-terminus, indicating that this region has no effect on *LCa$_v$1* kinetics.

Ca$_v$β subunit modulation of mammalian *Ca$_v$1.2* channel kinetics is highly dependent on the specific isoform that is expressed. Most mammalian *Ca$_v$β* subunits did not alter *Ca$_v$1.2* kinetics, however *Ca$_v$β$_{1a}$* and *Ca$_v$β$_{2b}$* were found to enhance inactivation (table 4.2), resulting in more rapidly inactivating whole-cell currents, while *Ca$_v$β$_{2a}$* had the opposite effect (Jangsangthong *et al.*, 2009; Yasuda *et al.*, 2004; Takahashi *et al.*, 2003; Helton and Horne, 2002). Only *Ca$_v$β$_{2b}$* was observed to mediate activation kinetics, resulting in a slight decrease in the latency to channel opening (Takahashi *et al.*, 2003). Some groups have reported that the length of the N-terminus, and not necessarily its structure, is critical in determining the kinetics of *Ca$_v$1.2* activation and inactivation (Herzig *et al.*, 2007; Jangsangthong *et al.*, 2009). For both *Ca$_v$β$_1$* and *Ca$_v$β$_2$*, shorter N-terminal domains produced *Ca$_v$1.2* currents which inactivated more rapidly. Is it possible then that the same could be true of the *LCa$_v$β* subunit? If this were true, then it is consistent with the hypothesis that no differences in *LCa$_v$1* kinetics were observed between *LCa$_v$β$_{A+}$* and *LCa$_v$β$_{B+}$*, since their N-terminal domains differ by only two amino acid residues in length (table 4.1 and 4.2). Investigation of N-terminal truncations of *LCa$_v$β* may help to illustrate this effect.

4.6 Conclusions

In conclusion, it has been shown that alternative splice isoforms of the *Lymnaea Ca$_v$β* subunit are present, and that they can modulate HVA calcium channels *in vitro*. Two novel isoforms,

$LCa_v\beta_{B+}$ and $LCa_v\beta_{B-}$, have been sequenced and cloned, both of which contain an alternative N-terminus.In addition, $LCa_v\beta_{B+}$ contains a small, optional insert in the HOOK region (exon 7B). Staining with fluorescent antibodies and analysis of whole-cell peak currents has revealed that both $LCa_v\beta_{A+}$ and $LCa_v\beta_{B+}$ were able to enhance membrane trafficking of *Lymnaea* calcium channels to some degree. Finally, it was shown that these novel $LCa_v\beta$ isoforms, as well as $LCa_v\beta_{A+}$, have the ability to modulate the biophysical properties of both LCa_v1 and LCa_v2 in a manner that is similar to $Ca_v\beta$ subunit modulation of mammalian HVA calcium channels. Understanding the effects of $Ca_v\beta$ subunit modulation of calcium channel function in the simplified invertebrate system of *Lymnaea* will contribute to our understanding of our own highly complex nervous systems.

4.7 Future Considerations

The findings of this project have shed light on some areas for future investigation which will help to clarify the roles of alternatively-spliced $Ca_v\beta$ subunits in HVA calcium channel modulation. In many of the datasets the standard error was quite large, often leading to statistical anomalies which need to be resolved. This could easily be accomplished by increasing the number of repeats (n-values) in each dataset in the hopes of decreasing the standard error (and the standard deviation used in the ANOVA). Increasing the n-values, and thereby hopefully decreasing the standard error, may reveal statistically significant differences that, at present, are not considered significant presenting a clearer picture of the true nature of $LCa_v\beta$ subunit modulation of invertebrate HVA calcium channels.

In order to truly understand the *LCa$_v$β* subunit modulation of *LCa$_v$1* it would be critical to have recordings in the absence of *Ca$_v$β* subunits, but this has not been possible to date (see section 4.2). Comparison of the biophysical properties of *LCa$_v$1* and rat *Ca$_v$1.2* channels has shown that these channels are nearly identical in their voltage-dependency on activation and inactivation as well as their gating kinetics (Senatore et al., unpublished data), and so it would be useful to include rat *Ca$_v$1.2* as a reference with which to compare the modulatory effects of *LCa$_v$β* subunits. By increasing the number of experimental repeats and including a *Ca$_v$1.2* comparison, it should be possible to gain further insight into the modulation of HVA calcium channels by *LCa$_v$β* subunit splice isoforms.

In order to identify the patterns of *LCa$_v$β* subunit expression, it would be helpful to perform quantitative real-time PCR on RNA extracted from various *Lymnaea* tissues (both neural and otherwise) at several developmental stages (eggs, juveniles and adults). Quantitative real-time PCR would identify where and when various *LCa$_v$β* subunit isoforms were expressed and to what extent they are present relative to other alternatively spliced isoforms. This information could provide clues as to the function of each *LCa$_v$β* isoform and the type of physiological or developmental effects it mediates. Along these same lines, the development of isoform-specific antibodies would allow for the determination of specific expression patterns in the *Lymnaea* central ring ganglia using fluorescently labeled secondary antibodies.

These antibodies could also be used for co-immunoprecipitation experiments to determine if there are any differences in the protein-protein interactions between alternatively spliced *LCa$_v$β* isoforms. It has been suggested that the largest role of the N-terminus of *Ca$_v$β*

subunits likely involves secondary protein interactions which act to fine-tune HVA calcium channel activity (Maltez *et al.*, 2005). Therefore, determining what, if any, differences are present in protein binding ability would help to fully evaluate the function of each $LCa_v\beta$ isoform, thereby enhancing our understanding of VGCC physiology.

Much work still needs to be completed in order to fully understand the roles of specific structural motifs found in $Ca_v\beta$ subunits, and how they affect channel electrophysiology. In order to tease apart the roles of the N-terminus and exon 7B in the modulation of channel gating and kinetics, a mutant $LCa_v\beta_{A-}$ subunit could be created that would contain exons A1 and A2 in the N-terminus but lack exon 7B (GVQFVSP) in the HOOK region. By creating and expressing $LCa_v\beta_A$-, it would be possible to determine with some degree of certainty which domains are responsible for the observed modulatory effects on LCa_v1 and LCa_v2. Also, creation of $LCa_v\beta$ subunit mutants which have been truncated at various methionine residues in the N-terminus may assist in determining if its length is indeed a factor affecting LCa_v1 modulation as was observed for mammalian $Ca_v1.2$ channels (Jangsangthong *et al.*, 2009; Herzig *et al.*, 2007). Finally, sequencing of the N-terminus of the $LCa_v\beta$ subunit should also be completed to confirm the genomic structure upstream of exon B. New primers targeting a combination of intron and exon sequence can be created and used in a similar fashion those described in the genomic sequencing of exons B, C and D and the introns between them.

The goal of this project was to enhance our understanding of how $Ca_v\beta$ subunits can modulate the expression and biophysical properties of VGCCs. Completion of further experimental repeats, quantitative real-time PCR and genomic sequencing, as well as the

inclusion of mammalian *$Ca_v1.2$* for biophysical comparison and creation of isoform-specific antibodies will improve the ability of future researchers to accomplish these goals.

Table 4.1: Effects of mammalian *Cavβ* subunit expression on the biophysical properties of L-type calcium channels. (Note that ND represents "no data available").

Beta subunit gene	Calcium channel type	N-terminal splice variant	Size of N-terminus	Name of exon 7 splice variant	Size of exon 7	Conductance	Peak Current	V0.5 activation	Ka	V0.5 inactivation	Ki	activation kinetics	inactivation kinetics	Reference
Cavβ1a	*Cav1.2*	A variant	57aa	7A	52aa	ND	increased	shifted left <10mV	ND	shifted left 12mV	ND	ND	2X faster	Jangsangthong et al., 2009
Cavβ1b	*Cav1.2*	A variant	57aa	7B	7aa	no effect	ND	no effect	decrease	shifted left 5mV	no effect	no change	no effect	Yasuda et al., 2004
Cavβ2a	*Cav1.2*	B variant	16aa	7A	45aa	decreased	ND	shifted left <5mV	no effect	shift right 7mV	increased	no change	drastically slower	Yasuda et al., 2004
Cavβ2b	*Cav1.2*	B variant	17aa	7B	7aa	ND	increased	ND	ND	no effect	no effect	slightly faster	faster	Takahashi et al., 2003
Cavβ3	*Cav1.2*	B variant	15aa	7B	7aa	no effect	ND	shifted left <5mV	no effect	shift left 5mV	no effect	no change	no effect	Yasuda et al., 2004
Cavβ4a	*Cav1.2*	B variant	15aa	7B	7aa	ND	increased 6X	no effect	slight decrease	no effect	no effect	ND	ND	Helton and Horne, 2002
Cavβ4b	*Cav1.2*	A variant	49aa	7B	7aa	no effect	increased 10X*	shifted left <5mV	slight decrease	shifted left <10mV	no effect	no effect	no effect	Yasuda et al., 2004; Helton and Horne, 2003*

Table 4.2: Effects of Cavβ subunit expression on the biophysical properties of neuronal voltage-gated calcium channels. The modulatory effects of snail (*LCavβ*), squid (*LoCavβ*) and mammalian (*Cavβ*) beta subunit expression on neuronal (Cav2) channels are summarized below, as are some of the structural properties of the N-terminus and HOOK regions. (Note that ND represents "no data available").

Beta subunit gene	Calcium channel type	N-terminal splice variant	Size of N-terminus	Name of exon 7 splice variant	Size of exon 7	Conductance	Peak Current	V1/2 activation	Ka	V1/2 inactivation	Ki	activation kinetics	inactivation kinetics	Reference
LCavβA+	*LCav2*	A variant	49aa	7B and 7A	51aa	no change	none	no effect	decreased	none	no change	no change	slower	N/A
LCavβB+	*LCav2*	B variant	47aa	7B and 7A	51aa	decreased	none	no effect	decreased	none	no change	no change	no change	N/A
LCavβB-	*LCav2*	B variant	47aa	7A	44aa	no change	increased 5X	no effect	decreased	none	decreased	no change	slower	N/A
LoCavβ1A+	*Cav2.3*	A variant	48aa	7B and 7A	49aa	ND	increased 15X	ND	ND	ND	ND	ND	ND	Kimura and Kubo, 2003
LoCavβ1A-	*Cav2.3*	A variant	48aa	7A	44aa	ND	increased 25X	ND	ND	shifted right	no change	slower	slower	Kimura and Kubo, 2003
LoCavβ1B+	*Cav2.3*	B variant	17aa	7B and 7A	49aa	ND	increased 10X	ND	ND	shifted right	no change	slower	slower	Kimura and Kubo, 2003
LoCavβ1B-	*Cav2.3*	B variant	17aa	7A	44aa	ND	increased 10X	ND	ND	ND	ND	ND	ND	Kimura and Kubo, 2003
Cavβ1b	*Cav2.2*	A variant	57aa	7B	7aa	increased	ND	no effect	slight decrease	shifted left 5mV	small decrease	no change	faster	Yasuda et al., 2004
Cavβ2a	*Cav2.2*	B variant	16aa	7A	45aa	increased	ND	shifted left <5mV	slight decrease	ND	ND	no change	drastically slower	Yasuda et al., 2004
Cavβ3	*Cav2.2*	B variant	15aa	7B	7aa	no effect	ND	shifted left <5mV	slight decrease	shifted left 9mV	no effect	no change	faster	Yasuda et al., 2004
Cavβ4a	*Cav2.2, Cav2.3*	B variant	15aa	7B	7aa	ND	increased 6x	no effect	decreased	no effect	no effect	ND	faster	Helton and Horne, 2002
Cavβ4b	*Cav2.2*	A variant	49aa	7B	7aa	Increased 2X	Increased 10X*	shifted left <5mV	slight decrease	shifted left <5mV	no effect	no effect	no effect	Yasuda et al., 2004; Helton and Horne, 2003*

References

Aparicio, S., Chapman, J., Stupka, E., Putnam, N., Chia, J., Dehal, P., Christoffels, A., Rash, S., Hoon, S., Smit, A., Gelpke, M. D. S., Roach, J., Oh, T., Ho, I. Y., Wong, M., Detter, C., Verhoef, F., Predki, P., Tay, A., Lucas, S., Richardson, P., Smith, S. F., Clark, M. S., Edwards, Y. J. K., Doggett, N., Zharkikh, A., Tavtigian, S. V., Pruss, D., Barnstead, M., Evans, C., Baden, H., Powell, J., Glusman, G., Rowen, L., Hood, L., Tan, Y. H., Elgar, G., Hawkins, T., Venkatesh, B., Rokhsar, D., & Brenner, S. (2002). Whole-genome shotgun assembly and analysis of the genome of fugu rubripes. *Science, 297*(5585), 1301-1310.

Arias, J. M., Murbartian, J., Vitko, I., Lee, J. H., & Perez-Reyes, E. (2005). Transfer of beta subunit regulation from high to low voltage-gated Ca2+ channels. *FEBS Letters, 579*(18), 3907-3912. doi:10.1016/j.febslet.2005.06.008

Arikkath, J., & Campbell, K. P. (2003). Auxiliary subunits: Essential components of the voltage-gated calcium channel complex. *Current Opinion in Neurobiology, 13*(3), 298-307.

Beguin, P., Nagashima, K., Gonoi, T., Shibasaki, T., Takahashi, K., Kashima, Y., Ozaki, N., Geering, T., Iwanaga, T., & Seino, S. (2001). Regulation of Ca2+ channel expression at the cell surface by the small G-protein kir/Gem. *Nature, 411*(6838), 701-706.

Bichet, D., Cornet, V., Geib, S., Carlier, E., Volsen, S., Hoshi, T., Mori, Y., & De Waard, M. (2000). The I-II loop of the Ca2+ channel alpha(1) subunit contains an endoplasmic reticulum retention signal antagonized by the beta subunit. *Neuron, 25*(1), 177-190.

Birnbaumer, L., Qin, N., Olcese, R., Tareilus, E., Platano, D., Costantin, J., & Stefani, E. (1998). Structures and functions of calcium channel beta subunits. *Journal of Bioenergetics and Biomembranes, 30*(4), 357-375.

Birnboim, H. C., & Doly, J. (1979). Rapid alkaline extraction procedure for screening recombinant plasmid dna. *Nucleic Acids Research, 7*(6), 1513-1523.

Brice, N. L., Berrow, N. S., Campbell, V., Page, K. M., Brickley, K., Tedder, I., & Dolphin, A. C. (1997). Importance of the different beta subunits in the membrane expression of the alpha 1A and alpha 2 calcium channel subunits: Studies using a depolarization-sensitive alpha 1A antibody. *European Journal of Neuroscience, 9*(4), 749-759.

Carbone, E., & Lux, H. D. (1984). A low voltage-activated, fully inactivating ca-channel in vertebrate sensory neurons. *Nature, 310*(5977), 501-502.

Castellano, A., Wei, X. Y., Birnbaumer, L., & Perezreyes, E. (1993). Cloning and expression of a 3rd calcium-channel beta-subunit. *Journal of Biological Chemistry, 268*(5), 3450-3455.

Castellano, A., Wei, X. Y., Birnbaumer, L., & Perezreyes, E. (1993). Cloning and expression of a neuronal calcium-channel beta-subunit. *Journal of Biological Chemistry, 268*(17), 12359-12366.

Catterall, W. A. (1996). Molecular properties of sodium and calcium channels. *Journal of Bioenergetics and Biomembranes, 28*(3), 219-230.

Chen, Y. H., Li, M. H., Zhang, Y., He, L. L., Yamada, Y., Fitzmaurice, A., Shen, Y., Zhang, H. L., Tong, L., & Yang, J. (2004). Structural basis of the alpha(1)-beta subunit interaction of voltage-gated Ca2+ channels. *Nature, 429*(6992), 675-680.

Chien, A. J., Carr, K. M., Shirokov, R. E., Rios, E., & Hosey, M. M. (1996). Identification of palmitoylation sites within the L-type calcium channel beta(2a) subunit and effects on channel function. *Journal of Biological Chemistry, 271*(43), 26465-26468.

Chien, A. J., Zhao, X. L., Shirokov, R. E., Puri, T. S., Chang, C. F., Sun, D., Rios, E., & Hosey, M. M. (1995). Roles of a membrane-localized beta-subunit in the formation and targeting of functional L-type Ca2+ channels. *Journal of Biological Chemistry, 270*(50), 30036-30044.

Cohen, J., Cohen, P., West, S. G., & Aiken, L. S. (2003). *Applied multiple Regression/Correlation analysis for the behavioral sciences* (3rd ed.). Mahwah, NJ: Lawrence Earlbaum Associates.

Cohen, R. M., Foell, J. D., Balijepalli, R. C., Shah, V., Hell, J. W., & Kamp, T. J. (2005). Unique modulation of L-type Ca2+ channels by short auxiliary beta(1d) subunit present in cardiac muscle. *American Journal of Physiology-Heart and Circulatory Physiology, 288*(5), H2363-H2374. doi:10.1152/ajpheart.00348.2004

Colecraft, H. M., Alseikhan, B., Takahashi, S. X., Chaudhuri, D., Mittman, S., Yegnasubramanian, V., Alvania, R. S., Johns, D. C., Marban, E., & Yue, D. T. (2002). Novel functional properties of Ca2+ channel beta subunits revealed by their expression in adult rat heart cells. *Journal of Physiology-London, 541*(2), 435-452. doi:10.1113/jphysiol.2002.018515

Dewaard, M., Pragnell, M., & Campbell, K. P. (1994). Ca2+ channel regulation by a conserved beta-subunit domain. *Neuron, 13*(2), 495-503.

Dubuis, E., Rockliffe, N., Hussain, M., Boyett, M., Wray, D., & Gawler, D. (2006). Evidence for multiple src binding sites on the alpha 1c L-type Ca2+ channel and their roles in activity regulation. *Cardiovascular Research, 69*(2), 391-401. doi:10.1016/j.cardiores.2005.11.006

Ebert, A. M., McAnelly, C. A., Handschy, A. V., Mueller, R. L., Horne, W. A., & Garrity, D. M. (2008). Genomic organization, expression, and phylogenetic analysis of Ca2+ channel beta 4 genes in 13 vertebrate species. *Physiological Genomics, 35*(2), 133-144. doi:10.1152/physiolgenomics.90264.2008 ER

Ebert, A. M., McAnelly, C. A., Srinivasan, A., Mueller, R. L., Garrity, D. B., & Garrity, D. M. (2008). The calcium channel beta 2 (CACNB2) subunit repertoire in teleosts. *Bmc Molecular Biology, 9* doi:10.1186/1471-2199-9-38 ER

Ferguson, G. A., & Takane, Y. (2005). *Statistical analysis in psychology and education* (6th ed.). Montreal, PQ: McGraw-Hill.

Fitzgerald, E. M. (2002). The presence of Ca2+ channel beta subunit is required for mitogen-activated protein kinase (MAPK)-dependent modulation of alpha 1B Ca2+ channels in COS-7 cells. *Journal of Physiology-London, 543*(2), 425-437. doi:10.1113/physiol.2002022822

Foell, J. D., Balijepalli, R. C., Delisle, B. P., Yunker, A. M. R., Robia, S. L., Walker, J. W., McEnery, M. W., January, C. T., & Kamp, T. J. (2004). Molecular heterogeneity of calcium channel beta-subunits in canine and human heart: Evidence for differential subcellular localization. *Physiological Genomics, 17*(2), 183-200.

Gao, T. Y., Chien, A. J., & Hosey, M. M. (1999). Complexes of the alpha(1C) and beta subunits generate the necessary signal for membrane targeting of class C L-type calcium channels. *Journal of Biological Chemistry, 274*(4), 2137-2144.

Gerster, U., Neuhuber, B., Groschner, K., Striessnig, J., & Flucher, B. E. (1999). Current modulation and membrane targeting of the calcium channel alpha(1c) subunit are independent functions of the beta subunit. *Journal of Physiology-London, 517*(2), 353-368.

Gonzalez-Gutierrez, G., Miranda-Laferte, E., Neely, A., & Hidalgo, P. (2007). The src homology 3 domain of the beta-subunit of voltage-gated calcium channels promotes endocytosis via dynamin interaction. *Journal of Biological Chemistry, 282*(4), 2156-2162. doi:10.1074/jbc.M609071200

Gonzalez-Gutierrez, G., Miranda-Laferte, E., Nothmann, D., Schmidt, S., Neely, A., & Hidalgo, P. (2008). The guanylate kinase domain of the beta-subunit of voltage-gated calcium channels suffices to modulate gating. *Proceedings of the National Academy of Sciences of the United States of America, 105*(37), 14198-14203. doi:10.1073/pnas.0806558105

Hanlon, M. R., Berrow, N. S., Dolphin, A. C., & Wallace, B. A. (1999). Modelling of a voltage-dependent Ca2+ channel B subunit as a basis for understanding its functional properties. *FEBS Letters, 445*(2-3), 366-370.

Harry, J. B., Kobrinsky, E., Abernethy, D. R., & Soldatov, N. M. (2004). New short splice variants of the human cardiac ca-v beta(2) subunit - redefining the major functional motifs implemented in modulation of the ca(v)1.2 channel. *Journal of Biological Chemistry, 279*(45), 46367-46372. doi:10.1074/jbc.M409523200

He, L. L., Zhang, Y., Chen, Y. H., Yamada, Y., & Yang, J. (2007). Functional modularity of the beta-subunit of voltage-gated Ca2+ channels. *Biophysical Journal, 93*(3), 834-845.

Helton, T. D., & Horne, W. A. (2002). Alternative splicing of the beta(4) subunit has alpha(1) subunit subtype-specific effects on Ca2+ channel gating. *Journal of Neuroscience, 22*(5), 1573-1582.

Hering, S. (2002). Beta-subunits: Fine tuning of Ca2+ channel block. *Trends in Pharmacological Sciences, 23*(11), 509-513.

Herzig, S., Khan, I. F. Y., Grundemann, D., Matthes, J., Ludwig, A., Michels, G., Hoppe, U. C., Chaudhuri, D., Schwartz, A., Yue, D. T., & Hullin, R. (2007). Mechanism of ca(v)1.2 channel modulation by the amino terminus of cardiac beta(2)-subunits. *Faseb Journal, 21*(7), 1527-1538. doi:10.1096/fj.06-7377com ER

Hille, B. (1992). *Ionic channels of excitable membranes* (2nd ed.). Sunderland, MA: Sinauer Associates.

Hong, X., Scofield, D. G., & Lynch, M. (2006). Intron size, abundance, and distribution within untranslated regions of genes. *Molecular Biology and Evolution, 23*(12), 2392-2404. doi:10.1093/molbev/msl111 ER

Huguenard, J. R. (1996). Low-threshold calcium currents in central nervous system neurons. *Annual Review of Physiology, 58*(1), 329-348.

Hullin, R., Singerlahat, D., Freichel, M., Biel, M., Dascal, N., Hofmann, F., & Flockerzi, V. (1992). Calcium-channel beta-subunit heterogeneity - functional expression of cloned cdna from heart, aorta and brain. *Embo Journal, 11*(3), 885-890.

Jangsangthong, W., Kuzmenkina, E., Khan, I. F. Y., Matthes, J., Hullin, R., & Herzig, S. (2009). Length-dependent modulation of cardiac L-type calcium channels by the N-terminus of a beta 1a subunit. *Naunyn-Schmiedebergs Archives of Pharmacology, 379*, 140.

Jarvis, S. E., & Zamponi, G. W. (2001). Distinct molecular determinants govern syntaxin 1A-mediated inactivation and G-protein inhibition of N-type calcium channels. *Journal of Neuroscience, 21*(9), 2939-2948.

Jones, S. W. (1998). Overview of voltage-dependent calcium channels. *Journal of Bioenergetics and Biomembranes, 30*(4), 299-312.

Kim, E., Niethammer, M., Rothschild, A., Jan, Y. N., & Sheng, M. (1995). Clustering of shaker-type K+ channels by interaction with a family of membrane-associated guanylate kinases. *Nature, 378*(6552), 85-88.

Kim, M. S., Morii, T., Sun, L. X., Imoto, K., & Mori, Y. (1993). Structural determinants of ion selectivity in brain calcium-channel. *FEBS Letters, 318*(2), 145-148.

Kimura, T., & Kubo, T. (2003). Cloning and functional characterization of squid voltage-dependent Ca2+ channel beta subunits: Involvement of N-terminal sequences in differential modulation of the current. *Neuroscience Research, 46*(1), 105-117.

Le Hir, H., Nott, A., & Moore, M. J. (2003). How introns influence and enhance eukaryotic gene expression. *Trends in Biochemical Sciences, 28*(4), 215-220. doi:10.1016/S0968-0004(03)00052-5 ER

Maltez, J. M., Nunziato, D. A., Kim, J., & Pitt, G. S. (2005). Essential ca-V beta modulatory properties are AID-independent. *Nature Structural & Molecular Biology, 12*(4), 372-377. doi:10.1038/nsmb909

Mannuzzu, L. M., Moronne, M. M., & Isacoff, E. Y. (1996). Direct physical measure of conformational rearrangement underlying potassium channel gating. *Science, 271*(5246), 213-216.

McPherson, P. S. (1999). Regulatory role of SH3 domain-mediated protein-protein interactions in synaptic vesicle endocytosis. *Cellular Signalling, 11*(4), 229-238.

Mintz, I. M., Venema, V. J., Swiderek, K. M., Lee, T. D., Bean, B. P., & Adams, M. E. (1992). P-type calcium channels blocked by the spider toxin omega-aga-iva. *Nature, 355*(6363), 827-829.

Montgomery, J. M., Zamorano, P. L., & Garner, C. C. (2004). MAGUKs in synapse assembly and function: An emerging view. *Cellular and Molecular Life Sciences, 61*(7-8), 911-929.

Moroz, L. L., Edwards, J. R., Puthanveettil, S. V., Kohn, A. B., Hla, T., Heyland, A., Knudsen, L., Sahni, A., Yu, F., Liu, L., Jezzini, S., Lovell, P., Iannucculli, W., Chen, M., Nguyen, T., Sheng, H., Shaw, R., Kalachikov, S., Panchin, Y. V., Farmerie, W., Russo, J. J., Ju, J., & Kandel, E. R. (2006). Neuronal transcriptome of aplysia: Neuronal compartments and circuitry. *Cell, 127*(7), 1453-1467. doi:10.1016/j.cell.2006.09.052

Neuhuber, B., Gerster, U., Mitterdorfer, J., Glossmann, H., & Flucher, B. E. (1998). Differential effects of Ca2+ channel beta(1a) and beta(2a) subunits on complex formation with alpha(1S) and on current expression in tsA201 cells. *Journal of Biological Chemistry, 273*(15), 9110-9118.

Nott, A., Muslin, S. H., & Moore, M. J. (2003). A quantitative analysis of intron effects on mammalian gene expression. *Rna-a Publication of the Rna Society, 9*(5), 607-617. doi:10.1261/rna.5250403 ER

Nowycky, M. C., Fox, A. P., & Tsien, R. W. (1985). 3 types of calcium channels in chick dorsal-root ganglion-cells. *Biophysical Journal, 47*(2), A67-A67.

Perezreyes, E., Castellano, A., Kim, H. S., Bertrand, P., Baggstrom, E., Lacerda, A. E., Wei, X. Y., & Birnbaumer, L. (1992). Cloning and expression of a cardiac brain beta-subunit of the L-type calcium-channel. *Journal of Biological Chemistry, 267*(3), 1792-1797.

Plummer, M. R., Logothetis, D. E., & Hess, P. (1989). Elementary properties and pharmacological sensitivities of calcium channels in mammalian peripheral neurons. *Neuron, 2*(5), 1453-1463.

Powers, P. A., Liu, S. Y., Hogan, K., & Gregg, R. G. (1992). Skeletal-muscle and brain isoforms of a beta-subunit of human voltage-dependent calcium channels are encoded by a single gene. *Journal of Biological Chemistry, 267*(32), 22967-22972.

Pragnell, M., Dewaard, M., Mori, Y., Tanabe, T., Snutch, T. P., & Campbell, K. P. (1994). Calcium-channel beta-subunit binds to a conserved motif in the I-ii cytoplasmic linker of the alpha(1)-subunit. *Nature, 368*(6466), 67-70.

Raghib, A., Bertaso, F., Davies, A., Page, K. M., Meir, A., Bogdanov, Y., & Dolphin, A. C. (2001). Dominant-negative synthesis suppression of voltage-gated calcium channel ca(v)2.2 induced by truncated constructs. *Journal of Neuroscience, 21*(21), 8495-8504.

Richards, M. W., Leroy, J., Pratt, W. S., & Dolphin, A. C. (2007). The HOOK-domain between the SH3 and the GK domains of ca-v beta subunits contains key determinants controlling calcium channel inactivation. *Channels, 1*(2), 92-101.

Ruth, P., Rohrkasten, A., Biel, M., Bosse, E., Regulla, S., Meyer, H. E., Flockerzi, V., & Hofmann, F. (1989). Primary structure of the beta-subunit of the dhp-sensitive calcium-channel from skeletal-muscle. *Science, 245*(4922), 1115-1118.

Sakharkar, M. K., Chow, V. T. K., & Kangueane, P. (2004). Distributions of exons and introns in the human genome. *In Silico Biology, 4*(4), 387-393.

Sokolov, S., Weiss, R. G., Timin, E. N., & Hering, S. (2000). Modulation of slow inactivation in class A Ca2+ channels by beta-subunits. *Journal of Physiology-London, 527*(3), 445-454.

Spafford, J. D., Munno, D. W., van Nierop, P., Feng, Z. P., Jarvis, S. E., Gallin, W. J., Smit, A. B., Zamponi, G. W., & Syed, N. I. (2003). Calcium channel structural determinants of synaptic transmission between identified invertebrate neurons. *Journal of Biological Chemistry, 278*(6), 4258-4267. doi:10.1074/jbc.M211076200

Spafford, J. D., van Minnen, J., Larsen, P., Smit, A. B., Syed, N. I., & Zamponi, G. W. (2004). Uncoupling of calcium channel alpha(1) and beta subunits in developing neurons. *Journal of Biological Chemistry, 279*(39), 41157-41167.

Spafford, J. D., & Zamponi, G. W. (2003). Functional interactions between presynaptic calcium channels and the neurotransmitter release machinery. *Current Opinion in Neurobiology, 13*(3), 308-314.

Stuhmer, W., Conti, F., Suzuki, H., Wang, X. D., Noda, M., Yahagi, N., Kubo, H., & Numa, S. (1989). Structural parts involved in activation and inactivation of the sodium-channel. *Nature, 339*(6226), 597-603.

Takahashi, M., Seagar, M. J., Jones, J. F., Reber, B. F. X., & Catterall, W. A. (1987). Subunit structure of dihydropyridine-sensitive calcium channels from skeletal-muscle. *Proceedings of the National Academy of Sciences of the United States of America, 84*(15), 5478-5482.

Takahashi, S. X., Mittman, S., & Colecraft, H. M. (2003). Distinctive modulatory effects of five human auxiliary beta(2) subunit splice variants on L-type calcium channel gating. *Biophysical Journal, 84*(5), 3007-3021.

Tanabe, T., Takeshima, H., Mikami, A., Flockerzi, V., Takahashi, H., Kangawa, K., Kojima, M., Matsuo, H., Hirose, T., & Numa, S. (1987). Primary structure of the receptor for calcium-channel blockers from skeletal-muscle. *Nature, 328*(6128), 313-318.

van Moorsel, C. H. M., van Nes, W. J., & Megens, H. J. (2000). A quick, simple, and inexpensive mollusc DNA extraction protocol for PCR-based techniques. *Malacologia, 42*(1-2), 203-206.

Vendel, A. C., Rithner, C. D., Lyons, B. A., & Horne, W. A. (2006). Solution structure of the N-terminal A domain of the human voltage-gated Ca2+ channel beta(4a) subunit. *Protein Science, 15*(2), 378-383.

Vendel, A. C., Terry, M. D., Striegel, A. R., Iverson, N. M., Leuranguer, V., Rithner, C. D., Lyons, B. A., Pickard, G. E., Tobet, S. A., & Horne, W. A. (2006). Alternative splicing of the voltage-gated Ca2+ channel beta(4) subunit creates a uniquely folded N-terminal protein binding domain with cell-specific expression in the cerebellar cortex. *Journal of Neuroscience, 26*(10), 2635-2644.

Vitko, I., Shcheglovitov, A., Baumgart, J. P., Arias-Olguín, I. I., Murbartian, J., Arias, J. M., & Perez-Reyes, E. (2008). Orientation of the calcium channel beta relative to the alpha(1)2.2 subunit is critical for its regulation of channel activity. *PLoS One, 3*(10)

Yamaguchi, H., Hara, M., Strobeck, M., Fukasawa, K., Schwartz, A., & Varadi, G. (1998). Multiple modulation pathways of calcium channel activity by a beta subunit - direct evidence of beta subunit participation in membrane trafficking of the alpha(1c) subunit. *Journal of Biological Chemistry, 273*(30), 19348-19356.

Yang, J., Ellinor, P. T., Sather, W. A., Zhang, J. F., & Tsien, R. W. (1993). Molecular determinants of Ca2+ selectivity and ion permeation in L-type Ca2+ channels. *Nature, 366*(6451), 158-161.

Yang, N. B., & Horn, R. (1995). Evidence for voltage-dependent S4 movement in sodium-channels. *Neuron, 15*(1), 213-218.

Yasuda, T., Chen, L., Barr, W., McRory, J. E., Lewis, R. J., Adams, D. J., & Zamponi, G. W. (2004). Auxiliary subunit regulation of high-voltage activated calcium channels expressed in mammalian cells. *European Journal of Neuroscience, 20*(1), 1-13. doi:10.1111/j.1460-9568.2004.03434.x ER

Zhou, W. B., Horstick, E. J., Hirata, H., & Kuwada, J. Y. (2008). Identification and expression of voltage-gated calcium channel beta subunits in zebrafish. *Developmental Dynamics, 237*(12), 3842-3852. doi:10.1002/dvdy.21776 ER